Quantum Chemical Models in Molecular Structure Elucidation

Jens Abildgaard

Dissertation in Chemistry

Department of Life Sciences and Chemistry

Roskilde University 1998

Quantum Chemical Models in Molecular Structure Elucidation

Jens Abildgaard
Department of Life Sciences and Chemistry, Roskilde University, 1998

Contents

"As far as the laws of mathematics refer to reality, they are not certain; and as far as they are certain, they do not refer to reality."

Albert Einstein

Introduction

Summary

The introductory *"Small Molecule Modeling"* (chapter 1) discusses the outline of an independent structure solution method based on quantum chemical structure calculations, validated by the fit of the calculated and experimental spectroscopic data. *"Protein Modeling"* is a description of the major obstacles that must be overcome before protein structure refinement reaches a level of accuracy allowing safe prediction of NMR chemical shifts. *"Models in Science"* restates one of the basic axioms of science; the fundamental dynamic of model and experiment.

In *"Quantum Mechanical Model Calculations in Chemistry"* (chapter 2) the methodology for testing calculations of molecular structure and selected spectroscopic data is presented. The model calculated data compared with experiment are: molecular geometry, electronic energy, vibrational frequencies, and ^{1}H and ^{13}C NMR nuclear shielding (chemical shifts). Though the survey is not exhaustive, the conclusions do point towards the Density Functional Theory (DFT) methods as the better choice in quantum chemical molecular orbital models, both with respect to precision of prediction and computational resources.

The article from Journal of the American Chemical Society *"Unraveling the Electronic and Vibrational Contributions to Deuterium Isotope Effects..."* (chapter 3) contains calculations of molecular structure and nuclear shielding in a series of aromatic compounds, displaying large variation in hydroxy hydrogen-deuterium substitution isotope effects on ^{13}C NMR chemical shifts. The DFT/GIAO (Gauge Including Atomic Orbital) calculated ^{1}H nuclear shielding is shown to be a sensitive and reliable probe for validating calculated hydrogen bond geometry. The theory of isotope effects being proportional to the gradient of the calculated nuclear shielding with respect to X-H(D) bond length is demonstrated (electronic contribution), and a new way of calculating the size of hydrogen-deuterium vibrationally average bond length shortening (vibrational contribution) further proves the theory by the exceptional good fit with experiment. Model calculations render probable a conclusion about the intramolecular steric cause of the large variation in hydrogen bond geometry in intramolecular hydrogen bonded o-hydroxy acyl aromatics.

One important feature of "*Ab initio Calculations of External Charge Effects...*" (chapter 4) is the new and simple formulation of the electric field effect on nuclear shielding described by the electric field component in the bond directions, and the size of the electric field determined at the atomic positions of the chemical bond. The model yields a quantification of the electric field effect on chemical shifts of acetamide, used as a small peptide bond model. This practical mathematical formulation using only molecularly fixed geometric parameters (atomic coordinates) is shown to work. This approach is not mathematically very different from the traditional formulation of the electric field, and electric field gradient effect in the three orthogonal nuclear shielding tensor directions, which must first be determined with respect to molecular coordinates.

The C_{2v} symmetric geometry of the title compound in *"Molecular and Vibrational Structure of 1,6,6aλ^4-Trithiapentalene..."* (chapter 5) is not a global energy minimum in neither restricted nor unrestricted Hartree Fock calculations, irrespective of basis set size. Including contributions from electron correlation with the MP2 method, results in the correct geometry which is electron correlation stabilized. The discussed "bell clapper" vibrational mode is calculated with a MP2=FULL/6-311G(d,p) normal mode analysis, but the use of the BPW91 and BLYP DFT functionals offers significantly improved correlation with experiment.

The calculations for *"The Vibrational Spectrum of Acenaphthylene..."* (chapter 6) unambiguously assign all allowed IR and RAMAN fundamental vibrational transitions, again demonstrating the superior quality of the DFT (BPW91/6-311G(d,p)) normal mode analysis. The availability of a neutron diffraction structure opens the possibility of comparing directly the calculated molecular geometries with the experimental. The MP2 and DFT calculated geometries both compare favorably with the neutron diffraction structure, and significantly better than the Hartree Fock and semi-empirical AM1 and PM3 methods.

Quantum Chemical Models in Molecular Structure Elucidation

The title of this dissertation is the result of an ongoing theme throughout the research I have been involved with. It can be described as work with "models yielding high resolution structural information validated by the combined use of quantum chemical calculated and experimental spectroscopic data". The research is and always was applied to the solution of specific chemical problems, as chemical modeling is inseparable from the experimental disciplines.

Having gone from inorganic synthesis [1] through experimental NMR-spectroscopy [2], over single crystal diffraction methods [1] and IR spectroscopy [3-4], the most resent work has mainly been within the field of computational chemistry, more accurately referred to as model chemistry [1,3-13].

Through the work with the last and academically rewarding research projects involving interpretation of NMR data with quantum chemical calculated nuclear shielding [1,6,7,11,12], I have personally become fascinated with these powerful techniques illuminating the fundamentals of chemistry. I am indebted to my supervisor professor **Poul Erik Hansen** from the Department of Life Sciences and Chemistry at Roskilde University for suggesting the work in this field.

Small Molecule Modeling

The present dissertation is about structural chemical modeling, applied to molecular systems of the humble size where we can still effectively correlate our calculations with experimental data. There is reason to believe that development in the combined use of NMR data and some variation of the Density Functional Theory (DFT) [14] models will result in an independent experimental structure solution method. "Experimental structure solution" simply meaning that a set of molecules is used for calibration having experimentally measured spectroscopic data to correlate with calculated values. The RMSD (Root Mean Squared Difference) between the experimental and calculated data are correlated with the RMSD between independently solved high resolution molecular structures (e.g. single crystal neutron diffraction) and calculated geometries to provide the structural resolution.

In the first chapter of this work, *"Quantum Mechanical Model Calculations in Chemistry: Structure, Vibrations, Chemical Shifts, and Isotope Effects on Chemical*

Shifts" (chapter 3 in the present work), an initial pilot attempt to correlate calculated and experimental molecular structure RMSD in atomic coordinates with RMSD in calculated spectroscopic data is presented [7] (chapter 2.3.6 Residual correlation).

While ^{13}C chemical shifts are sensitive to the directly covalent bonded structure, variations in bond lengths and angles, ^{13}C NMR data are rather insensitive (compared with the precision of their prediction) to the environmental conditions such as solvent effects and electric field perturbations. ^{1}H chemical shifts and isotope effects are insensitive to small geometric perturbations, but very sensitive to the environment (e.g. electric field effects) and hydrogen bond geometry [6] (chapter 4 in the present work). All the mentioned data are easily measured and suggests a multi-nuclear approach to a NMR structure solution method.

NMR chemical shifts probe, when uniquely assigned, local structure, and there is the possibility of grouping different types of atomic signals used in the correlation according to covalent bonding environment. Thus ^{13}C signals can be divided according to the level of saturation of the carbon atom as well as the types of atoms to which they are bonded, yielding a rich field of possible improvements in calibrations within the atomic subgroups and specific molecular fragments. Similar groupings could also be used in the calculations of RMSD between atomic coordinates in comparison between crystal diffraction solved molecular structures and calculated geometries for calibration. The mentioned type of localized systematic errors in the model calculations are sensitive to basis set saturation level, and a localized approach, a grouping according to bonding pattern, would to some extent remedy this kind of problems.

The power of modern molecular orbital calculations is demonstrated in the well established methodology for calculating IR vibrational frequencies. The normal mode analysis of the traditional Hartree Fock (HF), Second Order Møller Plesset Perturbation (MP2), and especially the relatively new Density Functional Theory (DFT) methods is the only practical way of assigning IR spectra. Furthermore the superior resolution of matrix isolation IR studies and the subdivision of the IR signals according to dipole allowed transition symmetry classes, by determining the transition moment direction in aligned molecules using polarized light, unambiguously determine and assign individual IR signals to the calculated molecular normal modes, thus offering the rare complete spectral assignment (chapter 5 and 6 in the present work). The combined use of the

best in state-of-the-art IR spectroscopy and model calculations of the mentioned type solves molecular symmetry ambiguities (chapter 5 in the present work) [3]. Complete and unambiguously assigned IR data could in principle also be used in conjunction with the model calculations as an independent structure solution method, provided that also the large and varied molecular calibration set could be obtained with independent experimentally determined high resolution structures.

To truly compare structures solved by crystal diffraction methods with molecular orbital calculated geometries, it is necessary to perform the geometry optimization within the periodic boundary conditions of the crystal spacegroups. No program has yet presented these capabilities with modern DFT functionals, and consequently comparison is tainted by the crystal packing effects, especially on low barrier torsion angles. Since the crystallographic community is rapidly waking up to the imperative benefit in quality of molecular orbital techniques, which of cause also provide the spatial electronic information relevant in x-ray diffraction studies, the missing capabilities in software is likely to be overcome in the near future. Combined with nuclear shielding calculation in a crystaline computational environment, such programs would also produce essential spectroscopic information for solid state NMR spectroscopy.

When comparing the molecular geometry from modern DFT calculations with high resolution neutron diffraction structures of planar aromatic hydrocarbons, possessing little conformational freedom, we find an excellent agreement [4] (chapter 7 in the present work), which we have also found in bond length and angle comparisons of systems with considerably more flexibility [11]. Ab initio molecular geometries, most notably geometries from some of the DFT methods, generally compare better with neutron diffraction structures than do the corresponding x-ray structures. We even find this when leaving out the hydrogen positions that are even more severely tainted by the systematic errors of the x-ray diffraction technique.

The last straw in the development and application of molecular orbital quantum chemical methods must be the return from the highly complex and involved mathematical calculations to a traditional picture of resonance structures describing the electronic structure. The electronic resonance picture has served the chemical society for more than a century, that is from well before the quantum mechanical description of

the chemical bond, and still is unsurpassed in conveying an intuitive understanding of this type of bonding phenomena in chemistry [4].

Protein Modeling

Having spent the larger part of my Ph.D. research trying to correlate NMR-spectroscopic data with structure in proteins [8-10,13], I admit to shy away from the cumbersome task of writing a thesis based on work where we have so far failed. We simply did not meet the required correspondence in the standard deviation between calculated and experimentally determined values, seen in the light of the variation within the measured data to be of interest or of any practical importance. We are of cause not alone in this [15-43], but we see no need to publish the material prematurely.

The prerequisite requirement for scaling up in size this type of quantum chemical prediction of chemical shifts to macro molecules is of cause that the calculations work in small molecule modeling. Furthermore the precision of the calculated chemical shifts in small molecules sets the limiting conditions for the expected precision in macro molecules.

In spite of the considerable success with predicting chemical shifts in small non-polar systems, we still need to extent this into more polar groups of molecules as e.g. ionic molecular aggregates in strongly solvating media [12]. Our experience is that the gas phase calculated nuclear shielding of organic compounds only compares well with chemical shifts of non-polar molecules in non-polar solvents like chloroform, dichloromethane, alkanes, etc.

Solvent and electric field effects in proteins are essential for understanding the variation in NMR data which are expected to be strongly influenced by the environment [8] (chapter 5 in the present work). The solution dynamic, both with respect to explicit solvent molecule modeling as well as electrostatics of solvation, is in our view also best studied by quantum chemical calculations of NMR parameters in model systems, most importantly the nuclear shielding compared with high resolution liquid state solution NMR.

A way of treating conformational dynamics and tautomeric equilibrium must be found for larger molecules, and the NMR data can be used to this end since the experimental average chemical shift is a linear combination of the nuclear shielding of

the populated molecular conformational states. The populations can be determined from the coefficients of a multi-linear regression analysis of the experimental chemical shifts and the calculated nuclear shielding of the contributing structures [11, 44]. It still, however, remains to be seen how many different conformers actually contribute to the description of protein dynamics, as reliable (not molecular mechanics) dynamics simulations have not yet been carried out.

Molecular orbital geometry optimization of sub-fragments of proteins, including both explicit solvent molecules as well as electrostatic solvent effects modeling, pieced together to make a complete protein structure, would answer many interesting questions in a much more convincing way than has hitherto been accomplished. There is at present uncertainty with respect to the respective energy contributions to protein stability from electrostatics (complex atomic multipole interaction), bond stretching and bending (gradients of the energy with respect to geometric perturbations), hydrogen bond geometry and stability, etc. If the energy gradients along the geometry optimization pathway is sampled and used for parameterization of a molecular force field, thus based on modern high level molecular orbital calculations, this molecular mechanics parameterization could be used for molecular dynamic refinement of the secondary and tertiary structure of the protein, the stationary points of which could be geometry optimized, further calibrating the molecular force-field etc.

Many proteins have coordinated transition metal centers, some of structural interest, some alostericly modifying the structure when changing oxidation states, and often directly involved in active catalytic sites. To complicate matters, unpaired metal electronic configurations require open shell calculations [45,46]. Modeling of transition metal complexes, a large field in its own right, is therefore also very relevant for macro molecule modeling, and must be fully tested in smaller and more manageable systems [1].

There is reason to believe that the presently ongoing and concerted development of "linear scaling" FMM (Fast Multipole Methods) [47-61] in quantum chemistry, new ways of treating localized "chromophores" by chopping large molecules into sections treated at different levels of [62-65], and the continuos improvement of computers and mathematical algorithms, eventually will bridge the gab between chemical modeling and structural molecular biology. Thus the problem of macro molecule modeling may be solved by the rapid introduction these and coming years of the emerging field of *Quantum biology*.

Models in Science

Models play a fundamental role in the sciences as the framework wherein we rationalize the increasing body of empirical observations and experimental data. Models, knowledge, theory, or even fundamental laws of nature are formulations that constantly change with new or more precise experimental evidence, and are thus neither absolute nor static but dynamic and in constant adaptation to the physical reality.

The reciprocal use and interdependence of model and experiment in the sciences is of cause not new, but characteristic of all scientific research. Historically the introduction of this dialectic process must necessarily mark the departure from the unverifiable speculations that characterized early natural philosophy.

> *"We can only speak of a scientific chemistry from the moment where we systematically, by the cooperation between theory and experiment, collect new experience, so that the theory is modified by the experiment, and from the modified theory new experiments can be planned etc."*
>
> K. A. Jensen, 1957

Scientific models vary in size and complexity; from the basic laws of arithmetic to the complex mathematical modeling of e.g. flow and equilibrium in economics or biological ecosystems, but the one outstanding characteristic of scientific models is that they can be tested against experiment. Without this test they are meaningless.

Complex mathematical models for large systems may incorporate a number of basic formulations and approximations which inevitably results in the accumulation of uncertainties. This, however, can be remedied by calibration against higher level observables. With increasing size and a corresponding sacrifice of precision and detail, the scientific description becomes more dependent on verification of the calculations against experimental data.

At the opposite end of the spectrum there have been attempts to formulate all-embracing fundamental laws of nature that covers the basic forces (strong and weak nuclear forces, electromagnetic, and gravitational forces) and the existence of all known fundamental subatomic particles ("the subatomic zoo"); a "Unified Field Theory". These attempts have if not largely failed then at least been beached on the energy

limitations that constrain terrestrial experimentation.

Having effectively parted with the idea of infinitely precise models for systems of any size or energy, we of cause do not have to part with modeling all together, which in effect would imply parting with modern science as we know it. Clearly defined validity limits and well established expected error values, determined by comparison with experiment, dispenses for a given model with the necessity of absolute laws. When using a specific model to predict new properties, we only have to refer to how well similar properties were predicted by the model in different systems within its field of validity.

Models in the exact sciences must be used and evaluated within well defined validity limits, and constantly checked against experimental data. If, however, too rigorous a formulations of "exact science" is used, only mathematics, the language of scientific modeling, would be left. In mathematics the experimental or the observable is slightly tricky to define (what experiment would prove "2", or indeed "5"), but even here the connection to reality is what makes mathematics stand out from pure philosophy.

If the exact sciences are characterized by the dynamic interplay between model and experiment, then the distinction between experimental and modeling (theoretical) sciences is artificial, though we do observe a natural tendency towards specialization. Some will focus on new and ever more rewarding experimental techniques applied on new systems of interest, "rewarding" meaning directly interpretable experimental results due to simple models. The theoretically oriented scientist on the other hand creates new models that rationalize new or existing empirical data or incorporates new selections of laws and formulations into original statements that predicts new or known, but hitherto unexplained properties and behavior.

Application of highly complex mathematical models employing ever more powerful computers does of cause not change the fundamental and integral role that models play in research and science, but for some reason, as popular models become available through windows interfaced graphically operated computer programs, we have a tendency to loose sight of the basic experimental foundation from which these models were once derived. Such models may predict properties of very large and complex systems, and we are inclined to believe what the machine tells us without questioning

the inherent precision of the basic model when applied to large systems, that is to check the field of validity.

The scientific touchstone in the use and application of models is, and always will be, whether the models produce data that can be tested directly against experiment, and how such a test turns out.

> *"The underlying physical laws necessary for the mathematical theory of a large part of physics and the whole of chemistry are thus completely known, and the difficulty is only that the application of these laws leads to equations much too complicated to be soluble. It therefore becomes desirable that approximate practical methods of applying quantum mechanics should be developed, which can lead to an explanation of the main features of complex atomic systems without too much computation"*
> P. A. M. Dirac, Proc. Roy. Soc. (London) Vol. CXXIII, p 714, April 1929.

References

1. *"Synthesis and ab-initio Model Calculations of the Nickel, Palladium, and Platinum(II) Complexes of Three o,o'-dihydroxy-azoarene-dyes. The Crystal Structures of ([5-chloro-2-hydroxy-phenylazo]-3-oxo-N-phenyl-butanamidat)-pyridine-nickel(II) and [5-chloro-2-hydroxy-phenylazo]-2-naphtholate)-tributyl-amin-platinum(II)"*, Abildgaard, J.; Josephsen, J.; Hansen, P. E.; Larsen, S. *Inorg. Chem.* (In preparation),
2. *"Assignment of the Ligating Nitrogen in o,o'-dihydroxy-azoarene Complexes of Nickel, Palladium, and Platinum(II) by ^{1}H- and ^{13}C-NMR Spectroscopy"*, Abildgaard, J.; Hansen, P. E.; Josephsen, J.; Lycka, A. *Inorg. Chem.* **33**, 5271 (1994),
3. *"Molecular and Vibrational Structure of 1,6,6aλ^4-Trithiapentalene. Infrared Linear Dichroism Spectroscopy and ab-initio Normal Mode Analyses"*, Andersen, K. B.; Abildgaard, J.; Radziszewski, J. G.; Spanget-Larsen, J. *J. Phys. Chem. Part A*, **101**, 4475 (1997)
4. *"The Vibrational Spectrum of Acenaphthylene: Linear Dichroism and ab-initio Model Calculations"*, Radziszewski, J. G.; Abildgaard, J.; Tulstrup, E. W. *Spectrochimica Acta Part A*, **53**, 2095 (1997)
5. *"Bent cyclopenta-2,4-dienylideneketene: Spectroscopic and ab-initio Study of Reactive Intermediate"*, Radziszewski, J. G.; Kaszynski, P.; Friderichsen, A.; Abildgaard, J. *Coll. Czech. Chem. Comm.* **63**, 1094 (1998)
6. *"Unraveling the Electronic and Vibrational Contributions to Deuterium Isotope Effects on ^{13}C Chemical Shifts by ab initio Model Calculations. Analysis of Isotope Effects on Sterically Perturbed Intramolecular Hydrogen Bonded o-Hydroxy Acyl Aromatics."*, Abildgaard, J.; Boldvig, S.; Hansen, P.E. *J. Am. Chem.*

Soc. **120 (35)**, 9063 (1998)
7. *"Quantum Mechanical Model Calculations in Chemistry: Structure, Vibrations, Chemical Shifts, and Isotope Effects on Chemical Shifts"*, Abildgaard, J.; Hansen, P. E., *Wiadomosci Chemiczne* (Chemical News), Polish Chemical Society, Ed. Koll, A. (1998) (in preparation)
8. *"ab-initio Calculations of External Charge Effects on the Isotropic ^{13}C, ^{15}N and ^{17}O Nuclear Shielding of Amides"*, Hansen, P. E.; Abildgaard, J.; Hansen, Aa. E. *Chem. Phys. Lett.* **224**, 275 (1994)
9. *"Isotope Effects on ^{13}C and ^{15}N Chemical Shifts in Proteins from Electric Field Effects"*, Abildgaard, J.; Hansen, P. E.; Hansen, Aa. E. Poster at "Frontiers of NMR in Molecular Biology IV", Keystone, Colorado, USA 3-9.4.1995. Abstract In *J. Cell. Biochem.* **Supplement 21B**, 68 (1995)
10. *"Structure Information Derived From Charge Induced Chemical Shift Changes"*, Hansen, P. E.; Abildgaard, J.; Hansen, Aa. E. Poster at "Frontiers of NMR in Molecular Biology III", Taos, New Mexico, USA 8-14.3.1993. Abstract In *J. Cell. Biochem.* **Supplement 17C,** 306 (1993)
11. *"Structural Studies of Tautomeric Systems based on DFT ab-initio Calculated Chemical Shifts and Isotope Effects on Chemical Shifts (β-thioxoketones)"*, Abildgaard, J.; Duus, F.; Hansen, P.E. *J. Am. Chem. Soc.* (In preparation)
12. *"Deuterium Isotope Effects on ^{15}N, ^{13}C and ^{1}H Chemical Shifts of Proton Sponges"*, Grech, E.; Kliemkiewicz, J.; Nowicka-Scheibe, J.; Pietrzak, M.; Stefaniak, L.; Bolvig, S.; Abildgaard J.; Hansen, P. E. *J. Am. Chem. Soc.* (In preparation)
13. *"Amide Deuterium Isotope Effects on Chemical Shifts in Proteins"*, Abildgaard, J.; Hansen, P. E.; Hansen, Aa. E.; Wang, A.; Bax, A. *J. Am. Chem. Soc.* (In preparation), *"Chemical Shifts as Probe for Geometric and Electronic Structure in Proteins"*, Abildgaard, J; Hansen, P. E.; Hansen, Aa. E., poster at "International Conference on Magnetic Resonance in Biological Systems" (ICMRBS), Veldhoven, Holland, 14-19.8 (1994), *"Correlation between ^{1}H Chemical Shifts and Electrostatic Properties from ab-initio and Semi-Empirical Molecular Orbital Calculations"*, Abildgaard, J.; Hansen, P. E.; Hansen, Aa. E., poster at 36th Experimental Nuclear Magnetic Resonance Conference (ENC), Boston, Massachusetts, USA, 26-30.3 (1995)
14. Foresman, J. B.; Frisch, Æ. Exploring Chemistry with Electronic Structure Methods; Gaussian, Inc.: Pittsburgh, PA (1996)
15. Augspurger, J. D.; Pearson, J. G.; Oldfield, E.; Dykstra, C. E.; Park K. D.; Schwartz, D. *J. Mag. Res.* **100**, 342 (1992)
16. Pearson, J. G.; Oldfield, E.; Lee, F. S..; Warshel, A. *J. Am. Chem. Soc.* **115**, 6851 (1992)
17. de Dios, A. C.; Oldfield, E. *Chem. Phys. Lett.* **205**, 108 (1993)
18. Oldfield, E.; de Dios, A. C.; Pearson, J. G. *Abs. Papers. Am. Chem. Soc.* **205**, 36 (1993)
19. Oldfield, E.; de Dios, A. C.; Pearson, J. G. *Abs. Papers. Am. Chem. Soc.* **206**, 256 (1993)
20. de Dios, A. C.; Pearson, J. G.; Oldfield, E. *Science.* **260**, 1491 (1993)
21. de Dios, A. C.; Pearson, J. G.; Oldfield, E. *J. Am. Chem. Soc.* **115**, 9768 (1993)
22. Augspurger, J. D.; Dykstra, C. E.; *J. Am. Chem. Soc.* **115**, 12016 (1993)
23. Augspurger, J. D.; de Dios, A. C.; Oldfield, E.; Dykstra, C. E.; *Chem. Phys. Lett.*

213, 211 (1993)
24. Laws, D. D.; DeDios, A. C.; Oldfield, E. *J. Biomol. NMR.* **3**, 607 (1993)
25. de Dios, A. C.; Oldfield, E. *J. Am. Chem. Soc.* **116**, 5307 (1994)
26. de Dios, A. C.; Oldfield, E. *J. Am. Chem. Soc.* **116**, 7453 (1994)
27. de Dios, A. C.; Laws, D. D.; Oldfield, E. *J. Am. Chem. Soc.* **116**, 7784 (1994)
28. de Dios, A. C.; Oldfield, E. *J. Am. Chem. Soc.* **116**, 11485 (1994)
29. Oldfield, E. *Abs. Papers. Am. Chem. Soc.* **208**, 146 (1994)
30. Le, H.; Oldfield, E. *J. Biomol. NMR*, **4**, 341 (1994)
31. Le, H.; Pearson, J. G.; de Dios, A. C.; Oldfield, E. *J. Am. Chem. Soc.* **117**, 3800 (1995)
32. Pearson, J. G.; Wang, J.-F.; Markley, J. L.; Le, H.; Oldfield, E. *J. Am. Chem. Soc.* **117**, 8823 (1995)
33. Laws, D. D.; Le, H.; de Dios, A. C.; Havlin, R. H.; Oldfield, E. *J. Am. Chem. Soc.* **117**, 9542 (1995)
34. Oldfield, E. *J. Biomol. NMR*, **5**, 217 (1995)
35. de Dios, A. C.; Oldfield, E. *Solid state NMR*, **6**, 101 (1996)
36. Feeney, J.; McCormick, J. E.; Bauer, C. J.; Birdsall, B.; Moody, C. M.; Starkmann, B. A.; Young, D. W.; Francis, P.; Havlin, R. H.; Arnold, W. D.; Oldfield, E. *J. Am. Chem. Soc.* **118**, 8700 (1996)
37. Le, H.; Oldfield, E. *J. Phys. Chem.* **100**, 16423 (1996)
38. Havlin; R. H.; Le; H.; Laws; D. D.; deDios; A. C.; Oldfield; E.; *J. Am. Chem. Soc.* **119**, 11951 (1997)
39. Pearson; J. G.; Le; H.; Sanders; L. K.; Godbout; N.; Havlin; R. H.; Oldfield; E.;; *J. Am. Chem. Soc.* **119**, 11941 (1997)
40. Heller; J.; Laws; D. D.; Tomaselli; M.; King; D. S.; Wemmer; D. E.; Pines; A.; Havlin; R. H.; Oldfield; E. *J. Am. Chem. Soc.* **119**, 7827 (1997)
41. Pearson, J. G.; Le, H.; Sanders, L. K.; Godbout, N.; Havlin, R. H.; Oldfield, E. *J. Am. Chem. Soc.* **119**, 11941 (1997)
42. Pearson, J. G.; Montez, B.; Le, H.; Oldfield, E.; Chien, E. Y. T.; Sligar, S. G.; *Biochem.* **36**, 3590 (1997)
43. McMahon, M. T.; deDios, A. C.; Godbout, N.; Salzmann, R.; Laws, D. D.; Le, H.; Havlin, R. H.; Oldfield, E. *J. Am. Chem. Soc.* **120**, 4784 (1998)
44. Hansen, P. E.; Langgaard, M.; Bolvig, S. *Polish J Chem.* **72**, 269 (1998)
45. Wilkens; S. J.; Xia; B.; Volkman; B. F.; Weinhold; F.; Markley; J. L.; Westler; W. M. *J. Phys. Chem. B,* **102**, 8300 (1998)
46. Xia; B.; Wilkens; S. J.; Westler; W. M.; Markley; J. L. *J. Am. Chem. Soc.* **120**, 4893 (1998)
47. Burant, J. C.; Strain, M. C.; Scuseria, G. E.; Frisch, M. J. *Chem. Phys. Lett.* **248**, 43 (1996)
48. Burant, J. C.; Strain, M. C.; Scuseria, G. E.; Frisch, M. J. *Chem. Phys. Lett.,* **258**, 45 (1996)
49. Lee, T.-S.; York, D. M.; Yang, W. *American Institute of Physics* **105**, 2744 (1996)
50. Perez-Jorda, J. M.; Yang, W. *J. Chem. Phys.* **104**, 8003 (1996)
51. Strain, M. C.; Scuseria G. E.; Frisch, M. J. *Science,* **271**, 51 (1996)
52. Challacombe, M.; Schwegler E.; Almlof, J. in Computational Chemistry: Review of Current Trends, Ed. J. Leczsynski *World Scientific* (1996)
53. Challacombe, M.; Schwegler, E. *J. Chem. Phys.* **105**, 4685 (1996)
54. White C. A.; Head-Gordon, M. *American Institute of Physics,* **105**, 5061 (1996)

55. White, C. A.; Head-Gordon, M. *J. Chem. Phys.* **104**, 2620 (1996)
56. Kutteh, R.; Apra E.; Nichols, J. *Chem. Phys. Lett.* **238**, 173 (1995)
57. Perez-Jorda, J. M.; Yang, W. Chem. Phys. Lett. 247, 484 (1995).
58. L. Greengard, *Science,* **265**, 909 (1994)
59. Petersen, H. G.; Soelvason, D.; Perram, J. W. *J. Chem. Phys.* **101**, 8870 (1994)
60. Greengard, L. MIT Press: Cambridge, MA, (1988)
61. Greengard, L.; Rokhlin, V. *J. Comput. Phys.* **73**, 325 (1987)
62. Dapprich, S.; Komaromi, I.; Byun, K. S.; Morokuma, K.; Frisch, M. J. *Theo. Chem. Act.* , in prep. (1998)
63. Svensson, M.; Humbel, S.; Froese, R. D. J.; Matsubara, T.; Sieber S.; Morokuma, K. *J. Phys. Chem.* **100**, 19357 (1996)
64. Humbel, S.; Sieber, S.; Morokuma, K. *J. Chem. Phys.* **105**, 1959 (1996).
65. Maseras, F; Morokuma, K. *J. Comp. Chem.* **16**, 1170 (1995)

Quantum Mechanical Model Calculations in Chemistry: Structure, Vibrations, Chemical Shifts, and Isotope Effects on Chemical Shifts.

Introduction

Models in Chemistry

The models used in chemistry are characterized by the ability to predict properties of new compounds, properties such as the molecular structure and energy, but a very exacting test for e.g. molecular orbital calculations is the ability to correctly calculate spectroscopic data.

One of the early models in chemistry, the valence bond theory surprisingly well predicts the structure of molecules despite the simple set of empirically derived rules on which it is based (see e.g. Figure 1).

This illustrates one of several aspects of chemical models. A model does not have to be universally correct and cover all systems to be of importance in the solution of chemical problems within a well defined field of chemistry.

The higher precision molecular orbital methods offer a quantitative and more detailed understanding of intramolecular phenomena as e.g. the vibrational explanation of isotope effects discussed at the end of this paper. On the other hand, the partial "black box" nature of the molecular orbital calculations in general reduces the intuitive understanding present in more simple models.

The comparison between experimental and calculated data is of central importance in all fields of science where models are used. The present paper gives an overview of semiempirical and *ab initio* calculations applied to a series of related problems; determining molecular geometry, calculating vibrational frequencies, nuclear shieldings (chemical shifts), and deuterium isotope effects on chemical shifts.

Despite the complex and involved computations, semiempirical and *ab initio* methods are now widely available. In most offices within the chemical scientific community, computers are present, that can perform calculations yielding precise information about real chemical problems, and in many cases solve specific ones.

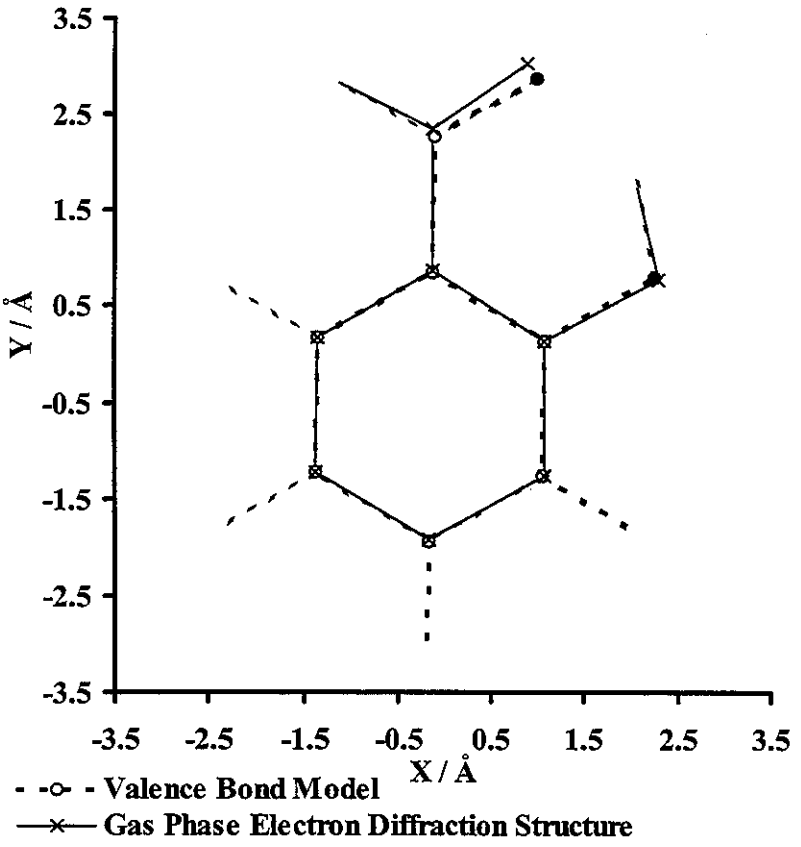

Figure 1. Comparison of salicylaldehyde molecular geometries obtained from the valence bond model * and from the experimental gas phase electron diffraction structure solution (table 1a) [45]. * (the bond lengths (R_{XY}=½R_{XX}+½R_{YY}) and angles (sp^2=120° and sp^3=109°) are in the gaussian input file in Appendix)

Today the quality of *ab initio* calculated IR [1-4] and NMR [5-11] spectroscopic data in moderate basis sets are of a quality that allows IR resonance's to be assigned to individual vibrational modes [1, 2], and the predictive power of calculated NMR nuclear shieldings (chemical shifts) is in our experience such that assignments may be made from the calculated values and misassignments are often revealed when comparing calculated and experimental NMR data [3].

Hydrogen-deuterium isotope effects on NMR chemical shifts, especially on ^{13}C NMR chemical shifts, have been investigated in detail and show large variations in *o*-hydroxy acyl aromatics with intramolecular hydrogen bonds upon substitution of the O-H hydroxy hydrogen with deuterium [4,12-24]. The results show a number of regularities relating deuterium isotope effects of *o*-hydroxy acetophenones to those of salicylaldehyde and *o*-hydroxy benzoic esters [17]. Deuterium isotope effects of intramolecularly hydrogen bonded systems are related to parameters like the oxygen-

oxygen ($R_{O...O}$) distances [5] and therefore among other things probe hydrogen bond strength [5, 12-26].

In order to dissect the interesting experimental trends of deuterium isotope effects on chemical shifts, theoretical calculations provide the testing ground for new ideas about the physical interpretation.

Aim and perspective

In the following an evaluation of the precision in predicting experimentally determined structures and spectroscopic data will be made of a selection of quantum mechanical models. The chemical system chosen is that of the intramolecularly hydrogen bonded *o*-hydroxy-acyl-aromatics and the example is salicylaldehyde (see Figure 1).

Calculation of molecular geometries and energies are clearly central points in the evaluation of the quality of theoretical calculations. Furthermore, the vibrational frequencies are calculated based on force constants, which are the second derivatives of the electronic energy with respect to atomic coordinate displacements. This means that the force constants can only be evaluated and used for the calculations of vibrational modes at the energy minimum nuclear configuration. The isotope effects on nuclear shielding depend on the first derivative of the nuclear shielding with respect to changes in bond length and bond angle (see later). A prerequisite for the calculation of these derivatives is a realistic calculation of the nuclear shieldings themselves.

It is not obvious that the calculated values for widely different parameters like molecular geometry, IR-frequencies, and NMR nuclear shieldings are calculated equally well by the same method. Furthermore, systematic errors in the calculated geometry may be compensated for by systematic errors in the calculation of spectral properties. Such example is seen for the AM1 calculations of IR frequencies (see later). The main objective here is to find a molecular orbital method that generates good results for all the spectroscopic properties mentioned above with due consideration of the computational effort involved.

Molecular orbital methods

The models tested are the well known semiempirical methods: AM1 [25], PM3 [26], CNDO [27], MNDO [28], MINDO3 [29], INDO [30], and the ab-initio methods: Restricted Hartree-Fock

(RHF) [31] also including Møller-Plesset second order electron correlation (MP2) [32] and various old and new Density Functional Theory (DFT) [33-38] methods. With the best of the DFT methods we have also tested a range of small basis sets. The intention is to make this investigation help in the selection between quantum mechanical methods, taking into account the resources, the magnitude of the problem, and the precision necessary for the solution of the problem at hand. Molecular mechanics methods routinely used to solve and refine structures of macromolecules like proteins [39] will not be dealt with. Excluded are also electron correlation methods above DFT and MP2.

The higher order electron correlation methods like Complete Active Space (CAS) [40], Configuration Interaction (CI) [41], Quadratic Configuration Interaction (QCI) [42], Coupled Cluster (CC) [43], and Full Configuration Interaction (Full CI) are all methods that require so much computational power that the majority of molecules relevant to physicists, organic and inorganic chemists are out of range. Likewise, in this work the calculations are not tested in the large basis sets normally used with high precision methods, like the higher order electron correlated methods, or typically used when calculating molecules with atoms from the third period and beyond.

Our choice of methods is motivated by a wish to present useful techniques to the practicing chemists. The DFT methods are so reliable that they compete favorably with more elaborate and expensive methods like MP2, and in most cases also with methods like CAS, CI, QCI, and CC. The improvements gained by using basis sets larger than the important and much used split-valence double-zeta gaussian type basis set 6-31G(d) with polarization functions of higher angular momentum than the valence shell on atoms in second period and higher, are generally expected to be small.

Bibliographic survey

In an attempt to describe the development of the use of molecular orbital calculations in chemistry over the last thirty years, we use the Chemical Abstracts Service (CAS) data base. The search terms "quantum", "orbital", "semiempirical" or "*ab-initio*" produce the data presented in the figure, which are numbers of hits in percentage of the total number of papers, books, and patent abstracts in CAS published in the respective years.

This is not an exhaustive investigation of the extent or importance of molecular orbital calculations in chemistry. For example no distinction is made between purely theoretical papers and papers in which theoretical models are used to solve practical chemical problems, and the mesh is maybe too fine, as the search terms could possibly have been used in a different context than the one discussed in this paper.

Despite the shortcomings, the data in the figure can be taken as evidence for a substantial increase in the relative number of papers dealing with molecular orbital calculations. In the period 1981-89 an almost linear increase of 0.08 % per year is seen, and over a period of 16 years from 1981-97 the number has grown exponentially leading to approximately 3.3% of the total 716564 abstracts in CAS 1997. The uncertainty however in this exponential trend is too large to safely allow prediction for the years to come.

The increase naturally coincides with the period in which computers have become ever faster, easier to operate, more common, and less expensive. The use of experimentally verifiable chemical models by definition and by its very nature, goes back as far as the historical records document the presence of a scientific chemistry discipline.

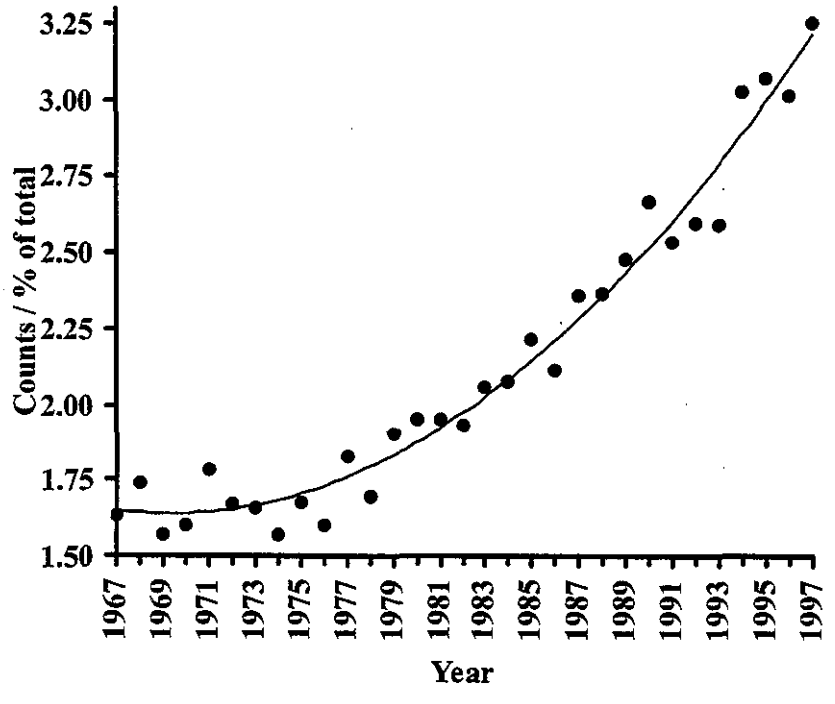

Figure: Number of papers, books, and patents found in Chemical Abstracts Services (CAS) database, searching the following words: "quantum", "orbital", "semiempiri-cal", or "ab-initio" in the title, the abstract, or in the index terms. The number of hits are shown as percentage of all abstracts in CAS for the years 1967 to 1997.

Experimental

The program

The program used is Gaussian94, [44] a program easily available at a reasonable price for academic institutions and a program that supports most computer platforms from PC´s to the most advanced parallel and vector processors. Gaussian94 is also an easily implemented package that includes the highest number of published molecular orbital models. Our experience tells us that the distributor furthermore is fast in implementing improvements and correcting errors, as these never fail to appear. Gaussian94 is a somewhat old fashioned FORTRAN type program with extensive output files containing loads of information and with few direct interfaces to programs for visualization of the results. This one drawback is likely to be remedied in the new integrated WINDOWS based GaussView program, also from Gaussian Inc. One very important advantage of Gaussian94 is the generally effective algorithms, especially the very efficient default geometry optimization routine.

Gaussian98 was released in the fall of 1998. For an outlay of the input files used in this work see Appendix.

Computers

The CPU times are included as the important parameter in weighing precision and computational resources between different methods. All calculations are done on the same type of computer executing one job at the time only. The calculations were done on an IBM SP2 R6000 with 133MHz 595-CPUs "wide-node" (256 bit data bus), no level2 cache and 2Gb of main memory. In our experience all of these calculations could also have been done on 200-450 MHz PC´s with 0.5-1 Mb level2 cache, the latter having a large effect on performance.

For the comparison of CPU times with other programs or computers, it is important to take into account the size of memory available and actually utilized by the program in every step of the specific calculation.

Salicylaldehyde

Salicylaldehyde (2-hydroxybenzaldehyde) was chosen as an example for several reasons, the most important being the available experimental structural and spectroscopic data. Recently an experimental gas phase electron diffraction structure

has been published [45]. This shows that the molecule is planar leaving no doubt about the main structural features. The hydrogen bond is of the medium to weak intramolecularly bonded type and a precise description of the hydrogen bond geometry is of the utmost importance. The hydrogen bond perturbs the spectroscopic data and is diagnostic of the precision of the molecular geometry and electronic structure.

Infra Red absorption data are given in refeferences 4, 46, and 47 for both O-H- and O-D-species. Assignments of ^{1}H and ^{13}C NMR spectra are at hand from standard literature [48] and deuterium isotope effects on ^{13}C chemical shifts [12, 13, 17] as well as primary isotope effects [49] have also been measured for salicylaldehyde.

Models

The calculations comprise of a series of closed-shell semiempirical and *ab initio* calculations. For the best of the latter (B3PW91, see later) the basis set has also been varied, testing all basis sets lower than 6-31G(d) and available with the distributed program [44].

The semiempirical methods are: CNDO [27], INDO [30], MNDO [28], MINDO [29], AM1 [25], and PM3 [26].

The classical *ab initio* method is RHF [31], in which the exchange term is either alone or combined with the second order electron correlation post HF-method MP2=FULL (MP2) [32]. The DFT *ab initio* methods can likewise be divided into two groups: the first, with the exchange term alone (the exchange term may either be Slater Local Spin Density exchange [33] (S), or Beckes exchange 1988 which includes the Slater exchange term combined with a correction for the electron density gradient [34] (B)), or combined with an electron correlation functional like Perdew electron correlation term Local (non-gradient corrected, (PL)) [35], Perdew and Wangs 1991 gradient corrected correlation functional (PW91) [36], or the Vosko-Wilk-Nussair correlation functional (also called Local Spin Density, (VWN5)) [37]. A more elaborate scheme is the important RHF/DFT 3-parameter hybrid functional [38] (B3PW91), in which the energy is calculated as a combination of the RHF and BPW91 functionals.

To sum up, the *ab initio* methods, mostly chosen to provide variation and to lead up to B3PW91, are: RHF, MP2, S, SVWN5, B, BPL, BPW91, B3PW91 all using the gaussian split-valence double-zeta basis set 6-31G(d) [50] with d-polarization functions on non-hydrogen atoms of salicylaldehyde. We refer to these as ab-initio methods in the Figures.

Table 1a. Experimental molecular geometry [45], IR frequencies [47,*], Chemical Shifts [48] and Isotope effects [12, 14, 17 ****]

Atomic Coordinates / Å			**Chemical Shift / ppm**		**IR Frequencies / cm^{-1}**	
	X	**Y**		**^{13}C**	**Symmetry*** **	**ν**
C1	0.000000	0.000000	**C1**	120.3	A'	275
C2	-1.418000	0.000000	**C2**	160.9	A'	410
C3	-2.139012	1.204723	**C3**	117.0	A'	455
C4	-1.438305	2.408658	**C4**	136.5	A'	565
C5	-0.036666	2.440466	**C5**	119.5	A'	660
C6	0.664627	1.240346	**C6**	133.4	A'	767
C7	0.761716	-1.247891	**C7**	196.2	A'	875
O8	0.247887	-2.359919	**O8**		A'	1030
O9	-2.117443	-1.168684	**O9**	**^{1}H**	A'	1110
H10 (H-CO)	1.867659	-1.153078	**H10**	9.91	A'	1145
H11 (O-H)	-1.429504	-1.873642	**H11**	11.03	A'	1207
H12 (C-H)	-3.221878	1.187712	**H12**	7.00	A'	1235
H13 (C-H)	-1.980007	3.354522	**H13**	7.52	A'	1324
H14 (C-H)	0.486778	3.396555	**H14**	7.02	A'	1350
H15 (C-H)	1.754612	1.246053	**H15**	7.58	A'	1386
					A'	1416
Bond length / Å			**Bond Angle / deg.**		A'	1460
C1-C2	1.4180		C1-C2-C3	120.9	A'	1487
C1-C6	1.4072		C1-C2-O9	120.9	A'	1591
C1-C7	1.4620		C1-C6-C5	121.5	A'	1622
C2-C3	1.4040		C1-C7-H10	116.5	A'	1682
C2-O9	1.3620		C1-C7-O8	123.8	A'	2850
C3-C4	1.3930		C2-C1-C6	118.2	A'	3040
C4-C5	1.4020		C2-C1-C7	121.4	A'	3089
C5-C6	1.3900		C2-C3-C4	118.9	A'	3120
C7-O8	1.2250		C2-O9-H11	104.8	A'	***3145*
C7-H10	1.1100		C3-C2-O9	118.2	A'	3200
O8-H11	1.7465		C3-C4-C5	121.5	A"	***149*
O9-H11	0.9850		C4-C5-C6	119.0	A"	225
C3-H12	1.0830		C6-C1-C7	120.4	A"	299
C4-H13	1.09		C7-O8-H11	98.6	A"	435
C5-H14	1.09		O8-C7-H10	119.7	A"	540
C6-H15	1.09		O8-H11-	150.5	A"	712
			C1-C6-H15	118.5	A"	750
Isotope Effects ** / ppm**			C2-C3-H12	120.0	A"	798
	$^{n}\Delta^{13}$C(OD)		C3-C4-H13	120.0	A"	855
C1	0.037		C4-C5-H14	120.0	A"	890
C2	0.228		C4-C3-H12	121.1	A"	940
C3	0.092		C5-C4-H13	118.5	A"	1010
C4	0.016		C5-C6-H15	120.0		
C5	-0.017		C6-C5-H14	121.0		
C6	-0.017					
C7	0.045					

* Gas phase signals at 260, 355, 399, 442, 600, 668, 700, 757, 883, 1020, 1175, 1197, 1290, 1339, 1450, 1471, 1488, 1705, and 2840 cm^{-1} have been omitted.

** Signal at 149 cm^{-1} is taken from RAMAN data, [46] and signal at 3145 cm^{-1} from pure liquid data.

*** Assignment based on B3PW91/6-31G(d) normal mode analysis (table 1b) and used only for correlation with this method.

**** Remeasured for present work.

Table 1b. B3PW91/6-31G(d) Calculated Structural and Spectroscopic data.

Atomic Coordinates / Å

	X	Y
C1	0.000000	0.644988
C2	-0.489130	-0.687570
C3	0.424007	-1.751430
C4	1.785784	-1.490920
C5	2.282470	-0.177610
C6	1.387541	0.876357
C7	-0.930100	1.757362
O8	-2.157030	1.639538
O9	-1.796870	-0.955900
H10 (H-CO)	-0.480930	2.770114
H11 (O-H)	-2.269030	-0.082980
H12 (C-H)	0.038363	-2.766200
H13 (C-H)	2.482315	-2.325870
H14 (C-H)	3.352839	0.003774
H15 (C-H)	1.744170	1.904983

Bond length / Å

C1-C2	1.4195
C1-C6	1.4067
C1-C7	1.4500
C2-C3	1.4020
C2-O9	1.3350
C3-C4	1.3865
C4-C5	1.4041
C5-C6	1.3827
C7-O8	1.2326
C7-H10	1.1079
O8-H11	1.7262
O9-H11	0.9924
C3-H12	1.0856
C4-H13	1.0873
C5-H14	1.0856
C6-H15	1.0887

Nuclear Shielding Gradients ($d\sigma^{13}C/dR_{O-H}$) / ppm Å^{-1}

	Bond direct. O-H stretch	Norm. mode O-H stretch
C1	5.4	6.2
C2	-25.3	-23.5
C3	-1.6	-2.9
C4	-2.3	-2.2
C5	5.5	5.5
C6	-0.2	0.4
C7	-2.4	0.5

Nuclear Shielding / ppm

	^{13}C
C1	79.0
C2	36.0
C3	80.4
C4	62.0
C5	80.5
C6	64.4
C7	5.6
O8	
O9	^{1}H
H10	22.36
H11	20.97
H12	25.32
H13	24.71
H14	25.33
H15	24.90

Bond Angle / deg.

C1-C2-C3	119.2
C1-C2-O9	121.8
C1-C6-C5	120.9
C1-C7-H10	116.2
C1-C7-O8	124.4
C2-C1-C6	119.6
C2-C1-C7	119.9
C2-C3-C4	119.8
C2-O9-H11	106.8
C3-C2-O9	119.0
C3-C4-C5	121.5
C4-C5-C6	118.9
C6-C1-C7	120.4
C7-O8-H11	99.2
O8-C7-H10	119.4
O8-H11-O9	147.9
C1-C6-H15	118.6
C2-C3-H12	118.6
C3-C4-H13	119.0
C4-C5-H14	120.3
C4-C3-H12	121.6
C5-C4-H13	119.4
C5-C6-H15	120.5
C6-C5-H14	120.7

IR Frequencies / cm^{-1}

Symmetry	υ
A'	285
A'	420
A'	469
A'	570
A'	677
A'	789
A'	895
A'	1061
A'	1150
A'	1187
A'	1239
A'	1273
A'	1354
A'	1396
A'	1428
A'	1454
A'	1515
A'	1544
A'	1649
A'	1691
A'	1751
A'	2982
A'	3188
A'	3203
A'	3226
A'	3233
A'	3323
A"	145
A"	215
A"	308
A"	438
A"	546
A"	732
A"	771
A"	827
A"	875
A"	953
A"	994
A"	1025

Basis set variation

The following basis sets are tested with the B3PW91 method: STO-3G, 3-21G, 4-21G, 4-21G(d), 4-21G(d, p), 4-31G, 4-31G(d), 4-31G(d, p), 6-21G, 6-21G(d), 6-31G, and 6-31G(d). The selection of methods and basis sets are in no way complete, but provide a good variation. B3PW91 was chosen to illustrate the basis set variation, as it has been shown to be the best DFT method in this, and in a number of other studies, both for IR [51-53] and for NMR data [11, 54]. The 6-31G(d) basis set is far from the Hartree Fock limit (the used atomic basis sets are optimized using the RHF method), but is a well balanced and commonly used basis set for organic molecules of the size of salicylaldehyde.

Results and discussion

Electronic energy

The electronic energy of differently optimized geometries are calculated using B3PW91/6-31G(d) single point energy calculations. For salicylaldehyde structures optimized with smaller basis sets, the B3PW91/basis set energies were always higher than the single point B3PW91/6-31G(d) calculation using this geometry. From Figure 5 it can be seen that the quality of the structure of the PM3 method is by far the best compared to the calculation time, and that the B3PW91/6-31G(d) energy of the PM3 geometry is comparable to those obtained with ab-initio methods. A word of caution is probably relevant at this point, as salicylaldehyde or similar structures could be included in the set of molecules that form the basis for the parameterization of the PM3 method [26].

Table 2. B3PW91 Calculated Electronic Energy of Salicylaldehyde Structures / a.u.

Geometry Optimization Method / Basis set	B3PW91/6-31G(d)	B3PW91/Basis Set
B3PW91/6-31G(d)	**-420.6418**	**-420.6418**
B3PW91/4-31G(d)	-420.6417	-420.2364
B3PW91/4-31G(d,p)	-420.6417	-420.2504
B3PW91/4-21G(d,p)	-420.6413	-419.9438
MP2=FULL/6-31G(d)	-420.6413	
B3PW91/6-21G(d)	-420.6408	-420.3083
B3PW91/4-21G(d)	-420.6408	-419.9277
BPW/6-31G(d)	-420.6405	
B3PW91/4-31G	-420.6402	-420.0890
SVWN5/6-31G(d)	-420.6398	
B3PW91/6-31G	-420.6397	-420.5270
PM3	-420.6393	
BPL/6-31G(d)	-420.6392	
B3PW91/3-21G	-420.6391	-418.3287
B3PW91/4-21G	-420.6389	-419.7551
B3PW91/6-21G	-420.6388	-420.1641
RHF/6-31G(d)	-420.6380	
AM1	-420.6373	
S/6-31G(d)	-420.6360	
CNDO	-420.6322	
B/6-31G(d)	-420.6306	
MNDO	-420.6297	
INDO	-420.6279	
B3PW91/STO-3G	-420.6276	-415.2936
MINDO3	-420.6218	

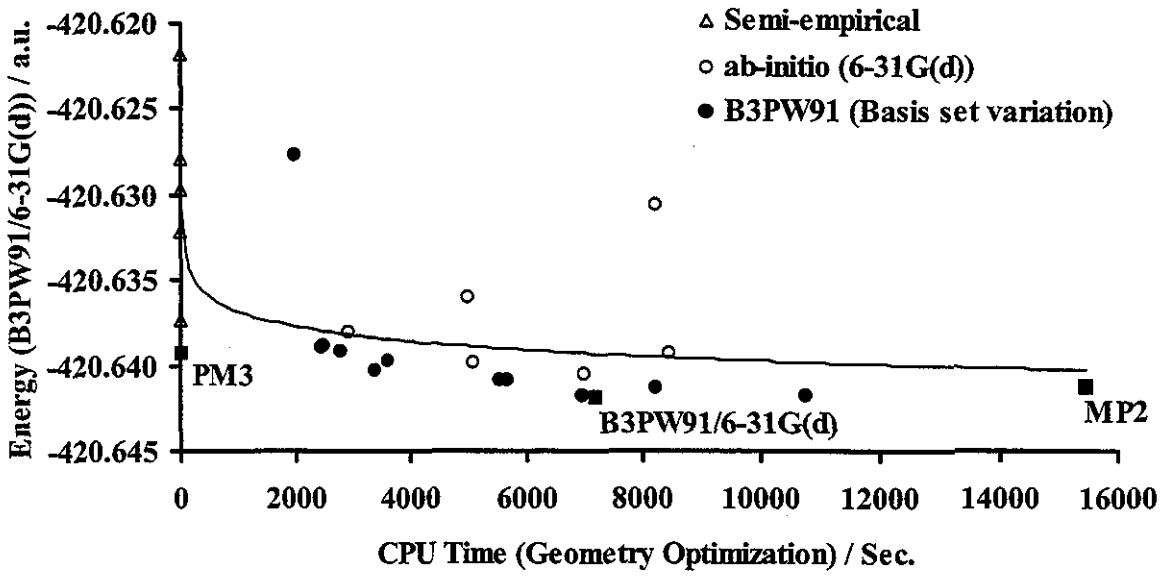

Figure 2. B3W91/6-31G(d) electronic energies of differently optimized salicylaldehyde geometries plotted vs. CPU time, the data are in Table 2.

Molecular geometry

The precision of the experimentally determined gas phase electron diffraction structure [45] is not as good as often found in low temperature single crystal x-ray studies, but is on the other hand not affected by crystal packing. In the gas phase structure the geometrical data for the aldehyde and hydroxy protons are realistic, which is not always the case for low resolution x-ray structures [55]. As mentioned, the experimental structure is planar within the experimental uncertainty. The bond lengths and bond angles transformed into the set of atomic coordinates used in the comparison with the calculated structures (Table 1).

All geometry optimizations used the same starting input parameters. Bond lengths: C-C 1.4 Å, C-O 1.35 Å, C=O 1.25 Å, C-H 1.1 Å, and O-H 1.0 Å, sp2 hybridized carbons and oxygen have bond angles of 120°, and the sp^3 hybridized hydroxy oxygen has a C-O-H angle of 109°, which is also the valence bond parameters in Figure 1. All geometry optimizations are done by the Gaussian94 program using analytical gradients of the energy with respect to atomic coordinates.

The calculated structures all turned out to be planar as the IR calculations did not have imaginary frequency values or in other words gave no negative force constants in the normal mode analysis.

Table 3. Molecular Geometry RMSD between Corresponding Atoms of Calculated and Superimposed Experimental Structure [45] / Å.

Geometry Optimization Method / basis set	CPU Time / sec.	All Atoms	H only	C and O only
B3PW91/6-31G(d)	7194	0.0066	0.0060	0.0102
B3PW91/4-31G(d)	6968	0.0078	0.0082	0.0100
B3PW91/4-31G(dp)	10785	0.0114	0.0124	0.0095
BPW/6-31G(d)	7003	0.0121	0.0092	0.0117
BPL/6-31G(d)	8453	0.0144	0.0089	0.0161
MP2/6-31G(d)	15469	0.0163	0.0068	0.0185
B3PW91/4-21G(dp)	8215	0.0190	0.0198	0.0137
B/6-31G(d)	8220	0.0211	0.0165	0.0170
B3PW91/4-31G	3383	0.0213	0.0147	0.0222
B3PW91/6-31G	3603	0.0227	0.0115	0.0266
B3PW91/6-21G(d)	5685	0.0233	0.0209	0.0216
B3PW91/4-21G(d)	5550	0.0235	0.0212	0.0218
S/6-31G(d)	4976	0.0240	0.0170	0.0196
PM3	14	0.0274	0.0103	0.0338
HF/6-31G(d)	2899	0.0281	0.0114	0.0286
B3PW91/6-21G	2475	0.0287	0.0270	0.0233
B3PW91/4-21G	2453	0.0292	0.0277	0.0235
B3PW91/3-21G	2762	0.0305	0.0292	0.0245
SVWN5	5096	0.0325	0.0301	0.0277
AM1	15	0.0625	0.0330	0.0763
CNDO	5	0.0632	0.0560	0.0560
B3PW91/STO-3G	1987	0.0730	0.0468	0.0797
INDO	7	0.0901	0.0808	0.0770
MNDO	16	0.1137	0.0771	0.1292
MINDO3	16	0.1396	0.1043	0.1515

The correlation between experimental and calculated structures were done by translation and rotation of the calculated structures to minimize the sum of distances between corresponding heavy atom coordinates including also the formyl and the hydroxy hydrogen. Figure 3 shows the experimental geometry and the projection of the best of the calculated structures.

The B3PW91/6-31G(d) structure gave the smallest deviation from the experimental molecular geometry, but the PM3 structure is an attractive alternative due to the much shorter time of calculations. Figure 4 shows the standard deviation between the calculated and experimentally determined atomic coordinates for all optimized structures against the CPU time. Plots of RMSD bond lengths or bond angles yield similar pictures, so that it is not possible to conclude which of these parameters contribute most to the deviation. For calculations done with B3LYP see ref [4].

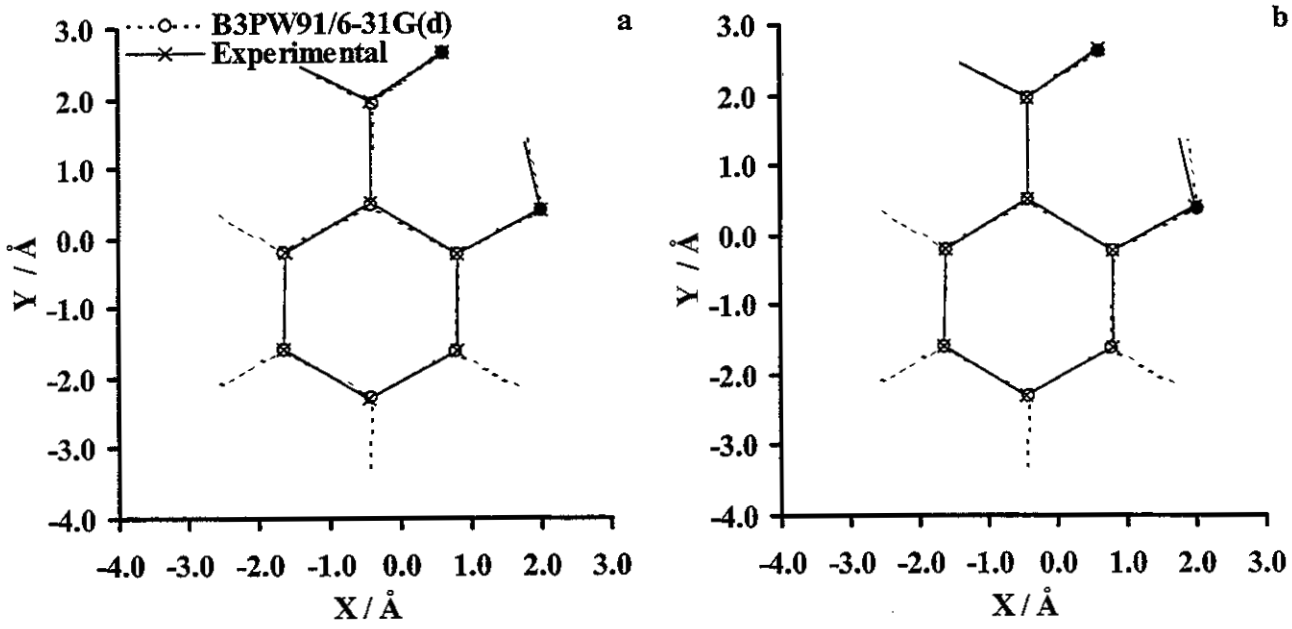

Figure 3. Projection of a) B3PW91/6-31G(d) and b) PM3 structures on the experimentally determined gas phase electron diffraction structure of salicylaldehyde [45].

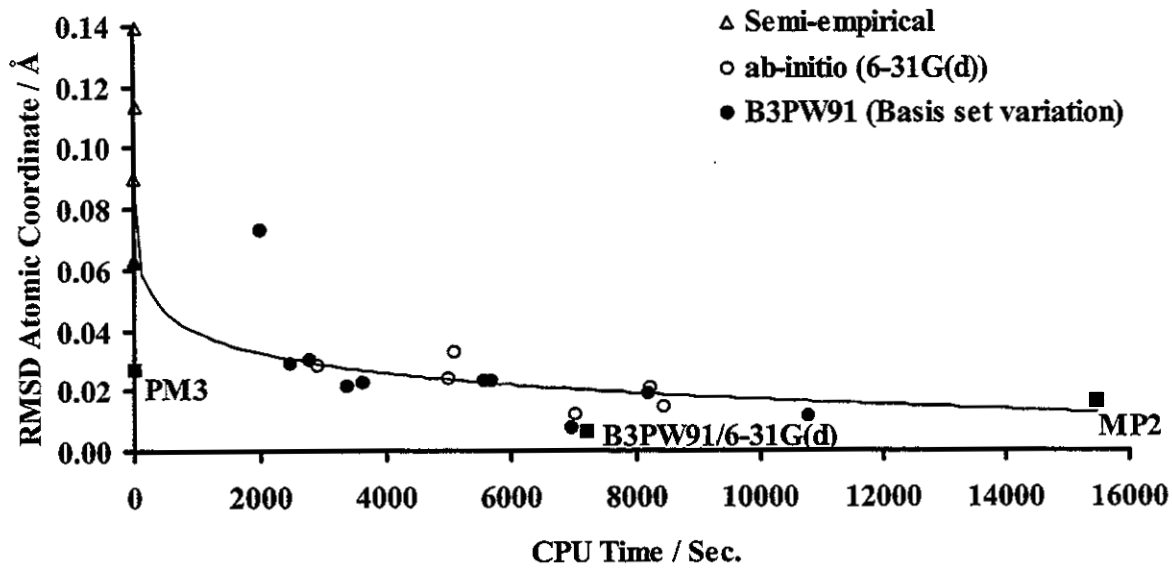

Figure 4. Standard deviations in C, O, aldehyde, and hydroxy hydrogen corresponding atomic coordinates of differently optimized salicylaldehyde geometries vs. CPU time, the data are in Table 3.

Linear Scaling

Quite often one finds a linear correlation between calculated and experimental spectroscopic data [52, 53]. For IR frequencies the scaling factor is slightly different from 1, [53] but the correlation line ideally goes through origo. Inspection of Figure 6 clearly establishes the soundness of applying linear scaling to compensate for systematic errors in calculated IR data.

In the NMR case the calculations produce nuclear shieldings (σ) . They are related to the experimental chemical shifts (δ) in the following fashion:

$$\delta = \alpha\,\sigma + \sigma_{reference}$$

The linear scaling factor α goes towards -1 for the best methods of calculation. [5,9,11] The nuclear shielding of the reference signal gives an extra parameter in the linear correlation, but the nuclear shielding of the reference compound is expected to vary more or less the same way α does with method and basis set.

No simple explanation can be given for this linearity between experimental and theoretically calculated data, or why the systematic deviation of the individual signals is proportional to the energy of the spectral transitions. However, this is often found [9, 52, 53] and also demonstrated in this paper.

Infra Red Frequencies

IR absorption signals can be assigned to transitions of different symmetry classes in symmetrical molecules by studies of oriented samples [1, 56, 57]. Furthermore, by isotope substitution localized modes can be assigned by observation of frequency ratios (see the calculation at the end of this paragraph). We were not aware of the experimental data in reference 4 when we did the comparison between the experimental and calculated IR frequencies. The gas phase IR data [46] has some additional signal, that are sorted out by comparison with the B3PW91/6-31G(d) calculation (see Table 1). This naturally biases the correlation towards this and the similar DFT methods.

IR frequency data are however in general not assigned and with the low symmetry of salicylaldehyde the possibility of comparing calculated and experimental frequencies depends to a large extent on the signals having the same order of frequencies in the experimental and calculated data, and that no interchange of the

signals occurs between the different calculations. This condition is not met, but an independent experimental vibrational mode assignment is not available, and using one of the better *ab initio* calculations for this purpose would even further bias the picture by making even better linear correlation between the experimental and calculated data of this and similar methods. Gross outliers will, in the present way of comparing the experimental and calculated values, shift the data and spoil correlation, whereas interchange of neighboring signal could artificially improve the linear regression.

The present method gives all calculated data the benefit of the doubt, though complete assignment of all IR transitions, by at least establishing the symmetry classes of the signals, would be ideal. We do however, find linear scaling factors of the various methods comparable to those in the literature [52, 53] and we find standard errors in the right order (see Figure 7 and Table 4). Therefore, we conclude that the possible problems of IR transition assignments, though serious, does not spoil the general picture, which is what we are after in the present context.

Figure 6a shows that the best agreement between experiment and calculation is found in the B3PW91/6-31-G(d) harmonic approximation frequency calculation. The best alternative is AM1 (Figure 6b). For a comparison of all methods see Figure 7. AM1 is in this case significantly better than PM3 in agreement with other reports [52]. This is very different from the calculations of energy and geometry (see previously), and from the calculation of chemical shifts (see later). The reason could be that the systematic errors in the geometries of the AM1 calculations are compensated for by systematic errors in the second derivatives of the energy with respect to changes in the atomic coordinates, or IR force constants. Another probable explanation would be gross mismatch of corresponding normal modes in the calculations.

Calculation of frequencies in the species deuteriated at the O-H position is straightforward. Ratios for those transitions perturbed, $O\text{-}H_{strecth}$, $O\text{-}H_{bend}$ and $O\text{-}H_{out\text{-}of\text{-}plane\text{-}bend}$ are close to 0.71 (inverse squareroot of ~2, see later) in B3PW91/6-31G(d) calculations (0.719 - 0.735).

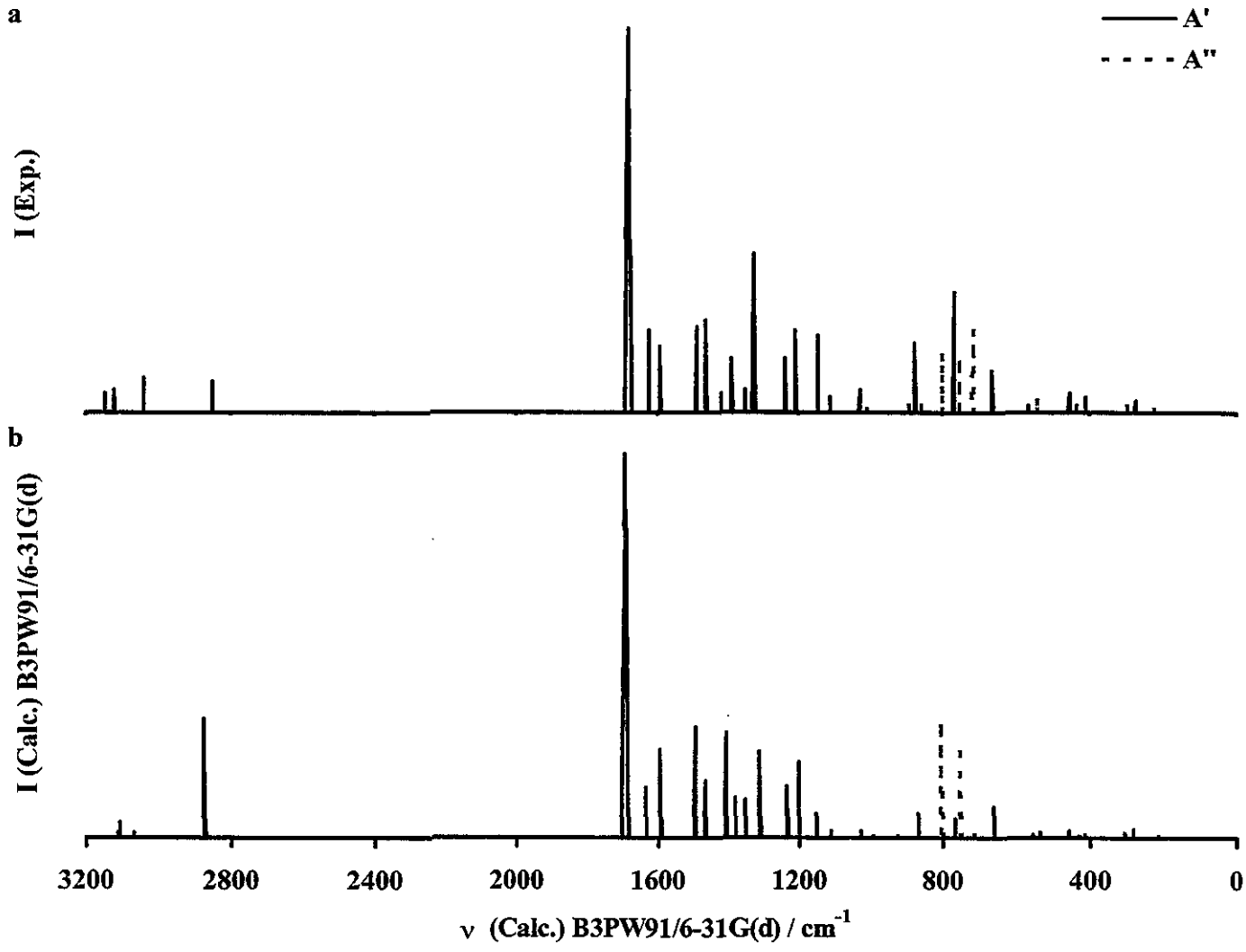

Figure 5. a) Synthetic experimental IR spectrum from data in reference 46, and b) spectrum from linearly scaled B3PW91/6-31G(d) harmonic approximation normal mode analysis calculated data (See figure 6a).

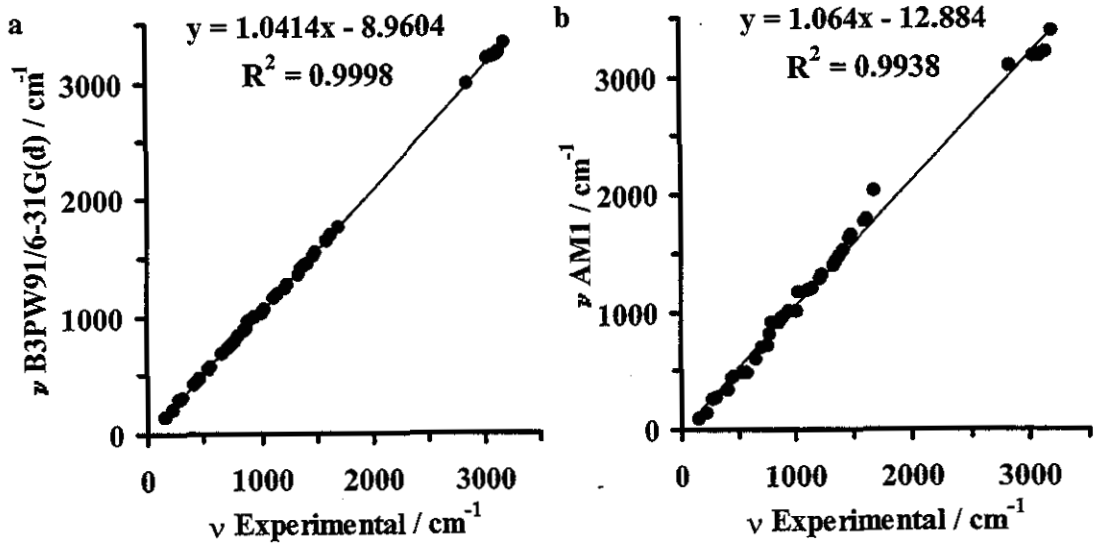

Figure 6. Calculated a) B3PW91/6-31G(d) and b) AM1 normal mode analysis calculated frequencies of salicylaldehyde vs. experimentally determined gas phase IR frequencies [4, 46,47, *].

* See footnotes to Table 1.

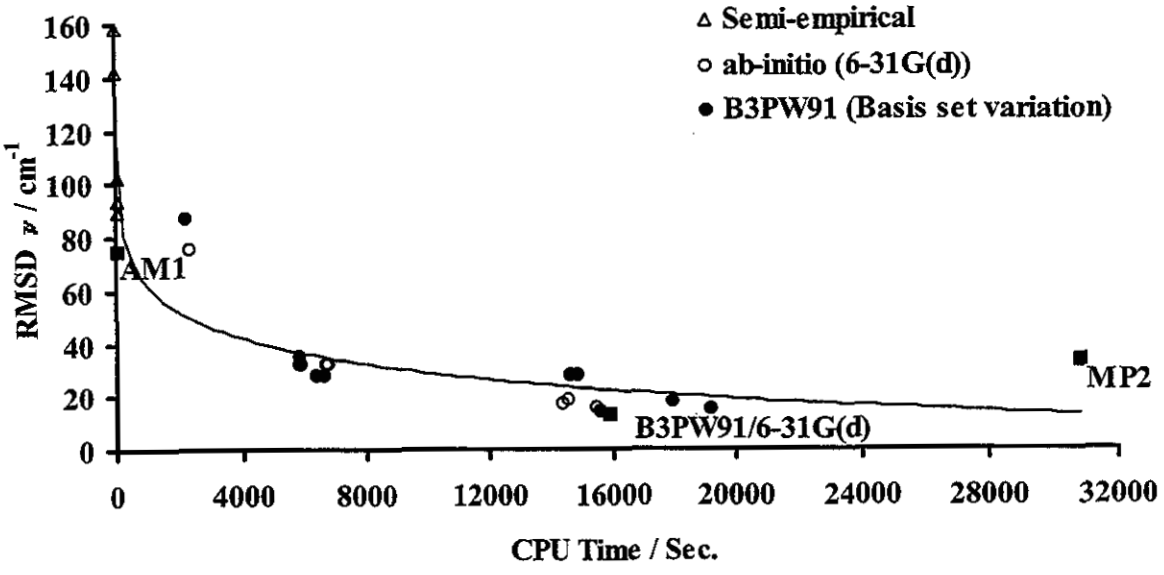

Figure 7. Standard deviations between experimental and calculated IR frequencies of salicylaldehyde vs. CPU time, the data are in Table 4.

Table 4. IR Frequency RMSD Between Calculated and Experimental Gas Phase Data / cm^{-1}

Geometry Optimization Method / basis set.	CPU time / Sec.	R-value	RMSD
B3PW91/6-31G(d)	**15910**	**0.9998**	**13.0**
B3PW91/4-31G(d)	15595	0.9998	14.4
B3PW91/4-31G(dp)	19218	0.9997	15.1
BPW/6-31G(d)	15480	0.9997	15.6
B/6-31G(d)	14390	0.9996	17.6
B3PW91/4-21G(dp)	17929	0.9996	18.2
BPL/6-31G(d)	14559	0.9996	18.5
B3PW91/4-21G(d)	14625	0.9990	28.0
B3PW91/6-31G	6599	0.9991	28.1
B3PW91/6-21G(d)	14833	0.9990	28.1
B3PW91/4-31G	6386	0.9990	28.5
B3PW91/6-21G	5878	0.9987	32.1
S/6-31G(d)	6681	0.9985	32.3
SVWN5	6727	0.9986	32.4
B3PW91/4-21G	5837	0.9987	32.8
MP2/6-31G(d)	30845	0.9988	33.2
B3PW91/3-21G	5801	0.9984	35.6
AM1	37	0.9938	75.1
HF/6-31G(d)	2334	0.9944	76.0
B3PW91/STO-3G	2203	0.9918	87.4
MINDO3	32	0.9932	89.2
MNDO	37	0.9922	93.6
PM3	38	0.9882	102.0
INDO	15	0.9897	141.9
CNDO	15	0.9879	158.3

^{1}H and ^{13}C nuclear shielding

^{1}H and ^{13}C chemical shifts are sensitive gauges of changes in molecular geometries and even small variations in chemical shifts have been used as indicators of structural changes. Especially ^{1}H chemical shifts of intramolecularly hydrogen bonded chelate protons have been used to describe hydrogen bond geometries [58].

The ^{1}H and ^{13}C nuclear shieldings are calculated using the Gauge Including Atomic Orbital (GIAO) [59] method. Other similar methods are the Localized Orbital/Local Origin (LORG) [60] and the Individual Gauge for Localized Orbitals (IGLO) [61] methods, both of which are different distributed gauge-origin variants of Coupled Hartree-Fock Theory (SCF perturbation methods) [see i.e. 62]. The three mentioned methods give comparable results [63].

It is important to notice that the present GIAO nuclear shielding calculation only is a partial DFT hybrid method [54], since it only includes the two exchange terms of the DFT hybrid functional (B3(PW91)). The correlation effects in the magnetic interaction is not included, although the method uses the fully B3PW91 converged molecular orbitals. This absence can possibly lead to systematic errors much the same way the

MP2 method is known for its systematic error in calculating too short bond lengths by overestimating the effect of electron correlation, whereas the HF method systematically calculates too long bonds.

It should be noted that the inexpensive PM3 geometry is a poor basis for calculations of ^{1}H chemical shifts (figure 8b and figure 10), properly because of the poor chelate hydrogen bond geometry (see also figure 3b), whereas most methods give reasonable ^{13}C chemical shifts $R^2 > 0.969$ (Figures 9 and 11). The importance of molecular geometries has recently been discussed by Forsyth [8].

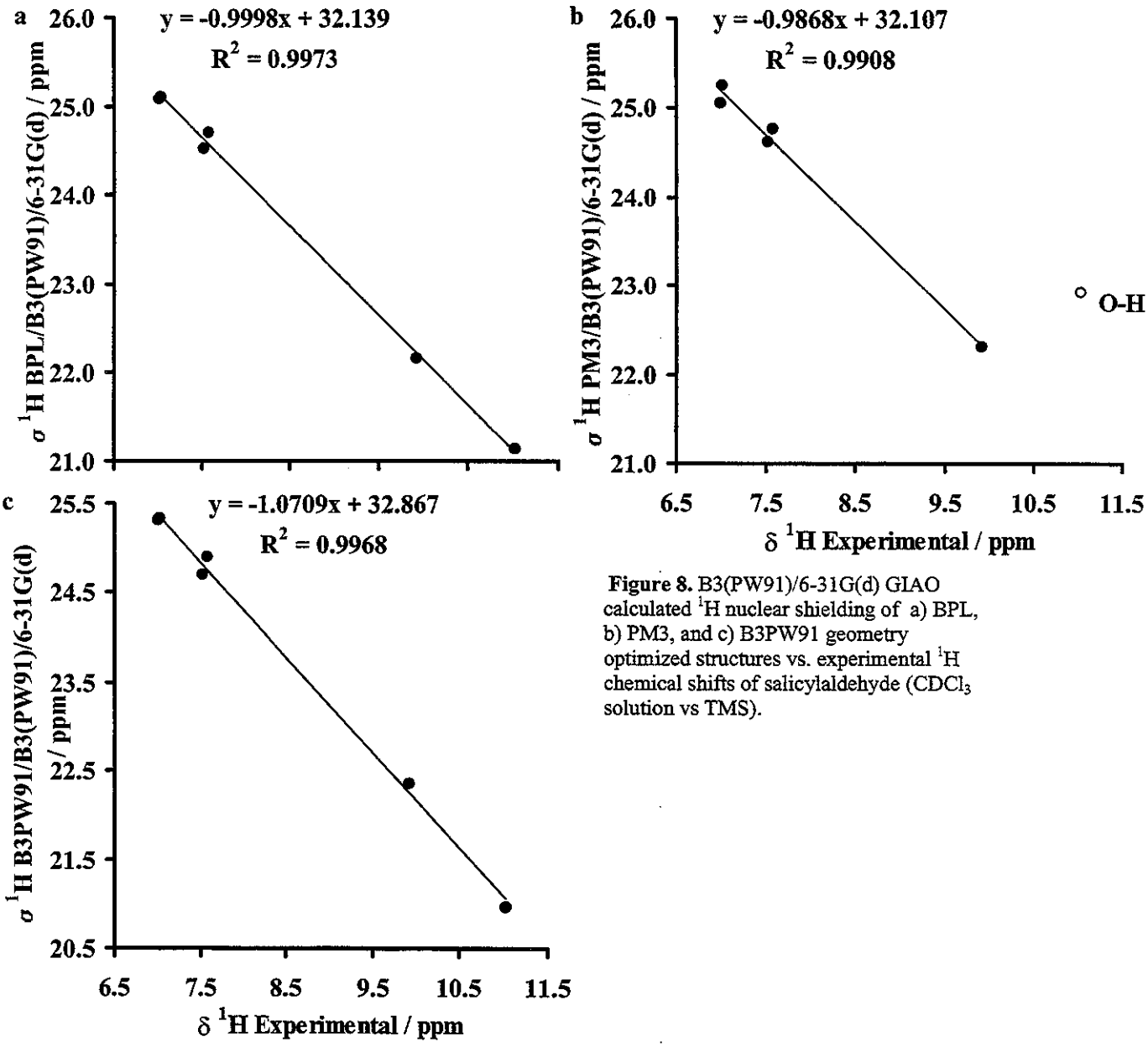

Figure 8. B3(PW91)/6-31G(d) GIAO calculated ^{1}H nuclear shielding of a) BPL, b) PM3, and c) B3PW91 geometry optimized structures vs. experimental ^{1}H chemical shifts of salicylaldehyde ($CDCl_3$ solution vs TMS).

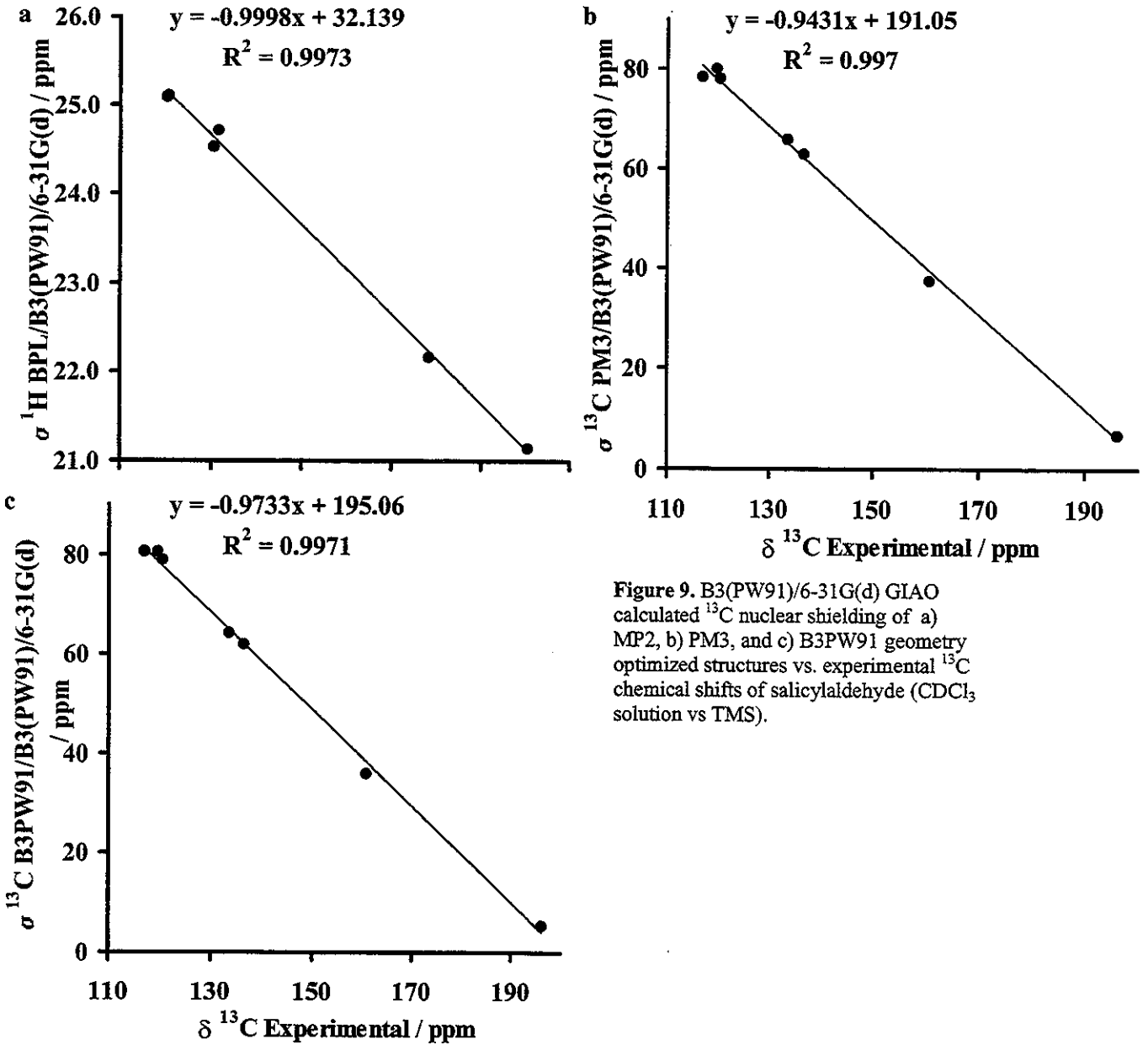

Figure 9. B3(PW91)/6-31G(d) GIAO calculated ^{13}C nuclear shielding of a) MP2, b) PM3, and c) B3PW91 geometry optimized structures vs. experimental ^{13}C chemical shifts of salicylaldehyde ($CDCl_3$ solution vs TMS).

Residual correlation

It is interesting to notice the parallel behavior seen when the precision of the different molecular orbital methods are compared. In Figure 12 we have plotted the RMSD of the spectroscopic data vs. the RMS of the absolute atom coordinate differences between the calculated and experimental geometry. The reason we do this is to investigate to what extent the calculated molecular geometries are reliable.

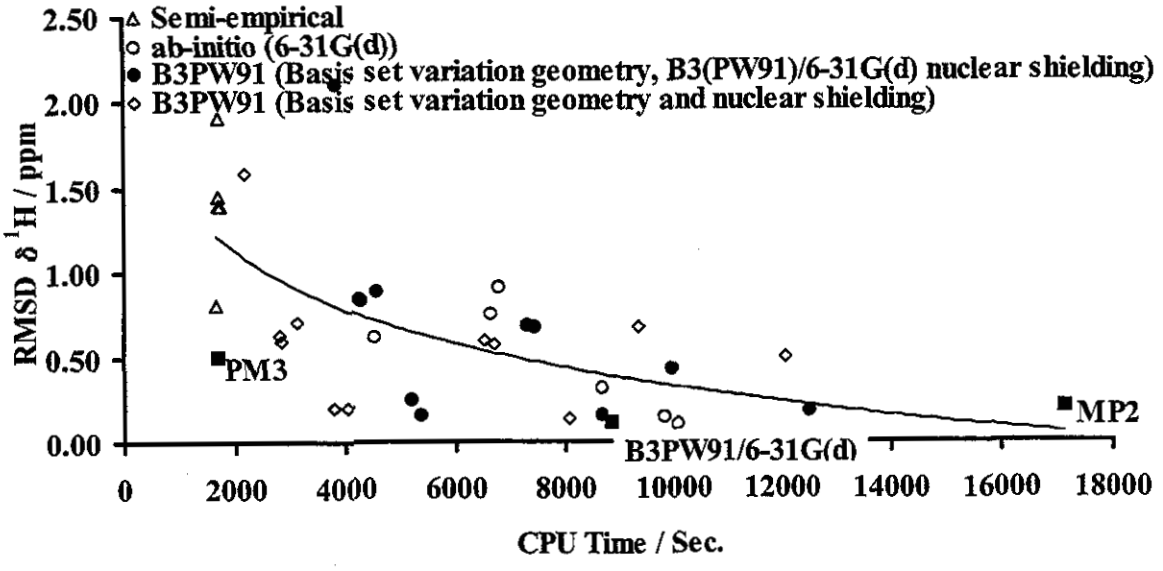

Figure 10. Standard deviations between experimental and calculated ^{1}H chemical shifts of salicylaldehyde vs. CPU times, the data are in Table 5.

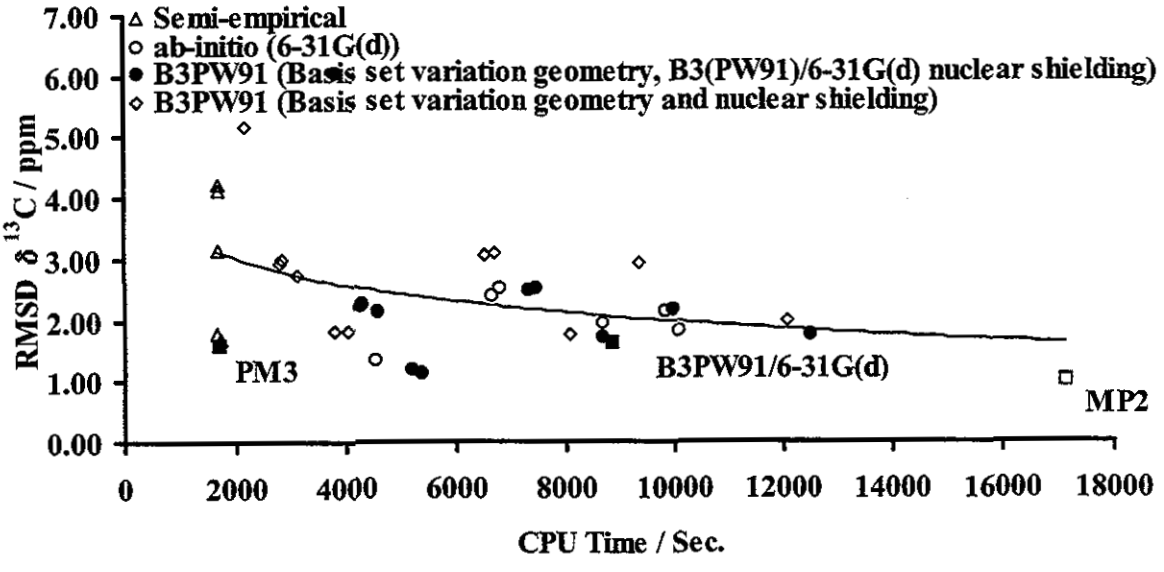

Figure 11. Standard deviations between experimental and calculated ^{13}C chemical shifts of salicylaldehyde vs. CPU time, the data are in Table 5.

The concerted fall in standard errors through the different methods does to some extent compensate for the obvious statistical shortcomings of using only one molecule in this type of investigation.

It is however readily foreseeable that calculated molecular structures will become an ever more important chemistry tool in the future, and that this kind of calibration will help to establish the quality of the calculated structure.

Table 5. RMSD Between B3(PW91)/GIAO Calculated Nuclear Shielding and Experimental Chemical Shift of Salicylaldehyde / ppm.

Geometry Optimization Method / Basis set	GIAO Basis Set	CPU time sec.	^{13}C R-value	RMSD	^{1}H R-value	RMSD
MP2/6-31G(d)	6-31G(d)	1639	**0.9990**	**1.0**	0.9867	0.20
B3PW91/6-31G	6-31G(d)	1783	0.9988	1.1	0.9943	0.16
B3PW91/4-31G	6-31G(d)	1810	0.9986	1.2	0.9886	0.24
RHF/6-31G(d)	6-31G(d)	1642	0.9978	1.3	0.7770	0.62
PM3	6-31G(d)	1653	0.9970	1.6	0.8638	0.51
B3PW91/6-31G(d)	6-31G(d)	1636	0.9971	1.6	0.9968	0.12
MNDO	6-31G(d)	1687	0.9963	1.7	0.0125	1.40
B3PW91/4-31G(d)	6-31G(d)	1703	0.9968	1.7	0.9943	0.16
B3PW91/4-31G(d,p)	6-31G(d)	1691	0.9968	1.8	0.9928	0.18
B3PW91/4-31G(d)	4-31G(d)	1087	0.9967	1.8	0.9959	0.13
AM1	6-31G(d)	1649	0.9965	1.8	0.5397	0.81
B3PW91/6-31G	6-31G	430	0.9970	1.8	0.9916	0.21
BPL/6-31G(d)	6-31G(d)	1629	0.9965	1.8	**0.9973**	**0.10**
B3PW91/4-31G	4-31G	399	0.9969	1.8	0.9924	0.21
BPW/6-31G(d)	6-31G(d)	1653	0.9961	2.0	0.9817	0.31
B3PW91/4-31G(d,p)	4-31G(d,p)	1300	0.9959	2.0	0.9629	0.50
B/6-31G(d)	6-31G(d)	1615	0.9951	2.1	0.9924	0.15
B3PW91/3-21G	6-31G(d)	1817	0.9957	2.1	0.9215	0.89
B3PW91/4-21G(d,p)	6-31G(d)	1756	0.9950	2.2	0.9706	0.43
B3PW91/4-21G	6-31G(d)	1809	0.9954	2.2	0.9259	0.85
B3PW91/6-21G	6-31G(d)	1810	0.9953	2.3	0.9276	0.83
S/6-31G(d)	6-31G(d)	1653	0.9942	2.4	0.9309	0.76
B3PW91/4-21G(d)	6-31G(d)	1759	0.9935	2.5	0.9417	0.69
B3PW91/6-21G(d)	6-31G(d)	1754	0.9935	2.5	0.9424	0.68
SVWN5/6-31G(d)	6-31G(d)	1660	0.9936	2.5	0.9168	0.91
B3PW91/3-21G	3-21G	345	0.9922	2.7	0.9532	0.71
B3PW91/4-21G(d,p)	4-21G(d,p)	1167	0.9892	2.9	0.9416	0.68
B3PW91/4-21G	4-21G	351	0.9911	2.9	0.9602	0.64
B3PW91/6-21G	6-21G	365	0.9907	3.0	0.9636	0.60
B3PW91/4-21G(d)	4-21G(d)	969	0.9885	3.0	0.9540	0.59
B3PW91/6-21G(d)	6-21G(d)	1022	0.9882	3.1	0.9560	0.58
CNDO	6-31G(d)	1681	0.9914	3.2	0.8667	1.39
INDO	6-31G(d)	1677	0.9851	4.1	0.8254	1.92
MINDO3	6-31G(d)	1684	0.9716	4.2	0.0020	1.46
B3PW91/STO-3G	STO3-3G	190	0.9436	5.2	0.8604	1.59
B3PW91/STO-3G	6-31G(d)	1851	0.9694	6.1	0.8208	2.10

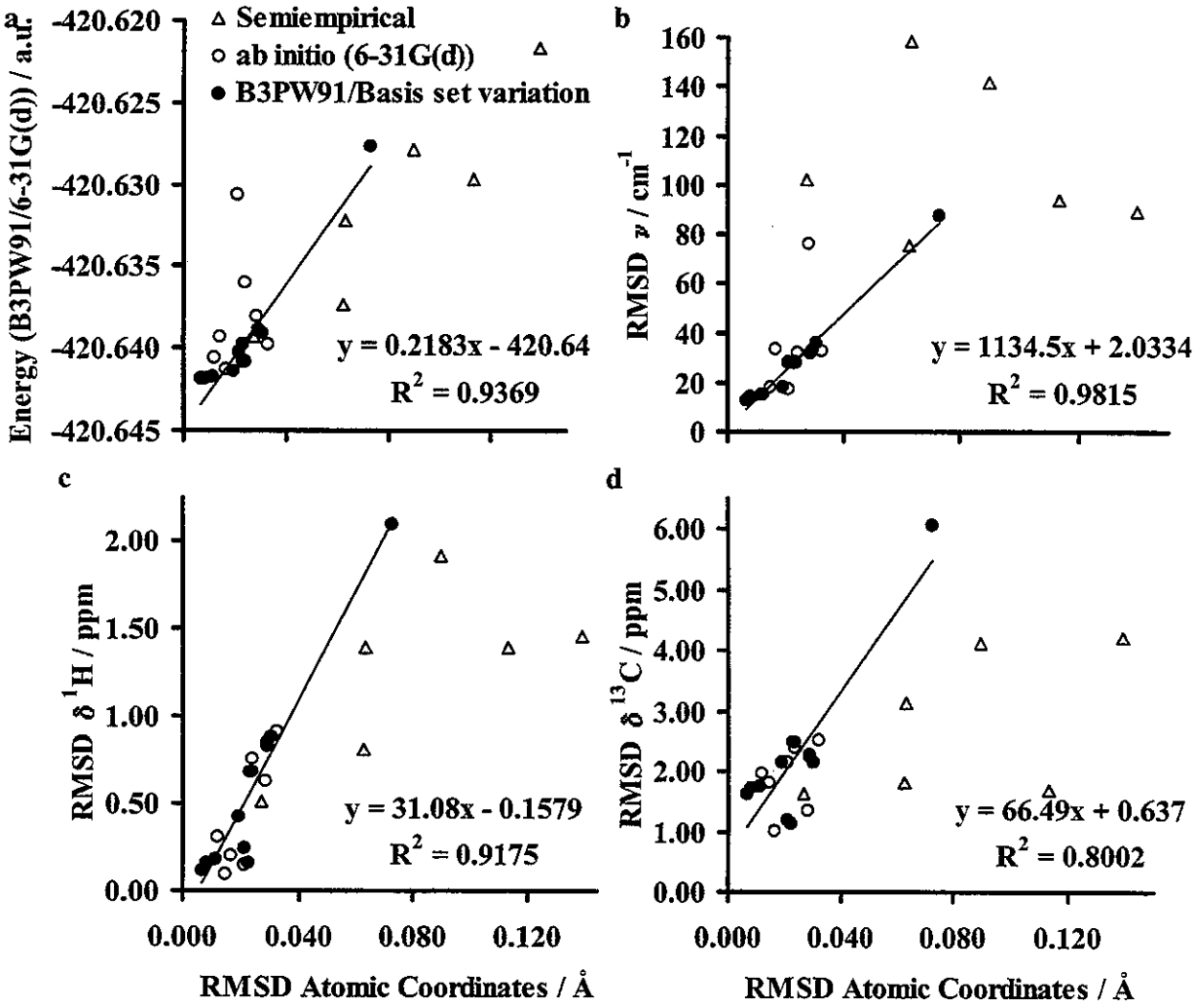

Figure 12. a) B3PW91/6-31G(d) electronic energy, b) Standard deviation between calculated and experimental IR frequencies, c) Standard deviations between experimental and calculated ^{1}H chemical shifts, and d) Standard deviations between experimental and calculated ^{13}C chemical shifts, all plotted against the standard deviation between corresponding atomic coordinates of the experimental and calculated molecular geometries of salicylaldehyde.

Deuterium isotope effects on chemical shifts

Isotope effects on chemical shifts is caused by differences in vibrational modes due to the different isotope masses. A hydrogen to deuterium substitution is a relatively large change of the atomic mass, a doubling, but the change in the total mass of the molecule is small. If the vibrational mode only involve movement of the hydrogen atom, while the rest of the molecule is immobile, then the IR frequency would change with a factor of inverse squareroot of 2 and the reduced masses would be 1 and 2 for the hydrogen and deuterium vibrations respectively. This is roughly what we find in the B3PW91/6-31G(d) IR frequency calculations (see previously). However, this picture is too simple as all nuclei move in the calculated harmonic force field in such a way that the center of mass of the molecule remains invariant. Upon deuteriation both frequency, amplitude, and direction of all atomic movements will change. The different isotopologs thus have different vibrational patterns (see e.g. Figures 13a and 13b).

The inspection of the IR frequency calculations of salicylaldehyde show three normal modes with frequency changes of more than 100 cm^{-1} upon deuterium substitution of the O-H proton (in reference 4 a similar conclusion is reached based on B3LYP calculations). The O-H out-of-plane-bending mode is anti-symmetrical with respect to the plane of the aromatic ring and thus does not lead to appreciable isotope effects, as we shall see later. Figures 13c and 13d clearly shows the O-H stretching mode to be very localized and similar to the O-D stretch, whereas the bending mode varies somewhat more (Figures 13a and 13b).

One-bond deuterium isotope effects on chemical shifts

One-bond isotope effects can be understood from a simple qualitative model in which deuterium substitution leads to a O-H(D) stretching mode vibrationally averaged shortening of the X-H bond (see Figure 14a). The nuclear shielding of the structure with shorter X-H distance leads to a larger nuclear shielding value. Translating this to chemical shift means a lower chemical shift for the deuterated species (low frequency or high field shift) which is the normal trend, also for zero (primary) and two bond isotope effects. However, to do this more quantitatively, we need to investigate the problem in depth.

The normal mode calculated at 827 cm-1 (607 O-D) is an out-of-plane bending mode anti-symmetrical around the molecular symmetry plane, and this leads to very

small isotope effects, if any at all.

The vibrational state found in the B3PW91/6-31G(d) normal mode analysis at 1453 cm-1 (1042 for O-D) is the in-plane bending mode which is not symmetrical in the two directions, as the O-H bond does not lie in an in-plane symmetry axis of the molecule. The much less strongly localized mode, which involves several other hydrogen bends, is nevertheless little anharmonic, and is of little interest in the context of hydrogen deuterium isotope effects (Figures 13a and 13b). Figure 14c shows the energy along the normal coordinates of the O-H(D) bending modes.

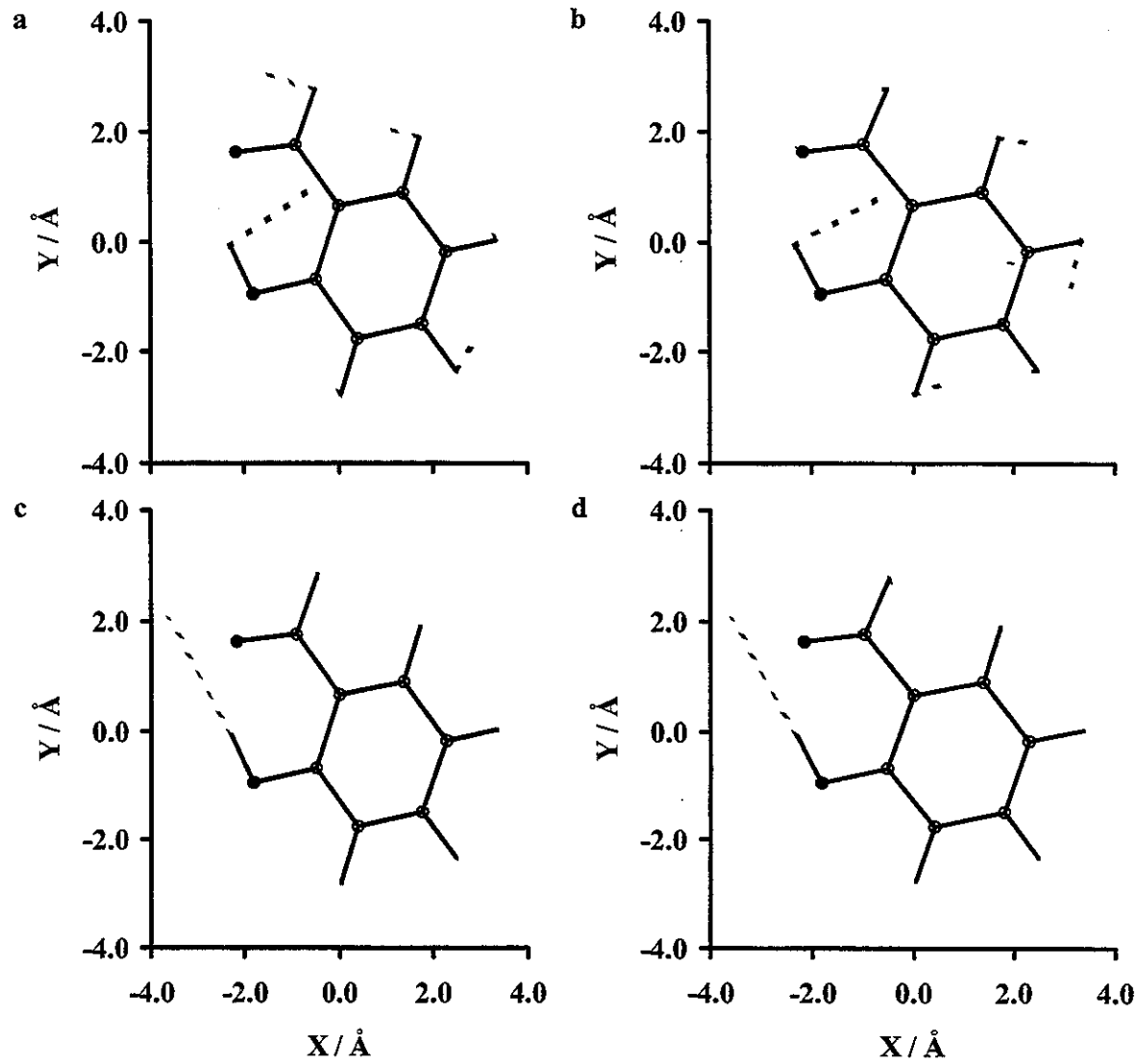

Figure 13. B3PW91/6-31G(d) harmonic approximation normal mode analysis calculated a) Bend type O-H normal mode at 1453 cm^{-1}, and b) O-D at 1042 cm^{-1} c) Stretch type O-H normal mode at 3324 cm^{-1}, and d) O-D at 2424 cm^{-1}. O-H and O-D normal modes are shown without mass weighting of the normal coordinate to illustrate the direction of the atomic movements for the two isotopologs of salicylaldehyde. The sum of atomic coordinate displacements are the same for the O-H and O-D modes.

Figure 14a shows the potential energy of salicylaldehyde as the atomic coordinates are moved along the O-H stretching normal coordinate. It is readily seen that the potential is highly unsymmetrical around the point of lowest energy, and quite similar for both the hydrogen and deuterium stretching modes. The energy difference between the lowest point on the potential and the vibrational state is the *zeropoint correction energy*.

The nuclear shielding surface for a set of different nuclear configurations can be calculated. In the present case the nuclear shielding profile along the O-H bond extension in the O-H bond direction is calculated and so are the nuclear shieldings for the geometries along the vibrational normal coordinate of the O-H and O-D stretching and in-plane-bending modes.

The nuclear shielding is seen to be linear in the region around the equilibrium geometry (Figure 14). Nuclear shieldings are shown to behave linearly with respect to small bond stretching perturbations in a number of cases [64, 65].

Figures 14b and 14d show the ^{13}C nuclear shielding of the carbon which displays the largest isotope effects, namely the carbon with the hydroxy substituent, and it is seen that the slope is nearly linear in the area of interest (normal coordinate = 0). The slopes of all carbons, or the nuclear shielding gradients with respect to O-H stretching normal coordinate perturbation, are proportional to the experimentally measured hydrogen-deuterium isotope substitution effects on the ^{13}C chemical shifts (Figure 15).

The nuclear shielding gradient is more readily obtained by calculating the nuclear shielding for a molecular geometry with the O-H bond shortened by 0.01 Å only. Figure 15a shows the calculated nuclear shielding gradients caused by 0.01 Å shortening of the hydroxy hydrogen O-H bond in the bond direction, and Figure 15b the corresponding plot of the calculated nuclear shielding gradients for the O-H and O-D stretching normal mode versus the experimental isotope effects. Because of the localized nature of the O-H stretching vibration, the plots are very similar and the improvement in correlation coefficient is not significant for choosing between the methods.

The more theoretically correct way of calculating the isotope effect on nuclear shielding would be to calculate the integrated nuclear shielding of the entire energy weighted molecular vibrational movement for the H- and D-species and subtract the two

values, and though this could be done, we satisfy ourselves with the present method inspired by the work of Cynthia Jameson [65, 66].

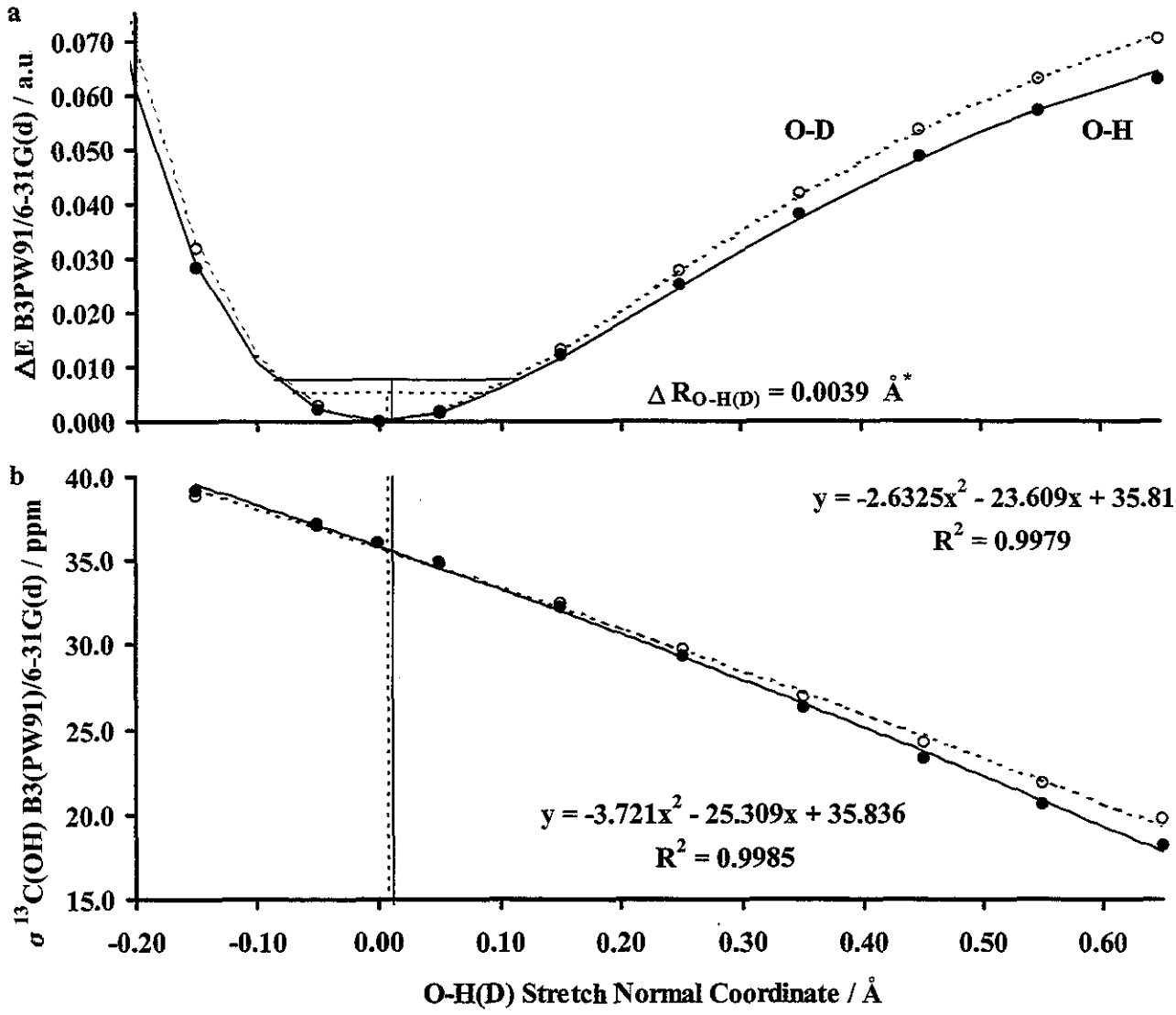

Figure 14. a) Stretch type potential curve for the O-H and O-D stretching normal modes. The normal coordinate (not mass weighted) is given by the sum of all the atomic coordinate changes. Morse functions are fitted to the data points (see text). b) ^{13}C-O nuclear shielding for the geometries along the O-H and O-D stretching normal coordinates corresponding to 14a.
* The corresponding value from the stretching potential with O-H movement only in the bond direction is 0.0035 Å.

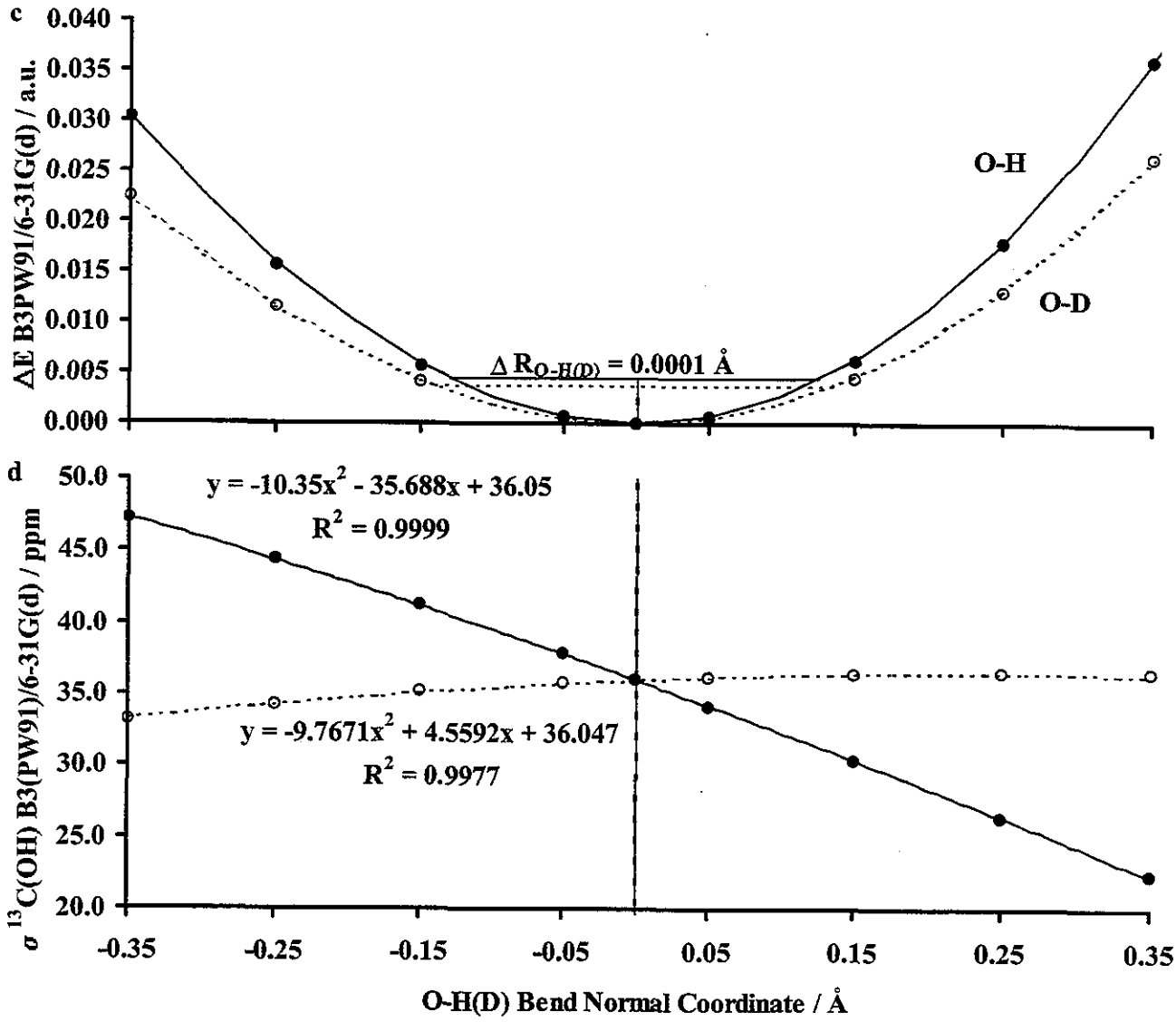

Figure 14. (Cont.) c) Bend type potential curve for the O-H and O-D in-plane bending normal modes d) ^{13}C-O nuclear shielding for the geometries along the O-H and O-D in-plane bending normal coordinates corresponding to 14c.

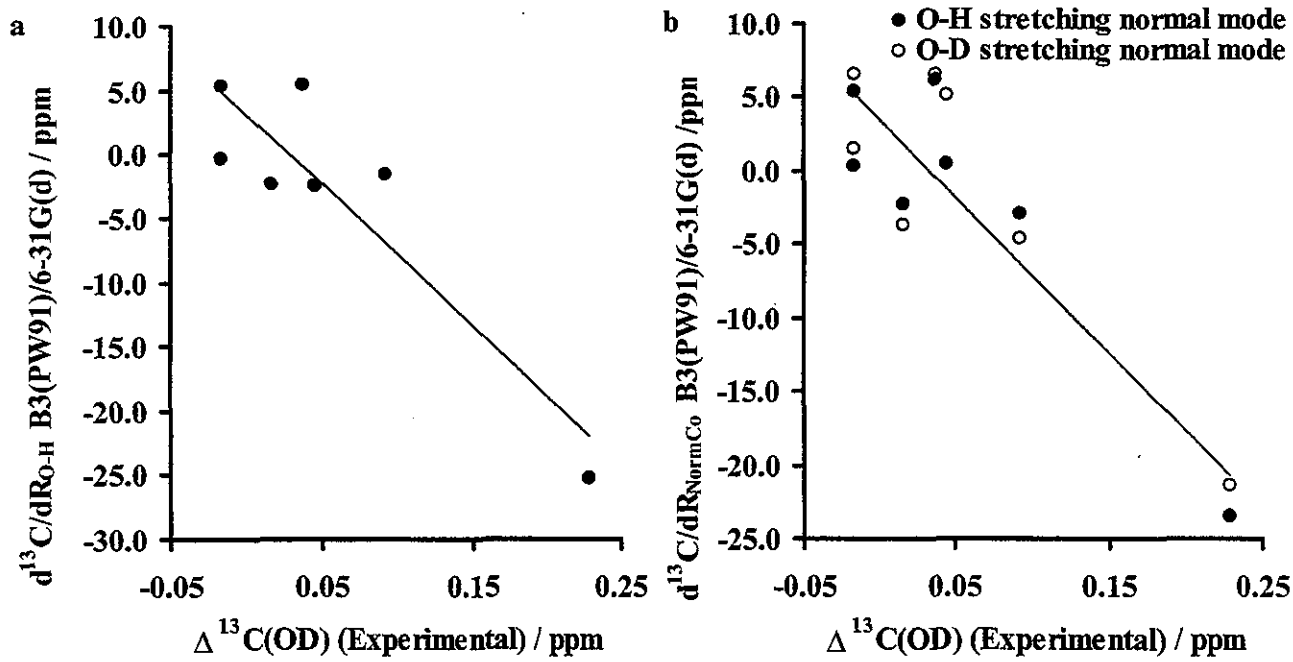

Figure 15. a) Plot of the ^{13}C nuclear shielding gradients, $d^{13}C/dR_{O-H}$, dR_{O-H} being the O-H coordinate in the bond direction, and b) plot of the ^{13}C nuclear shielding gradients, $d\sigma^{13}C/dR_{O-H\ Norm.\ Coor.}$, $dR_{O-H\ Norm.\ Coor}$ being the O-H(D) stretching normal coordinate, vs. the experimental isotope effects, $^{n}\Delta^{13}CO\text{-}H(D)$.

Two contributions to isotope effects: $d\sigma_i/dR_{X-H}$ and $\Delta R_{X-H(D)}$

In order to calculate the isotope effect it is necessary to know the change in the nuclear shielding with respect to either bond length or angle perturbations ($d\sigma_i/dR_{X-H}$, $d^2\sigma_i/d^2R_{X-H}$, and $d\sigma_i/d\alpha_{X-H}$) in which α is the bond angle. The two latter terms are usually of opposite signs and to some extent cancel [66]. Equally important is the size of the average geometry perturbation , that may vary between different molecular systems, and with different hydrogen bond geometries [5].

By scanning the O-H bond stretching, moving the hydroxy hydrogen only in the bond direction, and fitting a Morse function [67] to the resulting potential, we are able to calculate the change in the average hydrogen and deuterium position ($\Delta R_{O-H(D)}$).

Multiplying the nuclear shielding gradient of the individual nuclei (with respect to O-H bond perturbation) with the average change in O-H bond length, we arrive at the calculated isotope effects. Table 1b has the nuclear shielding gradient of salicylaldehyde with respect to O-H bond shortening. The calculated isotope effect can be determined by multiplying this gradient with the average geometry perturbation from the analytical solution to the fitted Morse function of the O-H bond stretching potential [67] (for the H displacement only in the bond direction, $\Delta R_{O-H(D)} = 0.0035$ Å).

The values are too small, indicating other contributions to the hydrogen

deuterium isotope effects than found in this somewhat simplistic approach.

We have used the normal mode analysis calculated reduced masses from the IR calculation, but it is possible to simply use the reduced masses of 1 and 2 for the hydrogen and deuterium species respectively, which are the reduced masses for the vibrational mode scanned when keeping the rest of the atomic coordinates constant.

Isotope effects in o-hydroxy acyl aromatics

In the work of differently substituted 2-hydroxy acetophenones [5] we observed extraordinary large two-bond isotope effects in some, but not all, of the species, while the calculated shielding gradients did not reflect this at all. We find that the gradients for 2-hydroxyacetophenone (**1**), 1,3-diacetyl-2,4-dihydroxybenzene (**2**), 1,3,6-triacetyl-2,4,6-trihydroxybenzene (**3**) and 1,5-diacetyl-2,4-dihydroxybenzene (**4**), are similar for corresponding carbons, but the experimental isotope effects vary up to a factor of ~2. The reason is that the major contribution to the variation in hydrogen-deuterium isotope effects stems from large differences in the average vibrational geometry. Using both the gradient and average geometry perturbation terms we reproduce the experimental isotope effects [5] (see figure 16 and 17).

If we compare the experimental isotope effects for the different types of compounds; *o*-hydroxy-ketones, -aldehydes, and -esters, the isotope effects are seen to be proportional within corresponding types of carbons [17]. This finding, and the finding that the calculated gradients are very similar for the differently substituted *o*-hydroxy-acylbenzenes, support the idea that the isotope effects to a first approximation can be presented as a product of $d\sigma_i/dR_{O\text{-}H(D)}$ and $\Delta R_{O\text{-}H(D)}$, both of which contribute significantly.

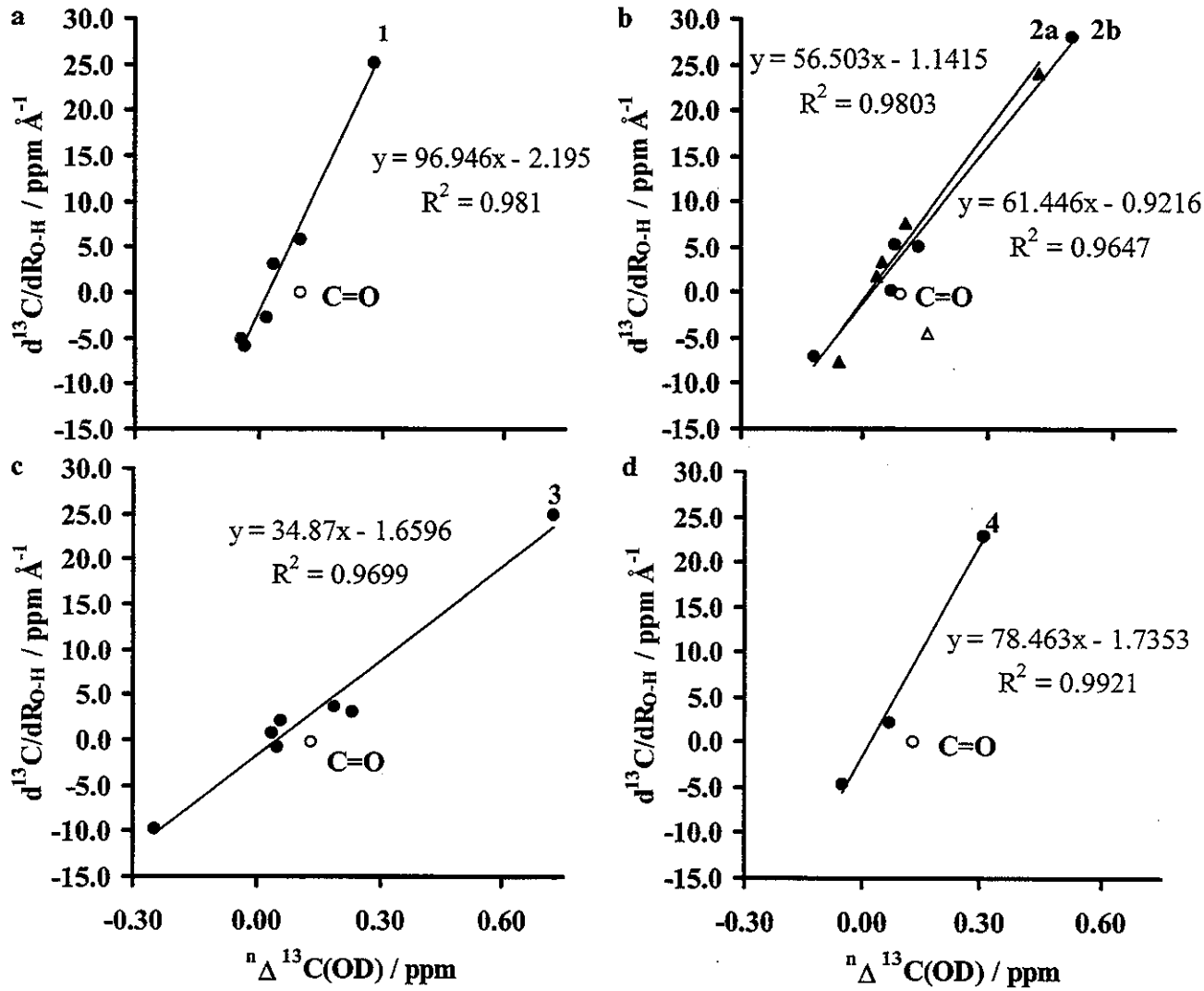

Figure 16. Calculated ^{13}C nuclear shielding gradients ($d\sigma^{13}C/dR_{O-H}$) plottet against the experimental isotope effects of **1** - **4** (a-d) [5].

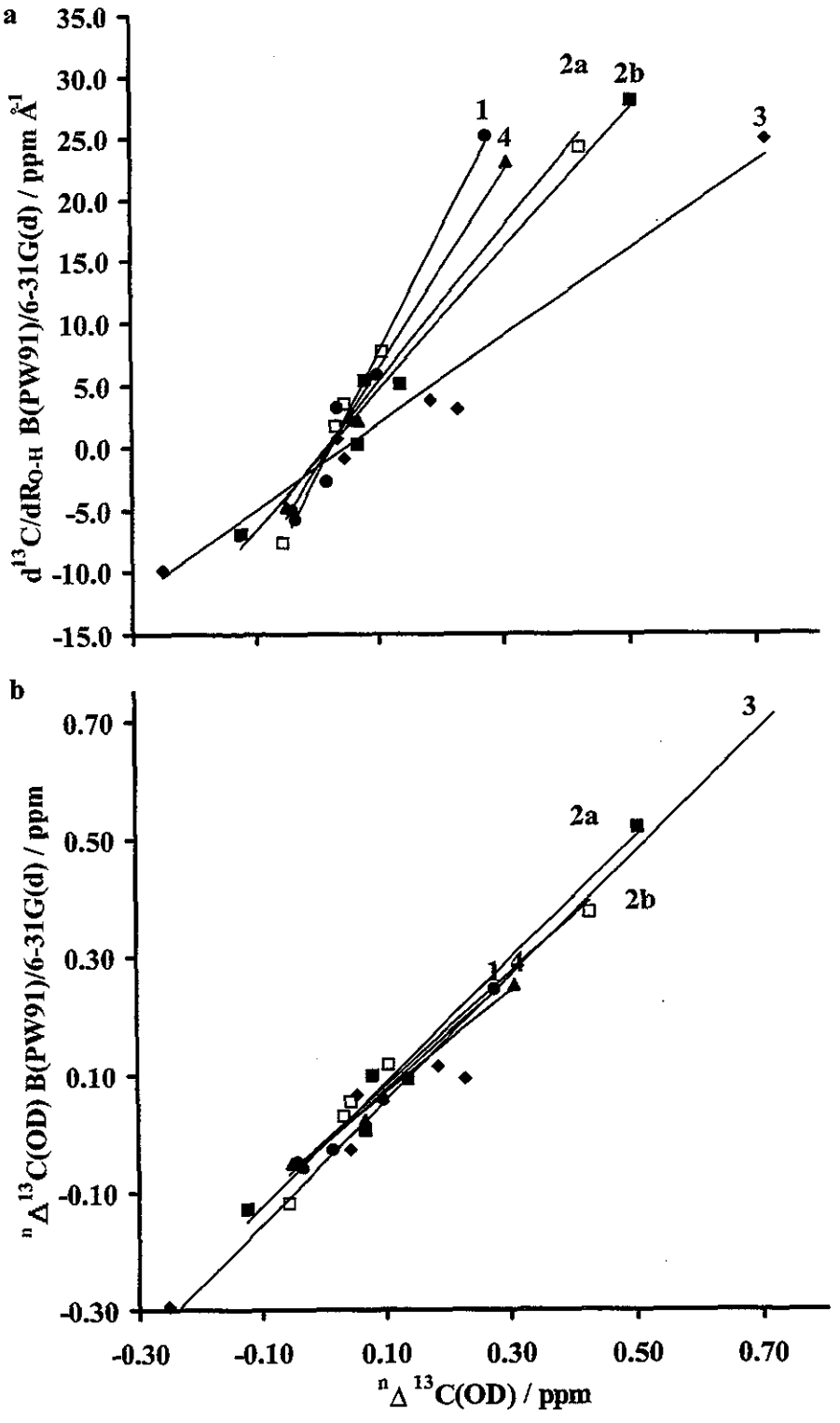

Figure 17. a) Calculated ^{13}C nuclear shielding gradients ($d\sigma^{13}C/dR_{O-H}$) plottet against the experimental isotope effects of 1 - 4. b) Calculated isotope effects using BPW91/6-31G/(d(p)) 5D normal mode analysis calculated reduced masses in the average geometry calculation, plottet against experimental values

Conclusion

As a consequence of the development of theory, computers, and computer software, molecular orbital model calculations are important tools in all branches of chemistry. These quantum mechanical models help us to explain, and to better understand, the physical cause of isotope substitution effects on NMR chemical shifts as demonstrated in the text.

The presence of a statistically significant correlation between experimentally determined and calculated spectroscopic data, meeting certain values of standard deviation means that calculated molecular geometry may be used as independent structure solutions, yielding reliable molecular geometries. The resolution is given by the residuals in the correlation between experimental and calculated data calibrated against the RMS absolute atom coordinate differences for molecules of experimentally determined high resolution structure. This is not so different from traditional methods, as we tend to overlook the model aspect of e. g. single crystal diffraction techniques.

Acknowledgments

The authors wish to thank the Danish Natural Science Research Council (Bonusudvalg) for allocation of time on UNI-C´s supercomputers, Ph. D. Søren Møller, Roskilde University Library for help in the literature study, and professor Aage. E. Hansen, University of Copenhagen for invaluable help and advice through the years.

References

1. Andersen, K. B.; Abildgaard, J.; Radziszewski, J. G.; Spanget-Larsen, J. *J. Phys. Chem.* **101**, 4475 (1997)
2. Radziszewski, J. G.; Abildgaard, J.; Thulstrup, E. W. *Spectrochimica Acta Part A*, **53**, 2095 (1997)
3. Martin, J. M. L.; El-Yazal J.; Francois, J.-P. *J. Phys. Chem.* **100**, 15358 (1996)
4. Lampert, H.; Mikenda, W.; Karpfen, A. *J. Phys. Chem.* **101**, 2254 (1997)
5. Abildgaard, J.; Bolvig, S.; Hansen, P. E. *J. Am. Chem. Soc.* **120** (35), 9063 (1998)
6. de Dios, A. C.; Oldfield, E. *Solid state NMR* **6**, 101 (1996)
7. de Dios, A. C. *J. Prog. NMR*, **29**, 229 (1996)
8. Barfield, M.; Fagerness, P. *J. Am. Chem. Soc.* **119**, 8699 (1997)
9. Hansen, P. E.; Langgård, M.; Bolvig, S. *Polish J. Chem.* **72**, 269 (1998)
10. De Dios, A. C.; Oldfield, E. *Chem. Phys. Lett.* **205**, 108 (1993)
11. Forsyth, D.; Sebag, A. B. *J. Am. Chem. Soc.* **119**, 9483 (1997)
12. O'Brien, D. H.; Stipanovich, R. D. *J. Org. Chem.* **43**, 1105. (1978)
13. Reuben, J. *J. Am. Chem. Soc.* **108**, 1735. (1986)
14. Hansen, P. E. *Org. Mag. Res.* **24**, 903. (1986)
15. Liepins, E.; Petrova, M. V.; Gudriniece, E.; Paulins, J.; Kuznetsov, S. L. *Mag. Res. Chem.* **27**, 907 (1989)
16. Reuben, J. *J. Am. Chem. Soc.* **109**, 316 (1987)
17. Hansen, P. E. *Mag. Res. Chem.* **31**, 23 (1993)
18. Hansen, P. E. *J. Mol. Struct.* **321**, 79 (1994)
19. Ng, S.; Lee, H -H.; Bennett, G. J. *Mag. Res. Chem.* **28**, 337 (1990)
20. Hansen, P. E.; Bolvig, S.; Duus, F.; Petrova, M. V.; Kawecki, R.; Krajewski, P.; Kozerski, L. *Mag. Res. Chem.* **33**, 621 (1995)
21. Hansen, P. E.; Duus, F.; Bolvig, S.; agodzinski, T. S. J. *J. Mol. Struct.* **378**, 45 (1996)
22. Khatipov, S. A.; Shapet'ko, N. N.; Bogavev, Yu. S.; Andreichikov, Yu. S.*Russ. J. Phys. Chem.* **59**, 2097 (1985)
23. Bolvig, S.; Hansen, P. E. *Mag. Res. Chem.* **34**, 467 (1996)
24. Hansen, P. E.; Ibsen, S. N.; Kristensen, T.; Bolvig, S. *Mag. Res. Chem.* **32**, 399 (1994)
25. Dewar, A. M.; Thiel, W. *J. Am. Chem. Soc.* **99**, 4499 (1977), Davis, L. P. et. al. *J. Comp. Chem.* **2**, 433 (1981), Dewar, M. J. S.; McKee, M. L.; Rzepa, H. S. *J. Am. Chem. Soc.* **100**, 3607 (1978), Dewar, M. J. S. et. al. *Organometallics* **4**, 1964 (1985), Dewar; M. J. S.; Zoebisch, E. G.; Healy, E. F. *J. Am. Chem. Soc.* **107**, 3902 (1985)
26. Stewart, J. J. P. *J. Comp. Chem.* **10**, 209 (1989), Stewart, J. J. P. *J. Comp. Chem.* **10**, 221 (1989)
27. Segal, G.; Pople, J. A. *J. Chem. Phys.* 3289 (1966)
28. Dewar, A. M.; Thiel, W. *J. Am. Chem. Soc.* **99**, 4499 (1977), Dewar; M. J. S.; Thiel, W. *J. Am. Chem. Soc.* **99**, 4899 (1977), Dewar, M. J. S.; Rzepa, H. S. *J. Am. Chem. Soc.* **100**, 777 (1978), Dewar, M. J. S.; McKee, M. L. *J. Comp. Chem.* **4**, 84 (1983), Davis, L. P. et. al. *J. Comp. Chem.* **2**, 433 (1981), Dewar, M. J. S.; McKee, M. L.; Rzepa, H. S. *J. Am. Chem. Soc.* **100**, 3607 (1978), Dewar; M. J. S.; Healy, E. F. *J. Am. Comp. Chem.* **4**, 542 (1983), Dewar, M. J. S.; Grady, G. L.; Stewart, J. J. P *J. Am. Chem. Soc.* **106**, 6771 (1984), Dewar, M. J. S. et. al. *Organometallics* **4**, 1964 (1985), Dewar; M. J. S.; Reynolds, C. H. *J. Comp. Chem.* **2**, 140 (1986)
29. Dewar, A. M.; Thiel, W. *J. Am. Chem. Soc.* **99**, 4499 (1977), Bingham, R. C.;

Dewar, M. J. S.; Lo?, *J. Am. Chem. Soc.* **97**, 1285 (1975)
30. Pople, J. A.; Beveridge D.; Dobosh, P. *J. Chem. Phys.* **47**, 2026 (1967)
31. Roothan, C. C. J. *Rev. Mod. Phys.* **23**, 69 (1951), Pople, J. A.; Nesbet, R. K. *J. Chem. Phys.* **22**, 571-574 (1959), McWeeny, R.; Dierksen, G. *J. Chem. Phys.* **49**, 4852 (1968)
32. Head-Gordon, M.; Pople, J. A.; Frisch, M. J. *Chem. Phys. Lett.* **153**, 503 (1988), Frisch, M. J. Head-Gordon, M.; Pople, J. A. *Chem. Phys. Lett.* **166**, 275 (1990), Frisch, M. J.; Head-Gordon M.; Pople, J. A. *Chem. Phys. Lett.* **166**, 281 (1990), Head-Gordon, M.; Head-Gordon, T. *Chem. Phys. Lett.* **220**, 122 (1994), Trucks, G. W.; Frisch, M. J.; Andres J. L.; Schlegel, H. B. *J. Chem. Phys.* submitted (1998?), Saebo, S.; Almlof, J. *Chem. Phys. Lett.* **154**, 83 (1989)
33. Hohenberg, P.; Kohn, W. *Physical Review* **136**, B864-B871 (1964), Kohn, W.; Sham, L. J.*Physical Review* **140**, A1133-A1138 (1965), Slater, J. C. *Quantum Theory of Molecular and Solids*. Vol. 4: *The Self-Consistent Field for Molecular and Solids,* McGraw-Hill: New York, 1974.
34. Becke, A. D. *Phys. Rev. A*, **38**, 3098 (1988)
35. Perdew, J. P.; Zunger, A. *Phys. Rev. B*, **23**, 5048 (1981)
36. Perdew J. P.; Wang, Y. *Phys. Rev. B*, **45**, 13244 (1992)
37. Vosko, S. H. Wilk L.; Nusair, M. *Canadian J. Phys.* **58**, 1200-1211 (1980)
38. Becke, A. D. *J. Chem. Phys.* **98**, 5648-5652 (1993)
39. Brünger, A. T.; Clore, G. M.; Gronenborn A. M.; Karplus, M.*Proc. Natl. Acad. Sci. (USA)*, **83**, 3801 (1986)
40. Hegarty D.; Robb, M. A. *Mol. Phys.* **38**, 1795 (1979), Eade R. H. E.; Robb, M. A. *Chem. Phys. Lett.* **83**, 362 (1981), Schlegel H. B.; Robb, M. A.*Chem. Phys. Lett.* **93**, 43 (1982), Bernardi, F.; Bottini, A.; McDougall, J. J. W.; Robb M. A.; Schlegel, H. B. *Far. Symp. Chem. Soc.* **19**, 137 (1984), Yamamoto, N; Vreven, T; Robb, M. A.; Frisch, M. J.; Schlegel, J. B. *Chem. Phys. Lett.* **250**, 373 (1996), Frisch, M. J.; Ragazos, I. N.; Robb M. A.; Schlegel, H. B. *Chem. Phys. Lett.* **189**, 524-28 (1992)
41. Foresman, J. B.; Head-Gordon, M.; Pople J. A.; Frisch, M. J. *J. Phys. Chem.* **96**, 135 (1992). Trucks G. W.; Frisch, M. J. in preparation? (1998) Pople, J. A.; Seeger R.; Krishnan, R. *Int. J. Quant. Chem. Symp.* **11**, 149 (1977), Krishnan, R.; Schlegel H. B.; Pople, J. A. *J. Chem. Phys.* **72**, 4654 (1980), Raghavachari K.; Pople, J. A. *Int. J. Quant. Chem.* **20**, 167 (1981)
42. Pople, J. A.; Head-Gordon M.; Raghavachari, K. *J. Chem. Phys.* **87**, 5968 (1987), Gauss J.; Cremer, C. *Chem. Phys. Lett.* **150**, 280 (1988), Trucks G. W.; Frisch, M. J. in preparation (1998?), Salter, E. A.; Trucks G. W.; Bartlett, R. J. *J. Chem. Phys.* **90**, 1752 (1989)
43. Pople, J. A.; Krishnan, R.; Schlegel H. B.; Binkley, J. S. *Int. J. Quant. Chem.* **XIV**, 545 (1978), Cizek, J. Adv. *Chem. Phys.* **14**, 35 (1969), Purvis G. D.; Bartlett, R. J. *J. Chem. Phys.* **76**, 1910 (1982), Scuseria, G. E.; Janssen C. L.; Schaefer, III, H. F. *J. Chem. Phys.* **89**, 7382 (1988), Scuseria G. E. ; Schaefer, III, H. F. *J. Chem. Phys.* **90**, 3700 (1989), Bartlett; R. J. Purvis, G. D. *Int. J. Quant. Chem.* **14**, 516 (1978)
44. Frisch, M. J.; Trucks, G. W.; Schlegel, H. B.; Gill, P. M. W.; Johnson, B. G.; Robb, M. A.; Cheeseman, J. R.; Keith, T.; Petersson, G. A.; Montgomery, J. A.; Raghavachari, K.; Al-Laham, M. A.; Zakrzewski, V. G.; Ortiz, J. V.; Foresman, J. B.; Peng, C. Y.; Ayala, P. Y.; Chen, W.; Wong, M. W.; Andres, J. L.; Replogle, E. S.; Gomperts, R.; Martin, R. L.; Fox, D. J.; Binkley, J. S.; Defrees, D. J.; Baker, J.; Stewart, J. P.; Head-Gordon, M.; Gonzalez, C.; Pople, J. A. Gaussian

94, Revisions B.3, C.3, and E1 Gaussian, Inc.: Pittsburgh, PA (1995)
45. Borisenko, K. B.; Bock, C. W.; Hargittai, I. *J. Phys. Chem.* **100**, 7426 (1996)
46. Singh, O. N.; Srivastava, M. P.; Singh, I. S. *Curr. Sci.* **23**, 630 (1967)
47. Radhi, M. M.; El-Bermani, M. F.*Spectrochim. Acta,* **46A**, 33 (1990)
48. Aldrich ^{13}C NMR Library.
49. Altman, L. A.; Laungani, D.; Gunnarson, G.; Wennerström H.; Forsén, S. *J. Am. Chem. Soc.* **100**, 8264 (1978)
50. Ditchfield, R.; Hehre W. J.; Pople, J. A.*J. Chem. Phys.* **54**, 724 (1971), Hehre, W. J.; Ditchfield R.; Pople, J. A. *J. Chem. Phys.* **56**, 2257 (1972), Hariharan P. C.; Pople, J. A. *Mol. Phys.* **27**, 209 (1974), Gordon, M. S. *Chem. Phys. Lett.* **76**, 163 (1980), Hariharan P. C.; Pople, J. A. *Theo. Chim. Acta.* **28**, 213 (1973)
51. Tozer, D. J. *J. Chem. Phys.* **104**, 4166 (1996)
52. Wong, M. W. *Chem. Phys. Lett.* **256**, 391 (1996)
53. Scott, A. P.; Radom, L. *J. Phys. Chem.* **100**, 16502 (1996)
54. Cheeseman, J. R.; Trucks, G. W.; Keith, T. A.; Frisch, M. J. *J. Chem. Phys.* **104** (14), 5497 (1996)
55. Wajsman, E.; Grabowski, M. J.; Stepien, A.; Cygler, M. *Chryst. Struct. Comm.* **7**, 233 (1978)
56. Michl, J.; Thulstrup, E. W. *Spectroscopy with polarized light, Solute alignment by photo selection, in Liquid Crystals, Polymers and Membranes*, VCH, New York (1995)
57. Thulstrup, E. W.; Michl, J. *Elementary Polarization Spectroscopy,* VCH, New York (1989)
58. Pardi, G.; Wagner; K. Wüthrich, *Eur. J. Biochem.* **137**, 445 (1983)
59. Wolinski, K.; Hilton J. F.; Pulay, P. *J. Am. Chem. Soc.* **112**, 8251 (1990), Dodds, J. L.; McWeeny R.; Sadlej, A. J. *Mol. Phys.* **41**, 1419 (1980), Ditchfield, R. *Mol. Phys.* **27**, 789 (1974), McWeeny, R. *Phys. Rev.* **126**, 1028 (1962), London, F. *J. Phys. Radium, Paris* **8**, 397 (1937)
60. Hansen Aa. E.; Bouman, T. D. in *Nuclear Magnetic Shieldings and Molecular Structure*, ed. J. A. Tossell, Kluwer Academic Publishing Dordrecht, (1993)
61. Hansen Aa. E.; Bouman, T. D. *J. Chem. Phys.* **82**, 5035 (1985), Bouman; T. D.; Hansen, Aa. E. *Intern. J. Quantum Chem. : Quantum Chem. Symp.* **23**, 381 (1989)
62. Kutzelnigg, W. *Isr. J. Chem.* **19**, 193 (1979), Schindler M.; Kutzelnigg, W. *J. Chem. Phys.* **76**, 1919 (1982), Schindler M.; Kutzelnigg, W. *J. Am. Chem. Soc.* **105**, 1360 (1983), Schindler M.; Kutzelnigg, W. *Mol. Phys.* **48**, 781 (1983), Kutzelnigg, W. *J. Mol. Struct. (Theochem)*, **202**, 11 (1989)
63. Facelli, J. C.; Grant, D. M.; Bouman, T. D.; Hansen, Aa. E. *J. Compt. Chem.* **11**, 32 (1990)
64. Munch, M.; Hansen, P. E.; Hansen, Aa. E.; Bouman, T. D. *Acta Chem. Scand.* **46**, 1065 (1992)
65. Jameson, C. J. in *Isotopes in the Physical and Biomedical Sciences, Isotopic Applications in NMR Studies*, edited by E. Buncel; J. R. Jones, p. 1. Elsevier, Amsterdam (1991)
66. Jameson, C. J. in *Encyclopedia of NMR*, **vol. 6.** , John Wiley, New York, (1995)
67. Dahl J. P.; Springborg, M. *J. Chem. Phys.* **88**, 4335 (1988)

Appendix.

Gaussian input-file.

```
%CHK=salialdh
%MEM=160000000
#B3PW91/6-31G(d) OPT

Salicylaldehyde (Geometry Optimization)

0 1
C
C 1 R2
C 2 R3 1 V3
C 3 R4 2 V4 1 D4
C 4 R5 3 V5 2 D5
C 5 R6 4 V6 3 D6
C 1 R7 2 V7 3 D7
O 7 R8 1 V8 2 D8
O 2 R9 3 V9 4 D9
H 7 R10 1 V10 2 D10
H 9 R11 2 V11 1 D11
H 3 R12 2 V12 1 D12
H 4 R13 3 V13 2 D13
H 5 R14 4 V14 3 D14
H 6 R15 5 V15 4 D15
Variables:
R2=1.4
R3=1.4
R4=1.4
R5=1.4
R6=1.4
R7=1.4
R8=1.25
R9=1.35
R10=1.1
R11=1.0
R12=1.1
R13=1.1
R14=1.1
R15=1.1
V3=120.
V4=120.
V5=120.
V6=120.
V7=120.
V8=120.
V9=120.
V10=120.
V11=109.
```

V12=120.
V13=120.
V14=120.
V15=120.
D4=0.
D5=0.
D6=0.
D7=180.
D8=0.
D9=180.
D10=180.
D11=0.
D12=180.
D13=180.
D14=180.
D15=180.

--Link1--
%CHK=salialdh
%MEM=160000000
#B3PW91/6-31G(d) GEOM=CHECK GUESS=READ FREQ

Salicylaldehyde (Vibrational Normal Mode Analysis)

0 1

--Link1--
%CHK=salialdh
%MEM=160000000
#B3PW91/6-31G(d) GEOM=CHECK GUESS=READ NMR

Salicylaldehyde (Nuclear Shielding Calculation)

0 1

Unraveling the Electronic and Vibrational Contributions to Deuterium Isotope Effects on ^{13}C Chemical Shifts Using ab Initio Model Calculations. Analysis of the Observed Isotope Effects on Sterically Perturbed Intramolecular Hydrogen-Bonded *o*-Hydroxy Acyl Aromatics

Jens Abildgaard, Simon Bolvig, and Poul Erik Hansen

Contribution from the Department of Life Sciences and Chemistry, Roskilde University, P.O. Box 260, DK-4000 Roskilde, Denmark

JOURNAL OF THE AMERICAN CHEMICAL SOCIETY®

Reprinted from
Volume 120, Number 35, Pages 9063–9069

J. Am. Chem. Soc. **1998,** *120,* 9063−9069

Unraveling the Electronic and Vibrational Contributions to Deuterium Isotope Effects on ^{13}C Chemical Shifts Using ab Initio Model Calculations. Analysis of the Observed Isotope Effects on Sterically Perturbed Intramolecular Hydrogen-Bonded *o*-Hydroxy Acyl Aromatics

Jens Abildgaard, Simon Bolvig, and Poul Erik Hansen*

Contribution from the Department of Life Sciences and Chemistry, Roskilde University, P.O. Box 260, DK-4000 Roskilde, Denmark

Received March 17, 1998

Abstract: Deuterium isotope effects on chemical shifts, $^{n}\Delta C(OD)$,have been measured in a series of *o*-hydroxy acyl aromatics of the type 2-hydroxyacetophenone (**1**) and 1,3,5-triacetyl-2,4,6-trihydroxybenzene (**3**). $^{2}\Delta C(OD)$ increase as the number of neighboring hydrogen-bonded moieties increase. The calculated molecular ab initio geometries with Density Functional Theory(BPW91/6-31G(d(p)) (5D) with p functions on the chelate protons only) show a large increase in R_{OH} in going from **1** to **3** and a large corresponding decrease in the C=O···H—O distance. $R_{O\cdots O}$, $A_{OH\cdots O}$, $R_{OH\cdots O}$, as well as R_{OH} and $R_{C=O}$ correlate linearly as do $^{2}\Delta C(OD)$ and $R_{O\cdots O}$. The nuclear shielding[1] and the first derivative of the ^{13}C nuclear shielding with respect to O-H bond stretching, $(d\sigma/dR_{OH})$, has been calculated with the 6-31G(d) (6D) basis set using the GIAO/B(PW91) method (exchange term only). (Chemical shift and nuclear shielding are used intermittently. It should be remembered that they lead to different signs.) The change in the R_{OH} distance upon deuteriation ($\Delta R_{OH(D)}$) was obtained from a potential scan of OH bond stretching and analyzing the data with a fitted Morse function. Isotope effects are calculated as the product of $d\sigma/dR_{OH}$ and $\Delta R_{OH(D)}$. The variations in the calculated $^{2}\Delta C(OD)$ are dominated by $\Delta R_{OH(D)}$. The calculated $^{n}\Delta C(OD)$ correlate well with experimental isotope effects. Three parameters, $^{2}\Delta C(OD)$, $\Delta R_{OH(D)}$, and $R_{O\cdots O}$ all show promise as gauges of hydrogen bond strength. Calculated O*H* and ^{1}H chemical shifts in general show good agreement with experimental values (RMSD = 0.40 ppm) as do the ^{13}C chemical shifts (RMSD = 1.9 ppm). The large experimental $^{2}\Delta C(OD)$ values can be understood in terms of a steric effect caused by the neighboring CH_3CO group leading to shorter OH···O and O···O distances and consequently stronger hydrogen bonds.

Introduction

Over the years much effort has been concentrated on characterization of hydrogen-bonded systems in order to provide parameters to describe hydrogen-bond strength and geometry.[1−6] Intramolecular hydrogen bonding of the resonance assisted (RAHB) type[1−4] as found in *o*-hydroxy acyl aromatics is a very common type of intramolecular hydrogen bond. NMR parameters often used to characterize hydrogen bonds are O*H* chemical shifts, primary isotope effects,[7−9] or secondary deuterium isotope effects on chemical shifts.[10−29] For ^{13}C the latter is defined as $^{n}\Delta C(OD) = \delta C(OH) - \delta C(OD)$. Deuterium isotope effects

* Address for correspondence: Professor Poul Erik Hansen, Department of Life Sciences and Chemistry, Roskilde University, P.O. Box 260, DK-4000 Roskilde, Denmark. Telephone: +45 46742432. FAX: +45 46743011. E-mail: POULERIK@virgil.ruc.dk.

(1) Gilli, G.; Bertolucci, F.; Ferretti, V.; Bertolasi, V. *J.Am. Chem. Soc.* **1989**, *111*, 1023.
(2) Gilli, G.; Bertolasi, V. In *The Chemistry of Enols*; Rappoport, Z.; Patai, S., Eds.; Wiley: Chichester, 1990.
(3) Gilli, P.; Ferretti, V.; Bertolasi, V.; Gilli, G. *Adv. Mol. Strut. Res.* **1996**, *2*, 67.
(4) Hansen, P. E.; Kawecki, R.; Krowcsynski, A.; Kozerski, L. *Acta Chem. Scand.* **1990**, *44*, 826.
(5) Lampert, H.; Mikenda, W.; Karpfen, A. *J. Phys. Chem.* **1996**, *100*, 7418.
(6) Borisenko, K. B.; Bock, C. W.; Hargittai, I. *J. Phys. Chem.* **1996**, *100*, 7426.
(7) Altman, L. J.; Laungani, D. L.; Gunnarson, G.; Wennerström, H.; Forsén, S. *J. Am. Chem. Soc.* **1978**, *100*, 8264.
(8) Dziembowska, T.; Rozwadowski, Z.; Hansen, P. E. *J. Mol. Struct.* **1997**, *436−437*, 189.
(9) Smirnov, S. N.; Golubev, N. S.; Denisov, G. S.; Benedict, H.; Schah-Mohameddi, P.; Limbach, H.-H. *J. Am. Chem. Soc.* **1996**, *118*, 4094.
(10) Hansen, P. E.; Bolvig, S. *Maun. Reson. Chem.* **1997**, *35*, 520.
(11) Shapet'ko, N. N.; Bogachev, Yu. S.; Radushnova, L. V.; Shigorin, D. N. *Dokl. Akad. Nauk, SSSR* **1976**, *231*, 409.
(12) O'Brien, D. H.; Stipanovich, R. D.; *J. Org. Chem.* **1978**, *43*, 1105.
(13) Hansen, P. E. *Prog. NMR Spectrosc.* **1988**, *20*, 207.
(14) Reuben, J. *J. Am. Chem. Soc.* **1986**, *108*, 1735.
(15) Hansen, P. E. *Org. Magn. Reson.* **1986**, *24*, 903.
(16) Liepins, E.; Petrova, M. V.; Gudriniece, E.; Paulins, J.; Kusnetsov, S. L. *Magn. Reson. Chem.* **1989**, *27*, 907.
(17) Reuben, J. *J. Am. Chem. Soc.* **1987**, *109*, 316.
(18) Hansen, P. E. *Magn. Reson. Chem.* **1993**, *31*, 23.
(19) Hansen, P. E. *J. Mol. Struct.* **1994**, *321*, 79.
(20) Ng, S.; Lee, H.-H.; Bennett, G. J. *Magn. Reson. Chem.* **1990**, *28*, 337.
(21) Hansen, P. E. In *The Chemistry of Double Bonded Functional Groups*; Patai, S., Ed.; Wiley: New York, 1989, p 83.
(22) Hansen, P. E.; Bolvig, S.; Duus, F.; Petrova, M. V.; Kawecki, R.; Krajewski, P.; Kozerski, L. *Magn. Reson. Chem.* **1995**, *33*, 621.
(23) Hansen, P. E.; Duus, F.; Bolvig, S.; Jagodzinski, T. S. *J. Mol. Struct.* **1996**, *378*, 45.
(24) Hansen, P. E.; Christoffersen, M.; Bolvig, S. *Magn. Reson. Chem.* **1993**, *31*, 893.
(25) Khatipov, S. A.; Shapet'ko, N. N.; Bogavev, Yu. S.; Andreichikov, Yu. S. *Russ. J. Phys. Chem.* **1985**, *59*, 2097.

S0002-7863(98)00905-6 CCC: $15.00
Published on Web 08/22/1998

on ^{13}C chemical shifts, $^{n}\Delta C(OD)$, have been studied extensively in intramoleculary hydrogen-bonded systems[4,10-29] and are shown qualitatively to describe hydrogen-bond strength. The latter is described e.g. by the oxygen−oxygen distance ($R_{O\cdots O}$).[30] A weakness so far has been the relatively narrow range of deuterium isotope effect values except in the case of indandiones.[16,22] With the present set of compounds this is now changed. Deuterium isotope effects on chemical shifts have likewise been shown to distinguish "localized" and tautomeric hydrogen-bonded systems,[10,11,15,26,27] and some interesting isotope effects in *o*-hydroxy acyl aromatic compounds in which the acceptor group (RCO) is sterically perturbed previously have been described.[28]

In recent years ab initio methods to calculate nuclear shieldings[31-37] and deuterium isotope effects on nuclear shieldings[38,39] have been developed to a high degree of accuracy and have become generally accessible due to still faster computers and commercial software. Furthermore, the theoretical developments of Jameson[40,41] and Chesnut[42] have made it possible to identify the important contribution to the secondary isotope effect to a product of the first derivative of the nuclear shielding with respect to O−H(D) bond stretching, $d\sigma/dR_{OH}$, and the change in the average O−H(D) bond length upon deuteriation, $\Delta R_{OH(D)}$.

The main aim of the present study is to demonstrate that deuterium isotope effect on chemical shifts and especially $^{2}\Delta C(OD)$ is a quantitative descriptor of hydrogen-bond strength and how these data are calculated theoretically. A further aim is showing that reliable structures can be obtained and very good ^{1}H and ^{13}C chemical shifts can be calculated in intramolecularly hydrogen-bonded cases.

Experimental Section

Compounds. Compound **2**[49] was synthesized as described but obtained only in a rather low yield from a chromatographic separation on silica gel (eluent: hexane/methylene chloride/methanol, 4:1:1). Compound **3** and its analogues[50] were prepared as described. An elemental analysis gave C: 57.34% and H 4.77% (theoretical C 57.14% and H 4.76%).

Table 1. BPW91/6-31G(d(P)) 5D Calculated Bond Lengths and Angles in **1**−**6**

	1	**2a**	**2b**	**3**	**4**	**5**	**6**
				Bond Length/Å			
R_{C1-C2}	1.437	1.441	1.443	1.444	1.452	1.422	1.438
R_{C2-O}	1.340	1.330	1.326	1.318	1.334	1.335	1.347
R_{O-H}	1.019	1.050	1.045	1.086	1.024	1.022	1.012
$R_{H\cdots O}$	1.577	1.461	1.467	1.360	1.562	1.566	1.607
$R_{O\cdots O}$	2.523	2.459	2.452	2.400	2.518	2.515	2.541
$R_{C7=O}$	1.258	1.268	1.265	1.274	1.259	1.258	1.255
R_{C1-C7}	1.468	1.454	1.469	1.458	1.464	1.470	1.478
				Bond Angle (deg)			
$V_{C1-C2-O}$	121.7	119.2	121.0	119.0	120.5	123.0	122.3
V_{C2-O-H}	104.4	104.0	103.9	103.7	104.6	103.8	104.5
$V_{O-H\cdots O}$	152.1	156.2	154.6	157.7	153.2	152.1	151.3
$V_{C7=O\cdots H}$	102.3	101.1	103.3	102.3	102.0	102.5	102.9
$V_{C1-C7=O}$	120.7	120.8	119.5	119.5	120.6	120.8	120.4
$V_{C2-C1-C7}$	118.6	118.6	117.7	117.8	119.1	117.8	118.7
$V_{C1-C7-C8}$	120.7	121.2	123.1	123.7	121.0	121.0	120.5

NMR. ^{1}H and ^{13}C NMR spectra were recorded on a Bruker AC250 MHz instrument using $CDCl_3$ as solvent except for low-temperature spectra for which CD_2Cl_2 was used. TMS was used as internal reference. ^{13}C NMR spectra were recorded with a spectral resolution of 0.55 Hz/point. COLOC[43] spectra were recorded as described earlier.[24]

Spectra of isotopologues were repeated with different deuterium contents.

Calculations. The molecular geometries were optimized using the Gaussian94 suite of programs[31] and BPW91 Density Functional Theory (DFT) (Beckes exchange[44] and Perdew−Wang correlation terms[45]), and a mix of the built-in Gaussian-type basis sets. The 6-31G(d) (5D) basis set was used at carbon, oxygen, and hydrogen bound to carbon. The 6-31G(d,p) basis set was used at hydrogens bound to oxygen (hydrogen-bonded chelate hydrogens). No symmetry constraints were used in the geometry optimizations, but all calculated structures were essentially flat with **3** converging toward C_{3h} symmetry, **4** and **5** towards C_{2v} symmetry, and **6** toward C_{2h} symmetry. The resulting geometries with some relevant bond lengths and angles are shown in Table 1 and in Scheme 1.

In addition to the compounds shown in Scheme 1, structures of compounds at the same level of calculations are given in Table 1S (Supporting Information): salicylaldehyde (**7**), 1-acetyl-2,4-dihydroxy-3-formylbenzene (**8**), 1-acetyl-2,6-dihydroxy-3-formylbenzene (**9**), 1,3-diformyl-2,4-dihydroxybenzene (**10**), 1,3-diacetyl-5-formyl-2,4-dihydroxybenznene (**11**), 1-acetyl-3,5-diformyl-2,4,6-trihydroxybenene (**12**), and 1,3,5-triformyl-2,4,6-trihydroxybenzene (**13**).

The NMR nuclear shieldings were calculated with the 6-31G(d) (6D) basis set using the GIAO[32,33] method and with the exchange term only on the fully converged molecular orbitals, B(PW91), recently shown to yield superior results relative to the RHF/GIAO method,[46] especially for nuclei other than carbon (Table 2). The correlation between the experimental chemical shifts and the calculated nuclear shielding is shown in Figure 1a,b for ^{1}H and ^{13}C signals, respectively.

The first derivative of the nuclear shielding with respect to the O−H bond lengths ($d^{13}C/dR_{O-H}$) was calculated simply by shortening the O-H bond by 0.01 Å and recalculating the nuclear shielding. The derivatives of the nuclear shielding with respect to O-H bond length are shown in Scheme 2.

The amount of the O−H bond shortening due to hydroxy deuterium isotope substitution ($\Delta R_{OH(D)}$) was calculated by scanning the O-H bond in the bond direction at the BPW91/6-31G(d(p)) level in eight increments of 0.05 Å around the equilibrium position, yielding a total

(26) Bordner, J.; Hammen, P. D.; Whipple, E. B. *J. Am. Chem. Soc.* **1989**, *11*, 6572.
(27) Bolvig, S.; Hansen, P. E.; *Magn. Reson. Chem.* **1996**, *34*, 467.
(28) Hansen, P. E.; Ibsen, S. N.; Kristensen, T.; Bolvig, S. *Magn. Reson. Chem.* **1994**, *32*, 399.
(29) Zheglova, D.; Genov, D. G.; Bolvig, S.; Hansen, P. E.; *Acta Chem. Scand.* **1997**, *51*, 1016.
(30) Hofacker, G. L.; Marchal, Y.; Ratner, M. A. In *The Hydrogen Bond*; Schuster, P.; Zundel, G.; Sandody, C.; Eds.; North-Holland: Amsterdam, 1976; p 1.
(31) Frisch, M. J.; Trucks, G. W.; Schlegel, H. B.; Gill, P. M. W.; Johnson, B. G.; Robb, M. A.; Cheeseman, J. R.; Keith, T. A.; Petersson, G. A.; Montgomery, J. A.; Raghavachari, K.; Al-Laham, M. A.; Zakrzewski, V. G.; Ortiz, J. V.; Foresman, J. B.; Peng, C. Y.; Ayala, P. A.; Wong, M. W.; Andres, J. L.; Replogle, E. S.; Gomperts, R.; Martin, R. L.; Fox, D. J.; Binkley, J. S.; Defrees, D. J.; Baker, J.; Stewart, J. P.; Head-Gordon, M.; Gonzalez, C.; Pople, J. A. *Gaussian94* (Revision C.3); Gaussian, Inc.: Pittsburgh PA, 1995.
(32) Ditchfield, R. *Mol. Phys.* **1974**, *27*, 789.
(33) Wolinski, K.; Hilton, J. F.; Pulay, P. *J. Am. Chem. Soc.* **1990**, *112*, 8251.
(34) Forsyth, D.; Sebag, A. B. *J. Am. Chem. Soc.* **1997**, *119*, 9483.
(35) de Dios, A. C.; Oldfield, E. *Solid State NMR* **1996**, *6*, 101.
(36) de Dios, A. C. *J. Prog. NMR* **1996**, *29*, 229.
(37) Barfield, M.; Fagerness, P. *J. Am. Chem. Soc.* **1997**, *119*, 8699.
(38) Hansen, P. E.; Langgård, M.; Bolvig, S. *Pol. J. Chem.*, in press.
(39) Munch, M.; Hansen, P. E.; Hansen, Aa. E. *Acta Chem. Scand.* **1992**, *46*, 1065.
(40) Jameson, C. J. In *Isotopes in the Physical and Biomedical Sciences, Isotopic Applications in NMR Studies*; Buncel, E., Jones, J. R., Eds.; Elsevier: Amsterdam, 1991; p 1.
(41) Jameson, C. J. In *Encyclopedia of NMR*; John Wiley: New York, 1995; Vol. 6.
(42) Chesnut, D. B.; Foley, C. K. *J. Chem. Phys.* **1986**, *84*, 852.
(43) Kessler, H.; Griesinger, C.; Zarbock, J.; Loosli, H. R. *J. Magn. Reson.* **1984**, *57*, 331.
(44) Becke, D. *Phys. Rev. A* **1988**, *38*, 3098.
(45) Perdew, P.; Wang, Y. *Phys. Rev. B* **1992**, *45*, 13244.
(46) Cheeseman, R.; Trucks, G. W.; Keith, T. A.; Frisch, M. J. *J. Chem. Phys.* **1996**, *104*, 5497.

Scheme 1. BPW91/6-31 G(d(p)) Optimized Structures with Some Relevant Geometric Features (Distances are in Å; $R_{O\cdots O}$ distances in bold.)

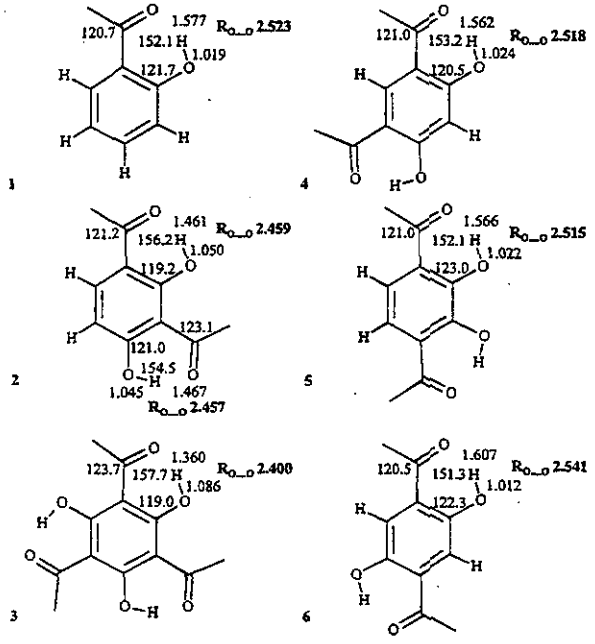

Table 2.

Experimental ^1H Chemical Shifts (δ^1H) (ppm)

	H1	H2	H3	H4	H5	H6
1	2.60	12.26	6.48	7.48	6.90	7.74
2	2.57	14.79	2.78	14.26	6.46	7.82
3	2.73	17.09				
4	2.64	13.09		6.36		8.22

GIAO B(PW91)/6-31G(d) Calculated ^1H Nuclear Shielding (σ^1H) (ppm)

	H1	H2	H3	H4	H5	H6
1	29.51	18.62	25.26	24.75	25.38	24.64
2	29.61	16.25	29.28	16.57	25.91	24.74
3	29.33	14.44				
4	29.58	18.47		26.06		24.46
5	29.51	18.20			25.29	
6	29.45	19.64		25.15		

Experimental Carbon Chemical Shifts ($\delta^{13}C$) (ppm)

	C1	C2	C3	C4	C5	C6	C7	C8	C9	C10
1	119.6	162.4	118.2	136.3	118.8	130.6	204.5	26.5		
2	112.0	168.2	109.9	170.9	109.6	137.8	202.9	26.2	205.6	33.5
3	103.2	175.7					205.0	32.9		
4	113.6	168.9	105.0			136.2	202.4	26.0		

GIAO B(PW91)/6-31G(d) (6D) Calculated ^{13}C Nuclear Shielding ($\sigma^{13}C$) (ppm)

	C1	C2	C3	C4	C5	C6	C7	C8	C9	C10
1	76.3	32.7	76.6	61.5	79.0	67.1	−2.8	163.0		
2	82.4	27.7	83.4	26.0	84.7	61.7	0.9	163.8	−3.4	155.8
3	87.8	23.0					−1.6	156.6		
4	81.6	28.8	89.7			63.0	−0.4	163.6		
5	74.6	38.0			79.9		−3.6	162.5		
6	72.0	41.6	76.8				−4.9	162.4		

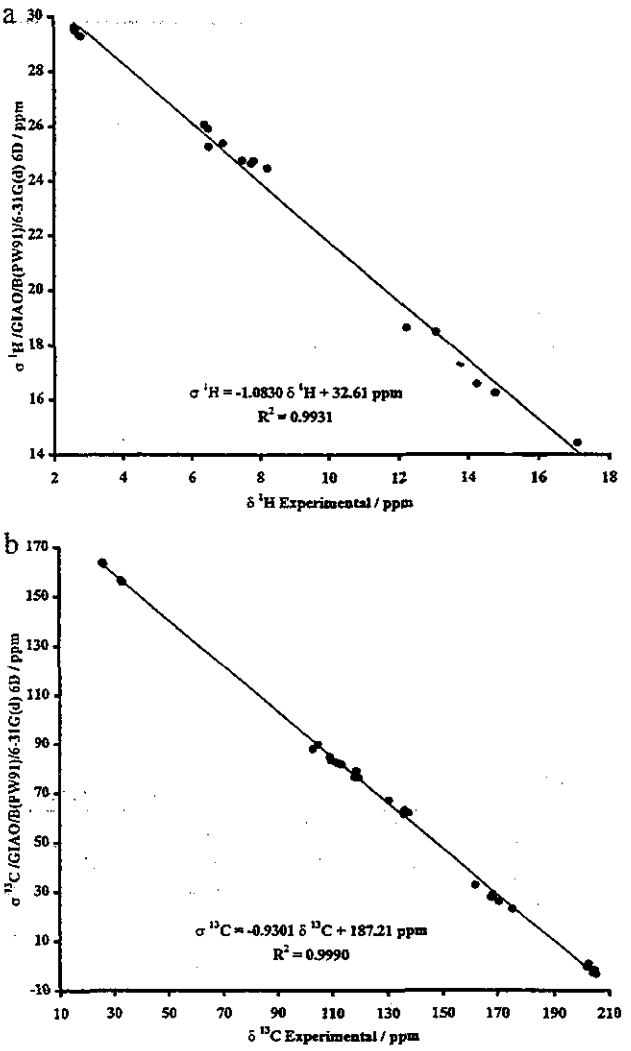

Figure 1. GIAO/B(PW91)/6-31G(d) (exchange term only) calculated nuclear shieldings vs experimental: (a) ^1H and (b) ^{13}C chemical shifts.

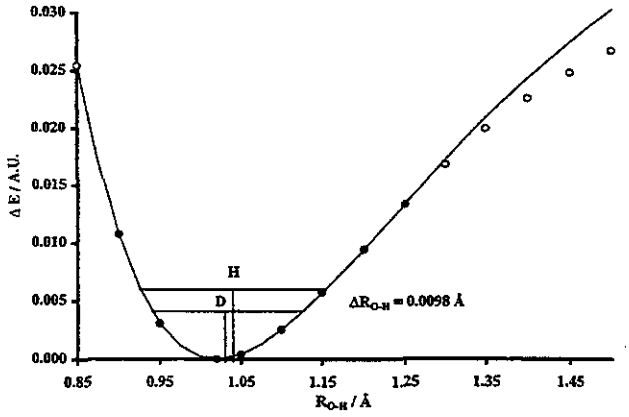

Figure 2. BPW91/6-31G(d(p)) calculated Morse function for O—H hydrogen displacements in the bond direction of **1**, including the average O—H(D) geometry and the zero-point energy for the two isotopologues. Open circles are calculated data not used in the fit.

of nine points. A Morse function was fitted to the points that were below three times the zero-point energy. The O-H bond length perturbation was calculated from the analytical solution to the Morse oscillator,[47,48] using the reduced masses, from a harmonic approximation normal mode analysis (IR frequency calculation). One example of such a potential energy scan is shown in Figure 2. The $\Delta R_{O-H(D)}$ values are

(47) Nieto, M.; Simmons, L. M., Jr. *Phys. Rev. A* **1979**, *19*, 438.

(48) Dahl, J. P.; Springborg, M. *J. Chem. Phys.* **1988**, *88*, 4335.
(49) Desai, R. D.; Ekhlas, M. *Proc. Ind. Acad. Sci.* **1938**, *8*, 194.
(50) Göschke, A.; Tambor, J. *Ber. Dtsch. Chem. Ges.* **1912**, *45*, 1237.

Scheme 2. GIAO/B(PW91)/6-31G(d) Calculated Nuclear Shielding Gradients for O-H ($d^{13}C/dR_{OH}$ are in units of ppm Å^{-1}; numbers in italics refer to **2b**; $\Delta R_{OH(D)}$, in bold.)

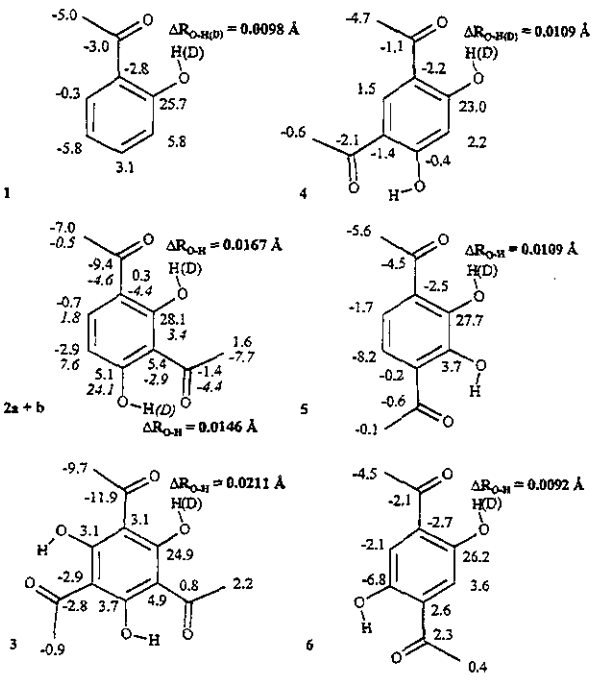

given in Scheme 2, and some of the results of the normal mode analysis and the Morse oscillator, in Table 3.

Assignments. The assignment of **2** was achieved by COLOC[43] experiments. ^{13}C chemical shifts are given in Table 2. The assignment of the isotope effects of compounds with more than one exchangeable OH proton was done in the following fashion. The isotope effects in *o*-hydroxy acyl aromatics were grouped into categories as described in refs 15 and 18 and are roughly similar to those of **1** (Scheme 3). As an example, at the methyl group of the *o*-acetyl group, a negative isotope effect proportional to δOH was observed. A very large and unusual four-bond isotope effect, $^4\Delta C(OD)$ is observed in compounds **2** and **3**. This is assigned to $^4\Delta C$-4(OD-2).

Temperature Effects. The deuterium isotope effects on ^{13}C chemical shifts are measured in one-tube experiments with both the protio and the deuterio species present and in varying ratios. A prerequisite for this type of measurement is slow exchange of the OH proton at the NMR time scale.

For **3**, the *OH* resonance was observed at high frequency, 17.09 ppm, and the C-2,C-4,C-6 carbon resonances showed one very large isotope effect (0.72 ppm) and two medium ones (0.229 and 0.186 ppm). Cooling had no effect on the magnitude of the isotope effects, indicating that tautomerism is not at play.

Results

Theoretical calculations. The ab initio geometries show (Scheme 1) that all of the carbons of the structures are in one plane. Furthermore, a large gradual increase in the OH bond length (R_{OH}) and a corresponding large gradual decrease in the C=O···H distance occurred when going from **1** to **2** to **3** with **4** being similar to **1**. The decrease in C=O···H distance is followed by a decrease in $R_{O\cdots O}$ (**1**, 2.523 Å; **4**, 2.518 Å; **2a**, 2.459 Å (steric compression at oxygen), **2b**, 2.457 Å (steric compression at methyl group); **3**, 2.400 Å. Plots of R_{OH}, $R_{C=O}$, and $R_{(O)H\cdots O}$ vs $R_{O\cdots O}$ or $\Delta R_{OH(D)}$ showed good correlation (Figure 3a,b).

A comparison of the calculated structures of **4** and **6** with the low-resolution X-ray structures[53,54] yielded average (RMSD) absolute atomic coordinate differences of 0.027 (0.011) and 0.032Å (0.020), respectively between corresponding heavy atoms in the superimposed geometries. Furthermore, plotting the data of $R_{O\cdots O}$ vs R_{OH} onto the graph of Steiner and Saenger[55] gave data points on the correlation line of that plot.

^1H and ^{13}C Chemical Shifts and Derivatives. The ^1H and ^{13}C chemical shifts are calculated very well using GIAO B(PW91)/6-31G(d) DFT ab initio methods as seen from Figure 1, which indicates that the quality of the calculated structures including the hydrogen-bond geometry is very good.

The first derivative of the nuclear shielding $d\sigma/dR_{OH}$ was calculated ab initio using the above-mentioned geometries (see Experimental Section) simply by shortening the OH bond 0.01 Å and recalculating the nuclear shielding. The $d\sigma/dR_{OH}$ is nicely correlated to the isotope effects within each compound and is seen not to vary much from compound to compound (Scheme 2 and Figure 4a) except for C-7, for which the $d\sigma/dR_{OH}$ decreased in going from **1** to **2** to **3**. Furthermore, those data for C-7 fall outside the correlation line for all the four compounds (One illustration is given in Figure 4a).

Changes in the Average Bond Length upon Deuteriation. Deuteriation at the OH position will lead to a change in the average OH(D) bond length, and as this vibrational mode is very localized and does not involve significant movement of other atoms in the molecule (Table 3) this will likely be the dominant effect of deuteriation for all other species than **3**. A potential scan of the OH bond stretching as described in the experimental section and shown in Figure 2 is constructed (BPW91/6-31G(d(p)) data). These data are fitted with a Morse function,[47,48] leading to the changes in the OH bond length upon deuteriation $\Delta R_{OH(D)} = R_{OH} - R_{OD}$ as seen in Scheme 2. We have scanned the entire vibrational normal coordinate from a harmonic approximation normal mode analysis for several systems, but the differences between this more rigorous treatment and the values shown here are negligible. To calculate the hydrogen displacement one needs the reduced masses, and we have just used those calculated in the normal mode analysis for OH and OD isotopologues, but again the differences between using the correct value or just values of 1 for H and 2 for D are negligible, except for **3**. The values presented are calculated from the analytical solution to the Morse oscillator.[47,48]

A dramatic increase is found in $\Delta R_{OH(D)}$ in going from **1** to **2** to **3**. Again, values for **4**−**6** are very similar to those of compound **1**. The $\Delta R_{OH-4(D)}$ of O−H4 in **2b** is seen to fall in between the value of **1** and $\Delta R_{OH-2(D)}$ of **2a**. R_{OH} and $\Delta R_{OH(D)}$ correlated well ($R = 0.982$) (Figure 3b).

By knowing the change in the bond length upon deuteriation as just described and the first derivative of the shielding, the isotope effects can be calculated as $d\sigma/dR_{OH} \times \Delta R_{OH(D)}$ (see Discussion). Figure 4b has the derivatives of the nuclear shieldings plotted against the experimental $^n\Delta C(OD)$ values and a plot of the experimental vs calculated isotope effects reveals a very good correlation, which improves when using the normal mode related reduced masses. Although the calculated values are slightly too small it is readily apparent that the slopes for each compound have become much more alike (not shown).

Two-Bond Deuterium Isotope Effects on ^{13}C Chemical Shifts, $^2\Delta C(OD)$. The $R_{O\cdots O}$ are distances correlated with $^2\Delta C$-(OD) ($R = 0.977$).

(51) Borisov, E. V.; Zhang, W.; Bolvig, S.; Hansen, P. E. *Magn. Reson. Chem.*, in press.
(52) Bax, A.; Freeman, R. *J. Am. Chem. Soc.* **1982**, *104*, 1099.
(53) Kokoila, M. K.; Nirmala, K. A.; Puttaraja; Shamala, N. *Acta. Crystallogr.* **1992**, *C48*, 1133.
(54) Wajsman, E.; Grabowski, M. J.; Stepien, A.; Cygler, M. *Cryst. Struct. Comm.* **1978**, *7*, 233.
(55) Steiner, Th.; Saenger, W. *Acta Crystallogr.* **1994**, *B50*, 348.

Table 3. O—H(D) Stretching Mode Morse Function Parameters and Normal Mode Analysis Calculated Reduced Masses and Vibrational Frequencies

	1	2a	2b	3	4	5	6
α^a (Å^{-1})	3.2	4.0	3.8	4.0	3.4	3.4	3.2
dissociation energy^a (kJ)	129.0	51.4	63.9	34.6	106.3	106.5	143.1
μ (O—H) reduced masses^b (amu)	1.0743	1.0995	1.0871	1.1385	1.0764	1.0748	1.0693
μ (O—D) reduced masses^b (amu)	2.3061	2.6591	2.5067	4.2013^c	2.3259	2.3137	2.2783
ν (O—H) vibrational frequency^b (cm^{-1})	2873	2420	2506	2049	2808	2838	3008
ν (O—D) vibrational frequency^b (cm^{-1})	2104	1811	1858	1639	2062	2080	2194

^{a} From Morse function fitted to O—H bond stretching BPW91/6-31 G(d(p)) 5D potential. ^{b} BPW91/6-31G(d(p)) 5D harmonic approximation normal-mode analysis calculated values. ^{c} The higher reduced mass for **3** is caused by coupling of the OD stretch vibration in this compound to other vibrational modes in particular the C=O stretch mode.

Scheme 3. Experimentally Observed Deuterium Isotope Effects on ^{13}C and ^1H Chemical Shifts (^1H chemical shifts are in italics.)[a]

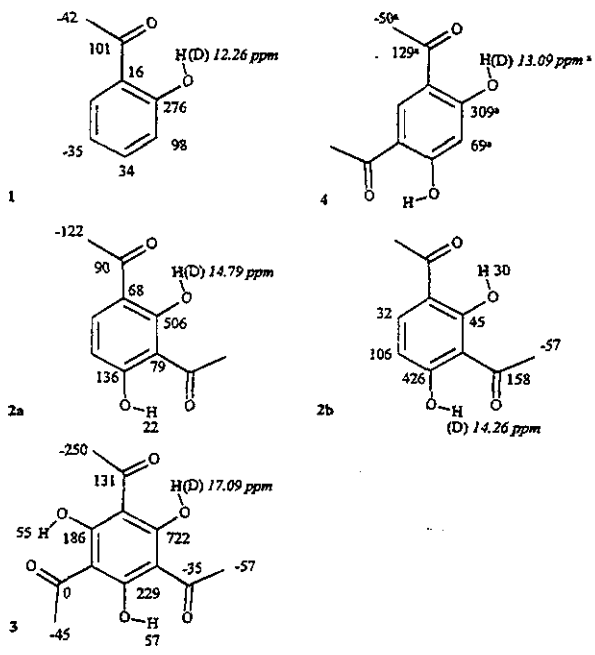

[a] 230 K in CD_2Cl_2. [b]$\Delta C(OD)$ for **2a** at 260 K in $CDCl_3$ C-1, 67 ppb; C-2, 416 ppb; C-4, 63 ppb; C-7, 104 ppb and C-8, −125 ppb. **2b** at 260 K in $CDCl_3$, C-2, 136 ppb; C-3, 86 ppb; C-4, 485 ppb; C-5, 124 ppb; C-6, 32 ppb; C-9, 159 ppb and C-10, −85 ppb. **3** at 250 K in CD_2Cl_2, C-2, 724 ppb.

A comparison of $^2\Delta$C-2(OD) of **1**−**4** revealed that **1** and **4** are very similar, but the values for **2** had increased dramatically and even more so for **3**. The increase from **1** to **2** to **3** can be ascribed to steric compression (see Discussion) leading to a shorter $R_{O\cdots O}$ and hence to a long R_{OH} and short $R_{OH\cdots O}$ distances. A small steric effect was found in 3,5-di-*tert*-butyl-2-hydroxyacetophenone,[10] and a large one also in the *tert*-butyl derivative, 2-pivaloyl-1,3-indandione.[16,22]

$^n\Delta C(OD)$. A comparison of the long-range isotope effects showed a very large four-bond effect, $^4\Delta$C-2(OD-4) in **2** and **3**. Another significant observation is the rather small $^4\Delta$CO-(OD-2) observed parallel with $^5\Delta CH_3$(OD-2) became more and more negative.

Steric Effects. The decrease in $R_{O\cdots O}$ is mainly coupled to a decrease in the C-1,C-2, O and C-2,C-1,C=O angles (see Scheme 1 and Figure 5a). This is seen from the following numbers: the angles (in degrees) (C-2,C-1,C=O and C-1,C-2,O): **1** (118.6; 121.7); **4** (119.0; 120.5); **2a** (118.6; 119.2); and for **2b** angles C-3,C-4,O; C-4,C-3,C=O, 121.0, 117.7; **3** (117.8; 119.0).

A comparison of calculated bond length of **3** and the corresponding molecules in which one, two, or three of the acetyl groups are replaced by formyl groups (**11**−**13**, for data see Table 1S) revealed that the $R_{O\cdots O}$ distances for an intramolecular hydrogen bond of $CH_3CO\cdots HO$ type are similar for similar steric motifs (Figure 5b) irrespective of the number of acetyl or formyl groups on the benzene ring. The same is true for a $HCO\cdots HO$ type of hydrogen bonds. For a $CH_3CO\cdots HO$ motif with Y = OH and X = CH_3C=O, $R_{O\cdots O} = 2.402 \mp 0.002$

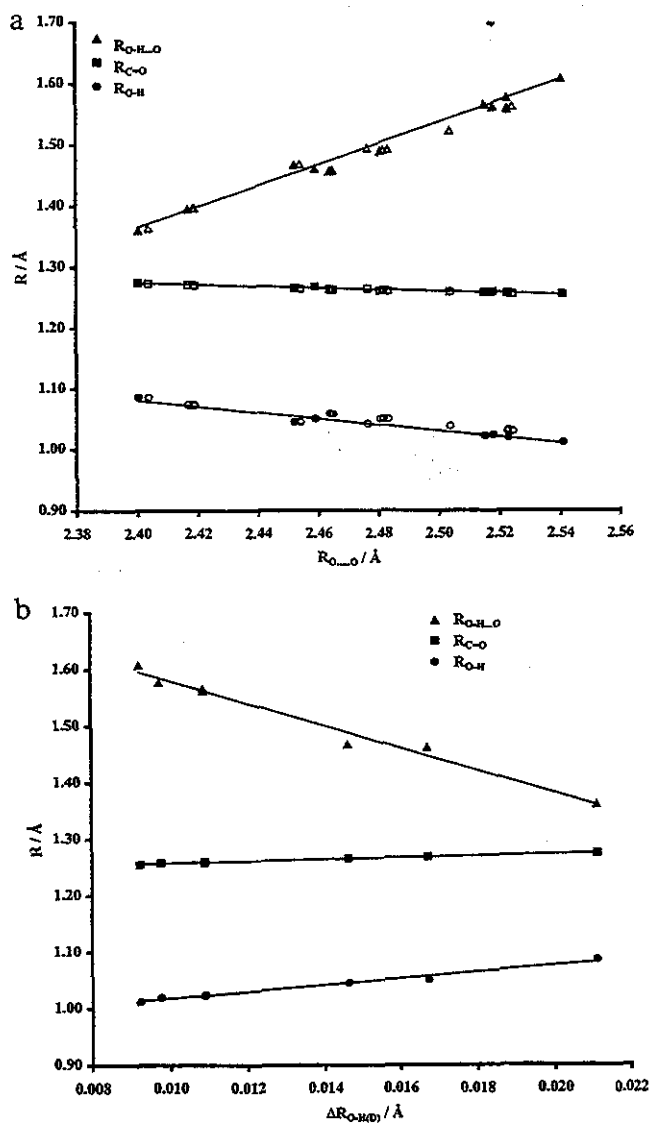

Figure 3. (a) Plot of $R_{(O)-H\cdots O}$, $R_{C=O}$, and R_{OH} distances vs $R_{O\cdots O}$ distances and (b) plot of $R_{(O)-H\cdots O}$, $R_{C=O}$, and R_{OH} distances vs $\Delta R_{OH(D)}$ distances. All data are from calculated structures. Open symbols are used for aldehyde analogues, compounds **7**−**13** (see Table s1); filled symbols, for compounds **1**−**6**. Regression line is based on data for compounds **1**−**6** only.

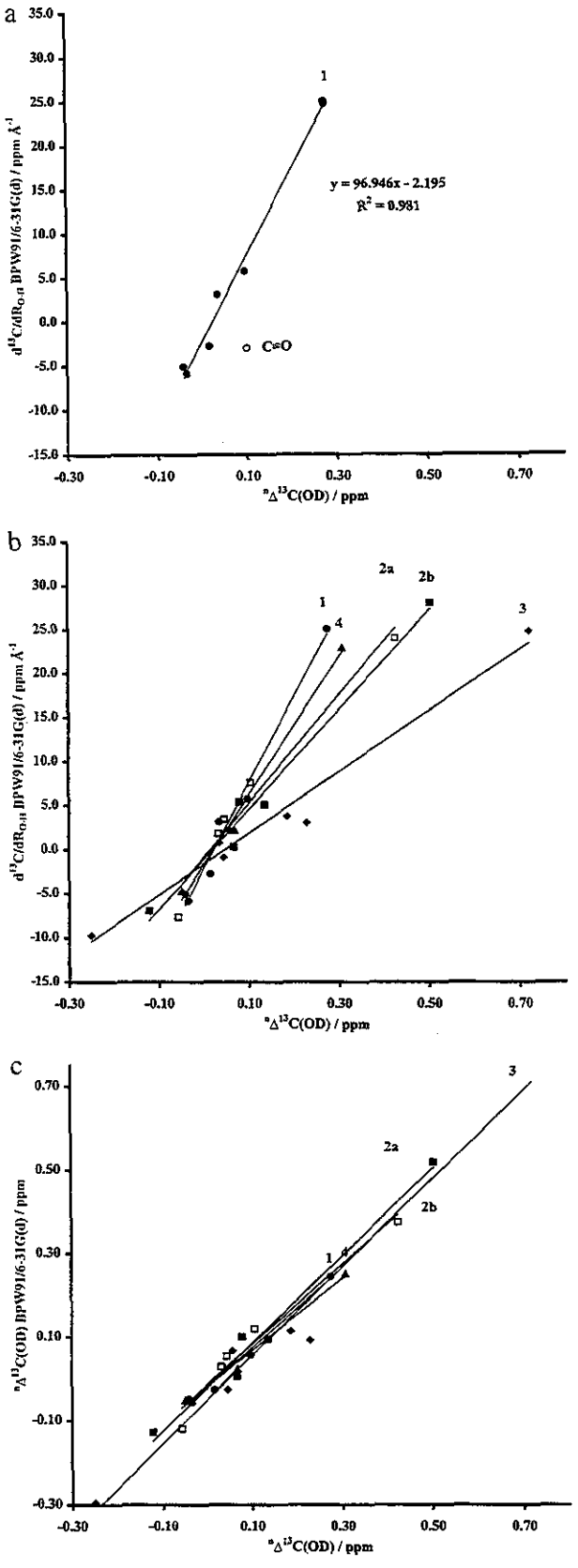

Figure 4. (a) Calculated ^{13}C Nuclear shielding gradients ($d^{13}C/dR_{OH}$) values plotted against the experimental isotope effects for **1** and (b) for **1**−**4**, and (c) calculated isotope effects using BPW91/6-31G(d(p)) 5D normal mode analysis calculated reduced masses in the average vibrational geometry calculation, plottet agains the experimental values.

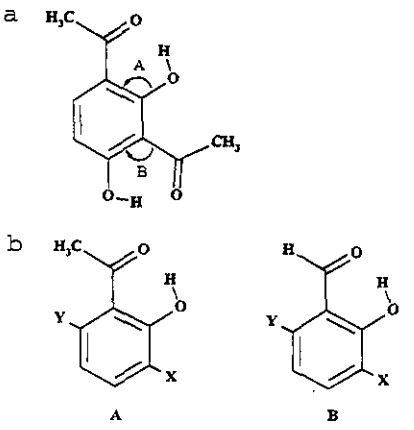

Figure 5. (a) Model for steric interactions and (b) steric motifs.

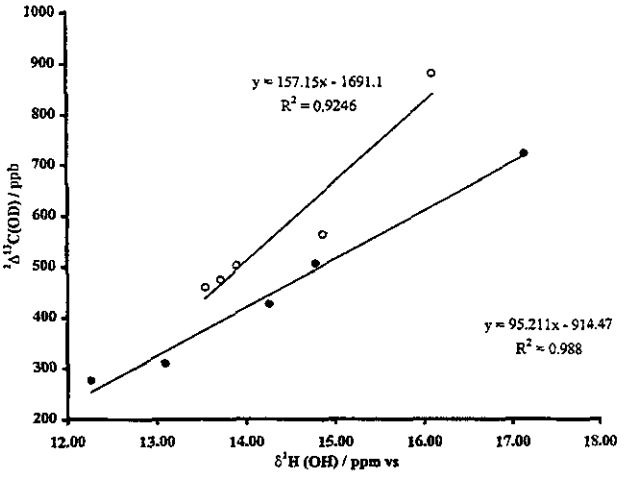

Figure 6. Plot of experimental δOH vs $^2\Delta C(OD)$: (●) *o*-hydroxy acyl aromatics and (○) indandiones from refs 16 and 22.

Å; Y = OH and X = HC=O, $R_{O\cdots O}$ = 2.418 ∓ 0.001 Å and Y = OH and X = H. $R_{O\cdots O}$ = 2.456 Å. For HC=O···HO with Y = OH and X = CH_3C=O, $R_{O\cdots O}$ = 2.464 ∓ 0.001 Å; Y = OH and X = HC=O, $R_{O\cdots O}$ = 2.482 ∓ 0.001 Å and Y = OH and X = H, $R_{O\cdots O}$ = 2.524 Å. For **2** and **7**−**10** similar relations can be written. Combining these results, it is found that an acetyl group ortho to the OH group of an intramolecular hydrogen bond causes a decrease in $R_{O\cdots O}$ of 0.017 Å more than for a compounds with a formyl group in the ortho position.

δOH vs $^2\Delta C(OD)$. The unusually large $^2\Delta C(OD)$ isotope effects for benzene derivatives observed in this study allowed an extension of the range previously studied.[10,15,17,18] As seen from Figure 6 a reasonable correlation is found between δOH and $^2\Delta C(OD)$(R = 0.93). The data for the indandiones[22] show possibly a steeper slope (0.157) than those of the benzene derivatives (0.095) and larger $^2\Delta C(OD)$ (Figure 6).

$^6\Delta OH(OD)$. Relatively large deuterium isotope effects on O*H* chemical shifts are observed over six bonds, $^6\Delta OH(OD)$ in **2** and **3**. For **2**, $^6\Delta$OH-2(OD-4) < $^6\Delta$OH-4(OD-2).

Discussion

The following discussion of deuterium isotope effects and their correlation to hydrogen bond strength is based on the assumption that the isotope effects to a large extent can be approximated by the term, $d\sigma/dR_{OH} \times (\Delta r - \Delta r^*)$. The former is termed, by Jameson, the electronic factor and tells how the effect is transmitted through the bonds. The latter is the change in the mean O-H distance upon deuteriation (called $\Delta R_{OH(D)}$ in

this paper). A justification for leaving out terms involving bond angle deformations and second order terms are given by Jameson[40,41] and by the results on second-order derivatives by Chesnut.[42] Other important points are that the displacements are close to the equilibrium geometry and that the nuclear shielding is linear in this region.[39,41,56] A further basic assumption is that hydrogen bond strength can be described by the $R_{O\cdots O}$ distance.[30]

The study of *o*-hydroxy acyl aromatics and the corresponding aldehydes showed that the isotope effects of the two types of compounds were proportional, supporting the idea that the isotope effect depended on two factors, $d\sigma/dR_{OH}$ and $\Delta R_{OH(D)}$. The present study shows that the latter factor is very important (Scheme 2) as the former is more or less constant for all compounds (Scheme 2). It is also interesting to notice that the calculated slopes, $d\sigma^{13}C\text{-}x/dR_{OH}$ for **1** compare quite well with the transmission coefficients estimated in ref 18.

Hydrogen-Bond Strength. A very important task is the development of parameters to gauge the strength of the hydrogen bond. As mentioned in the introduction, $^2\Delta C(OD)$ and δOH have been used extensively.[10,13,16] The plot of $R_{O\cdots O}$ vs $^2\Delta C$-(OD), the former based on calculations, shows a good correlation thereby confirming that $^2\Delta C(OD)$ is a proper gauge for hydrogen bond strength. $\Delta R_{OH(D)}$ is the factor determining the magnitude of isotope effects in these intramolecularly hydrogen-bonded systems. This parameter is shown to be proportional to R_{OH}, which is again proportional to $R_{O\cdots O}$ so many parameters are actually good descriptors of hydrogen-bond strength.

The correlation between R_{OH} and $R_{O\cdots O}$ shows a good agreement with the data of Gilli et al.[3], but less so with those of Ichikawa.[57]

^{1}H Chemical Shifts. OH and NH chemical shifts of hydrogen-bonded systems have been used extensively as markers of hydrogen bonding.[4,11,12,14,25] The *OH* chemical shifts are calculated very well in the RAHB cases of this paper even using moderate basis sets (see the Experimental Section). This is not the case for e.g. NH protons of proteins[56] in which environmental factors other than the hydrogen-bond partner may contribute significantly and the geometrical uncertainties likewise.

^{13}C Chemical Shifts. Calculation of ^{13}C chemical shifts have been discussed with respect to different methods. No significant differences were found[60] between LORG[58] and the IGLO[59] method or between the LORG and the GIAO[32,33] methods.[56] Recently, ^{13}C chemical shifts have been calculated on the basis of MM3, MMX, or B3LYP optimized structures.[34] Calculations of ^{13}C chemical shifts have also been investigated in protein fragments (end-capped amino acids)[56] and in proteins in general.[35] In the present case a very good correlation is found (Figure 1b). ^{13}C chemical shifts can be predicted to an accuracy of 2 × 1.85 ppm (2 × RMSD), which is extraordinary. A slope different from −1 is obtained (see Figure 1b), as has also been found in other studies.[34] A key to the successful calculations is the blend of DFT theory in the BPW91 version with only the exchange terms in the calculation of chemical shifts,[46] the use of fully optimized DFT ab initio geometries,[34] and probably to a lesser extent use of polarization basis functions at the chelate proton in the geometry optimization.

Steric Factors. The effect of steric hindrance can be divided into two, in some instances possibly mutual interactions as demonstrated in Figure 5a. One is the steric effect on the OH group caused by the methyl group of an acetyl group leading to a decrease in the angle A (Figure 5a) and the other one is steric compression of a carbonyl group caused by an oxygen and the methyl group of the acetyl group leading to a decrease of angle B. This is also seen from the angles C-2,C-1,C=O and C-1,C-2,O (see previously). A support for a steric model is the finding that structure calculations of **7**−**13** clearly show how the acetyl group leads to a larger decrease of $R_{O\cdots O}$ compared to a formyl group. For a given steric motif the results are similar whether a formyl or acetyl group are in the noninteracting positions (compare e.g. **3** and **11**). This is interesting as the formyl and acetyl groups are electronically different.

Conclusions

Structures of intramolecularly hydrogen-bonded *o*-hydroxy acyl aromatics are calculated to a good accuracy using DFT methods.

OH chemical shifts of these systems can be calculated to a very good accuracy using ab initio methods in moderate basis sets. In addition ^{13}C chemical shifts can be calculated well. A prerequisite is the use of fully optimized DFT geometries.[42,43]

It is demonstrated that $^2\Delta C(OD)$ isotope effects and δOH reflect the strength of the hydrogen bond well. The dominant factor of the $^n\Delta C(OD)$ isotope effects is the variation of the vibrational average of the O−H(D) bond length upon deuteriation rather than the derivative of the nuclear shielding with respect to OH bond shortening, $d\sigma/dR_{OH}$.

For the benzene derivatives having multiple OH and acyl groups, $^n\Delta C(OD)$ and the hydrogen bond strength are seen to increase due to an inductive effect (small) combined with a stronger steric compression effects.

Acknowledgment. The authors thank Anne Lise Gudmundsson for valuable help in recording some of the spectra and preparing some of the compounds and docent Aa. E. Hansen, University of Copenhagen for support. The Danish Science Research Council is thanked for support to S.B. and for providing computer CPU time.

Supporting Information Available: Two figures showing plots of experimentally determined $^n\Delta C(OD)$ isotope effects vs $d^{13}C/dR$, $^n\Delta C(OD)$ and plots of $A_{C-C(=O)CH_3}$ vs $R_{O\cdots O}$ and $A_{C1,C2-O(H)}$ vs $R_{O\cdots O}$ and a table giving calculated distances for **7**−**13** (6 pages, print/PDF). See any current masthead page for ordering information and Web access instructions.

JA9809051

(56) Abildgaard, J.; Bax, A.; LiWang, A.; Hansen, P. E. Manuscript in preparation.
(57) Ichikawa, M. *Acta Crystallogr.* **1978**, *B34*, 2074.
(58) Hansen, Aa. E.; Bouman, T. D. *J. Chem. Phys.* **1985**, *82*, 5035.
(59) Kutzelnigg, W. *Isr. J. Chem.* **1980**, *19*, 193.
(60) Facelli, J. C.; Grant, D. M.; Bouman, T. D.; Hansen, Aa. E. *J. Compt. Chem.* **1990**, *11*, 32.

Reprinted from

CHEMICAL PHYSICS LETTERS

Chemical Physics Letters 224 (1994) 275–282

Ab initio calculations of external charge effects on the isotropic ^{13}C, ^{15}N and ^{17}O nuclear shieldings of amides ☆

Poul Erik Hansen [a], Jens Abildgaard [a], Aage E. Hansen [b]

[a] *Department of Life Sciences and Chemistry, Roskilde University, P.O. Box 260, DK-4000 Roskilde, Denmark*
[b] *Chemical Laboratory IV, The H.C. Ørsted Institute, Universitetsparken 5, DK-2100 Copenhagen Ø, Denmark*

Received 18 February 1994; in final form 16 May 1994

ELSEVIER

15 July 1994

ELSEVIER

Chemical Physics Letters 224 (1994) 275–282

CHEMICAL PHYSICS LETTERS

Ab initio calculations of external charge effects on the isotropic ^{13}C, ^{15}N and ^{17}O nuclear shieldings of amides ☆

Poul Erik Hansen [a], Jens Abildgaard [a], Aage E. Hansen [b]

[a] *Department of Life Sciences and Chemistry, Roskilde University, P.O. Box 260, DK-4000 Roskilde, Denmark*
[b] *Chemical Laboratory IV, The H.C. Ørsted Institute, Universitetsparken 5, DK-2100 Copenhagen Ø, Denmark*

Received 18 February 1994; in final form 16 May 1994

Abstract

$^{13}C{=}O$, $^{13}CH_3$, ^{15}N and ^{17}O isotropic NMR shieldings of model amides, acetamide and N-methylacetamide, in the presence of point charges and of hydrogen fluoride simulating dipolar perturbations, have been calculated by the ab initio LORG method. Positive and negative charges produce similar but opposite changes. The calculated effects are exaggerated compared to experiment, but the trends are reproduced. The results are analyzed in terms of electric field effects and contributions along the bond directions, assuming a $\cos\theta$ angular dependence between the charge and the bond that is polarized, and a $1/r^2$ distance dependence. The parametrized expressions can form a basis for a protocol for analyzing changes in ^{13}C, ^{15}N and possibly ^{17}O amide and peptide shieldings caused by charged perturbers. Conversely, the location of an atom or group changing charge can be inferred from the chemical shift response of nuclei in its vicinity.

1. Introduction

Charges can have important effects on nuclear magnetic shieldings, as revealed e.g. through titration experiments for ^{13}C in amino acids [1,2], peptides [3–5] and proteins [6,7], and for ^{15}N [8,9] and ^{17}O [10]. In addition genetic engineering and new NMR techniques [11,12] have made ^{13}C and ^{15}N shielding data of proteins increasingly accessible, challenging interpretations of the wide range of these shieldings. Early interpretations [13] suggested electric field effects; a theoretical framework for such effects was developed by Stephen [14] and Buckingham [15] (see also Riley and Raynes [16]), and applied in more detail by Batchelor [17–19]. The focus was on the polarization of X–^{1}H bonds, although the method has also been applied to ^{13}C–C single bonds [10,21]. But until quite recently, the more general problem of the shieldings of the heavy nuclei in the peptide unit had hardly been treated theoretically.

However, ab initio calculations of NMR shieldings have now reached a stage, where results of an accuracy comparable to experiments can be obtained [22], and ab initio studies of charge and field effects on NMR shieldings have been reviewed by de Dios and Jameson [23]. In the peptide–protein context, ab initio calculations of charge, dipolar and quadrupolar perturbations of small molecules have been used to model local environmental effects on the CO shielding in carbon-monoxy ligated heme proteins [24] and to rationalize chemical shift ranges in proteins [25], and an ab initio charge-field approach has been applied to predict nuclear shieldings in proteins [26]. In the present work we use the localized or-

☆ Presented in part at "Frontiers of NMR in Molecular Biology", Taos, New Mexico, March 1993.

SSDI 0009-2614(94)00545-2

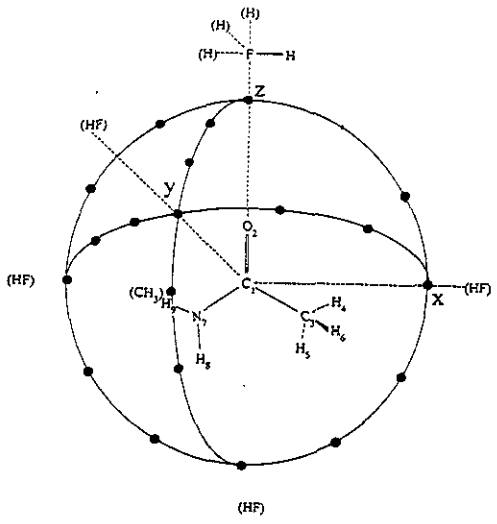

Fig. 1. Molecular geometry of ACAM and MEACAM with charge and HF positions.

bital–local origin (LORG) ab initio method [27,28] to study the shielding of all (non-hydrogenic) nuclei of model amides in the presence of positive and negative point charges simulating charged groups, and with hydrogen fluoride arranged as a dipolar fragment. The positions are chosen to yield balanced maps of the influence of charges and dipoles, and we show that the computed shieldings can be represented to a high degree of accuracy by a charge perturbation model providing a protocol for the dependence on distances and angles for charge and dipolar effects on the C, O and N nuclei of the amide unit.

2. Computational method and results

The amide models chosen were acetamide (ACAM) and N-methylacetamide (MEACAM); the ACAM molecular geometry was obtained from a BIOGRAF force field calculations [1] with the N–CH_3 unit in MEACAM grafted onto an unrelaxed ACAM structure (Table 1). Point charges are placed on domes centered on the carbonyl carbon atom, as shown in Fig. 1 for the positions chosen on a dome of 4 Å radius. Four ACAM calculations were performed both with a positive and a negative unit charge (i.e. 1 au) in the indicated positions on domes of radii 4 and 6 Å. Additional points in the direction of the C–CH_3 bond, at 5 and 7 Å distances, and at 6 Å in this direction at 30° above and below the N–CO–C plane were also included. For MEACAM only points with negative charges on the 6 Å dome were included. To simulate dipolar perturbations, hydrogen fluoride (HF) was placed as shown in Fig. 1 for half of the orientations at one of the five positions (in the other half H and F are interchanged). The HF distance was fixed at the experimental value of 0.917 Å [29].

SCF results were obtained with GAUSSIAN 90 [30], and for the amides we used a [3s2p/2s] basis [31], yielding ground state energies of −207.907651 and −246.924937 E_h for ACAM and MEACAM, respectively, varying up to 0.06 E_h with charges in different positions. For HF we used a [3s3p1d/2s] basis, based on the [3s2p] functions of Ref. [31] mutatis mutandis basis B of Ref. [27], and with a 50–50 contraction of gaussians with exponents 1.05

[1] Biograf, Biodesign Inc., Pasadena, USA.

Table 1
Atomic coordinates and absolute shieldings for the heavy nuclei in ACAM and MEACAM [a]

Atom	Coordinates (Å) [b]			σ(ACAM) [c] calc.	σ(MEACAM) [c] calc.
	x	y	z		
C_1	0.0000	0.0000	0.0000	−7.65	−4.73
O_2	0.0000	0.0000	1.2658	−185.69	−167.12
C_3	1.3254	0.0000	−0.6731	168.73	169.19
N_7	−1.0912	0.0579	−0.7237	171.34	167.53
C_9	−2.4527	0.0857	−0.2255		168.66

[a] See text and Fig. 1 for abbreviations and coordinate system.
[b] The bond lengths are chosen to mimic a peptide.
[c] Isotropic shieldings (in ppm) for the unperturbed molecules.

and 0.30 for the d component. This basis was chosen to ensure proper description of the lone pairs on F and of the virtual space in that region, and gave a ground state energy of $-100.040737\ E_h$. The dipole moment was 1.935 D (exp. 1.826 D [29]), and Mulliken populations gave partial atomic charges of +/− 0.561859 au, varying up to 0.01 au for different orientations of HF in the complexes.

The ab initio shielding calculations employed the LORG method [27,28,32], which is a variant of the coupled Hartree–Fock theory (see e.g. Ref. [28]) where local gauge origins are associated with localized (occupied) orbitals. Because of the strong polarization of the C=O and C–N bonds, care had to be exercised in the choice of localization and of the RMIN parameter [27,33] defining the LORG assignment of the local origins. We used a localization generating a σ, π bond structure for the N–C=O unit, and a value of RMIN identifying the σ(C–N), the σ(C–O) and the σ(C–C) orbitals as bonded to the carbonyl carbon, while the polarization of the π orbitals is so pronounced that their centroids are outside the RMIN radius relative to that atom.

Results for the heavy nuclei in the unperturbed molecules are given in Table 1 [2], with the computed shieldings within the expected range [33,34]. Figs. 2a–2d show the change, i.e. σ(charged) − σ(neutral), in the calculated carbonyl ^{13}C and ^{17}O, the N–methyl ^{13}C and the ^{15}N shieldings for in-plane charges plotted against the angle from the charge to the C=O bond (see Fig. 1). Negative and positive charges show almost exactly opposite effects. For the carbonyl ^{13}C (Fig. 2a) a large effect is found for charges along the C–C bond (angle 118°), with smaller effects for charges along the C=O and N–C(carbonyl) bonds and for charges behind the C–C bond (angle −62°); not unexpectedly, the largest effects are for short distances. MEACAM follows the ACAM trend, except that charges along the N–C(carbonyl) bond contribute slightly more in the former. The ^{17}O shielding (Fig. 2b) is almost unperturbed, except for charges along the C=O bond, while for N–methyl ^{13}C and for ^{15}N (Figs. 2c and 2d), the dominant perturbations lie along the C–C and N–C(carbonyl) directions, respectively. Note that the variations appear less regular for ^{17}O, N–methyl ^{13}C and ^{15}N since the domes are centered on the carbonyl carbon.

[2] Complete tables of computed results are available from the authors upon request.

3. Simulations

In an electric field perturbation approach, the variation in the nuclear shieldings can be modelled by an expression of the following form (see Fig. 3) [5,20]:

$$\Delta\sigma = q \sum_n \sum_{i=0,1} k_{n,i} \cos\theta_{n,i} / r_{n,i}^2 \,. \qquad (1)$$

Here $\Delta\sigma = \sigma(\text{charged}) - \sigma(\text{neutral})$ is the shielding difference of a particular atom induced by the charge q. n indexes a bond to the atom under observation, i indexes the end of the bond where the field component is determined ($i=0$ for the atom under observation and $i=1$ for the atom bonded to it), and the bond coefficients $k_{n,i}$ parametrize the field effects. In their electrostatic treatment of induced charges Schneider et al. [20,21] employ an expression of the same form, but use the midpoint of the bonds as reference points.

Here we test three different simulation schemes for expiscating bond contributions according to Eq. (1) by application of a multivariable linear regression analysis to the entire set of computed shieldings (i.e. 142 and 21 values for ACAM and MEACAM, respectively). The first scheme uses the field components along the bond directions at the nucleus under observation, giving $k_{n,0}$ coefficients ($i=0$ only). The second uses the components along the bond direction at the atoms bound to this nucleus, yielding $k_{n,1}$ coefficients ($i=1$ only), and the third scheme includes both atoms in the bonds (full Eq. (1)). In each of the two methyl groups the C–H bonds are treated as one effective contribution by assigning to the three bonds the same $k_{n,i}$ parameters. For the point charge results we use the actual charges (+/− 1 au), while for the dipolar results we use the average of the partial atomic charges for the various arrangements of the HF fragment (±0.5615 au) (see Section 2).

The results are shown in Table 2. The absence or presence of $k_{n,0}$ and $k_{n,1}$ values reflects the three simulation schemes as described. The relatively large standard deviations found in particular for the $k_{n,0}$ values may indicate that these are not completely independent of the $k_{n,1}$ variables and that for a given

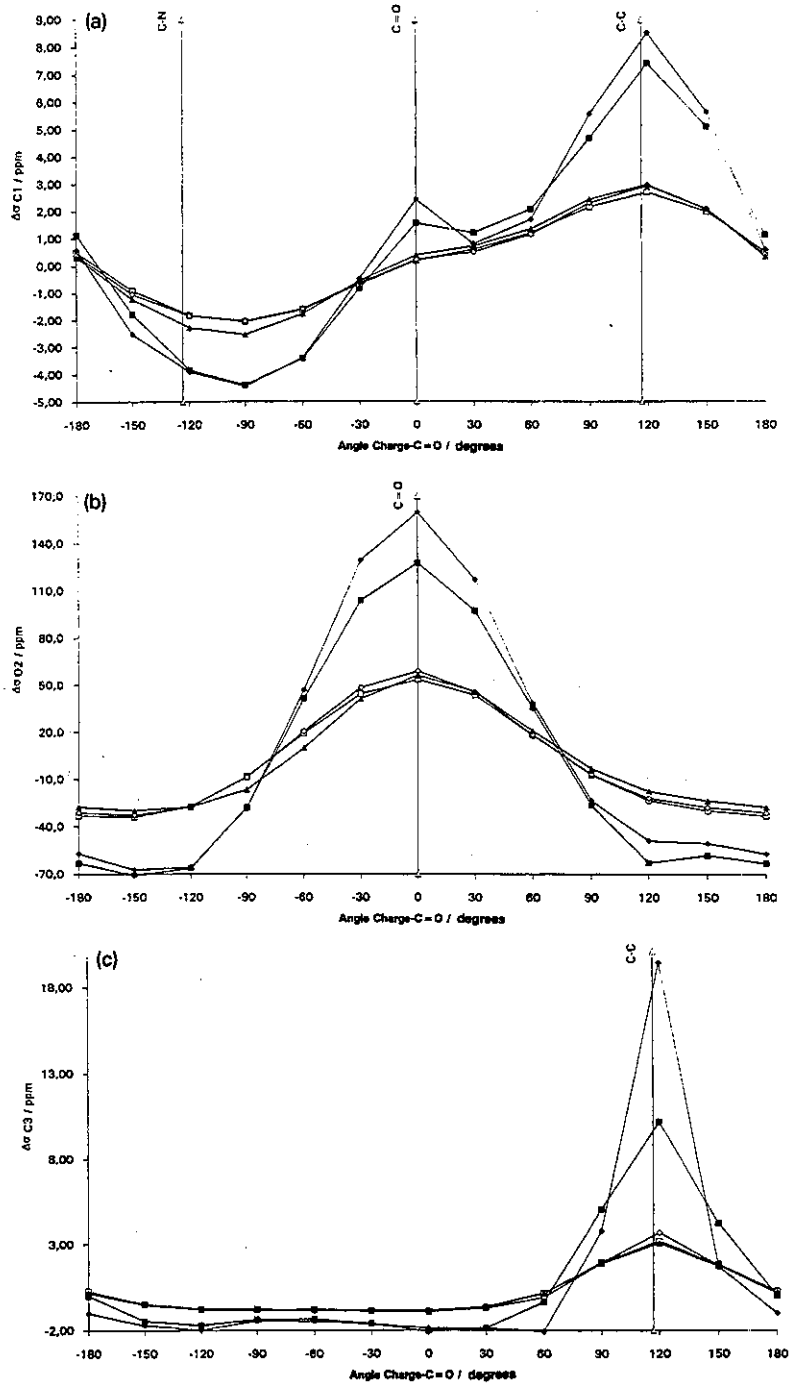

Fig. 2. Changes in isotropic nuclear shieldings (the nuclear shieldings of the figure are multiplied by the point charge sign) of (a) carbonyl carbon, (b) carbonyl oxygen, (c) methyl nitrogen and (d) amide nitrogen versus angles charge-C=O for ACAM and MEACAM. (■) Positive charges, 4 Å; (□) positive charges, 6 Å; (◆) negative charges, 4 Å; (◇) negative charges, 6 Å; (▲) N-methylacetamide, negative charges, 6 Å; (△) bond directions.

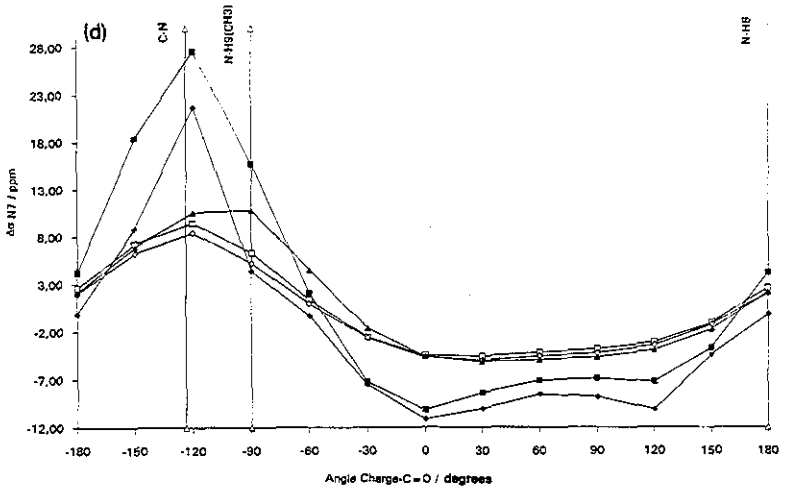

Fig. 2. Continued.

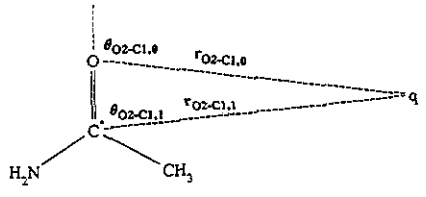

Fig. 3. Example of angles and distances used as geometrical input in Eq. (1). Those shown are the ones used for the ^{17}O nuclear shielding simulation.

atom only one particular direction, not necessarily along any of the actual bonds, may contribute effectively to $\Delta\sigma$ at the nucleus under observation.

As expected, the best fits are obtained when the field components at both atoms of the bonds are included in the simulation for the various nuclei. The parameters are quite sensitive to the choice of simulation, but experimentation with the use of bond midpoints, or other intermediate bond points, following Refs. [20,21] did not suggest consistent improvements relative to the end point simulations (i.e. $i=0$ or $i=1$ only). Between the latter two simulations, the $i=0$ only results are generally better except for the carbonyl ^{13}C nucleus, where the fact that $i=1$ gives the better simulation may be related to the effective electron deficiency of this nucleus caused by the strong bond polarizations discussed above. The accuracy of the full Eq. (1) (six-parameter) simulation of $\Delta\sigma$ for the carbonyl ^{13}C nucleus in ACAM is evident in Fig. 4.

The charge effects at the oxygen shielding are dominated exclusively by contributions along the C=O bond and a simple relationship is thus obtained.

4. Discussion

The main features of isotropic NMR shieldings are generally quite local, making the carbonyl ^{13}C in the present model systems probably the most realistically represented nucleus in terms of polypeptide or protein simulation. The accuracy of the protocol for this nucleus, as evidenced in Fig. 4, is particularly encouraging in terms of potential predictive and analytical value. Specifically, we find that for distances larger than 5 Å the data for carbonyl carbons can to good precision be analyzed in terms of a shielding polarization along the C–C bond using either a three-parameter model, or to higher accuracy a six-parameter model. In addition, there is a significant difference between the results for charge perturbations in front of and behind the C–C bond. Similar trends are seen for the ^{15}N and $^{13}CH_3$ nuclear shieldings, and a combination of titration shifts for these nuclei can therefore be used to locate the charge.

Our approach is different from that the Schneider et al. who calculated atomic charges and used these to estimate the changes in nuclear shielding [21], and from the ab initial work of de Dios et al. [26] which deals with specific shifts in selected proteins. In the

Table 2
Coefficients, R values and standard deviations obtained in fitting the calculated data for $^{13}C{=}O$, ^{17}O, $^{13}CH_3$, ^{15}N and $^{13}CH_3N$ nuclei to Eq. (1)

Atom	Compound	$k_{n,0}$			$k_{n,1}$			R value	Stdv (ppm)	Range (ppm)
		C1–O2	C1–C3	C1–N7	C1–O2	C1–C3	C1–N7			
$^{13}C{=}O$	ACAM	203.4(80.7) [a]	255.4(77.3)	179.5(82.6)				0.851	0.80	15.96
					12.3(2.2)	56.4(2.0)	−17.7(2.3)	0.930	0.55	
		−81.7(27.6)	−28.8(26.3)	−61.2(28.2)	34.0(1.6)	39.9(1.3)	−12.2(1.6)	0.986	0.25	
	MEACAM	−44.3(72.6)	16.6(64.0)	−82.1(78.8)				0.932	0.43	5.53
					0.0(7.1)	45.1(5.8)	−37.0(7.7)	0.951	0.36	
		−47.5(13.8)	14.3(11.8)	−12.8(15.0)	35.5(2.6)	29.9(1.7)	−31.7(2.7)	0.998	0.08	
		O2–C1			O2–C1					
$^{17}O{=}C$	ACAM	−1343.9(26.4)						0.948	8.1	87.9
					−1595.5(49.6)			0.880	3.81	
		−907.4(36.9)			−611.0(45.5)			0.977	6.0	
	MEACAM	−1376.9(52.2)						0.972	5.55	86.4
					−1464.7(114.2)			0.892	9.0	86.4
		−1159.6(144.0)			−257.5(160.0)			0.975	4.4	86.4
		C3–C1	C3–Hx		C3–C1	C3–Hx				
$^{13}CH_3{-}C$	ACAM	309.3(167.0)	356.2(157.5)					0.822	1.0	29.5
					−124.5(8.0)	−68.2(7.5)		0.663	1.4	29.5
		506.6(121.0)	553.5(115.7)		−9.5(7.0)	−38.4(4.1)		0.914	0.71	29.5
	MEACAM	391.4(110.8)	442.1(104.8)					0.973	0.19	3.9
					−52.1(31.4)	3.0(30.7)		0.759	0.55	3.9
		503.3(75.6)	544.3(72.5)		4.6(7.5)	−16.2(6.8)		0.999	0.12	3.9
		N7–C1	N7–H8	N7–H9 or CH_3	N7–C1	N7–H8	N7–H9 or CH_3 [b]			
^{15}N	ACAM	1788.1(492.3)	1787.8(444.2)	1976.6(491.7)				0.891	1.90	49.3
					−210.0(15.6)	0.40(10.1)	8.6(10.0)	0.795	2.60	49.3
		506.0(400.4)	651.3(361.9)	663.3(401.9)	−92.1(11.8)	−70.6(9.4)	−32.5(8.2)	0.937	1.45	49.3
	MEACAM	2076.1(908.7)	2081.4(819.2)	2359.7(907.3)				0.972	0.91	16.0
					−198.0(31.3)	35.9(24.8)	88.1(22.6)	0.951	1.21	16.0
		1678.1(492.3)	1725.3(417.8)	1823.1(467.0)	−70.0(17.4)	−52.1(128.7)	64.0(10.2)	0.995	0.42	16.0
		C9–N7	C9–Hx		C9–N7	C9–Hx				
$^{13}CH_3{-}N$	MEACAM	44.5(2.7)	−9.5(4.5)					0.947	0.31	4.8
					33.07(7.3)	−19.0(3.7)		0.916	0.39	4.8
		70.4(18.6)	24.1(20.9)		31.7(31.5)	30.8(11.3)		0.963	0.27	4.8

[a] Standard deviations are given in brackets. [b] CH_3 for MEACAM.

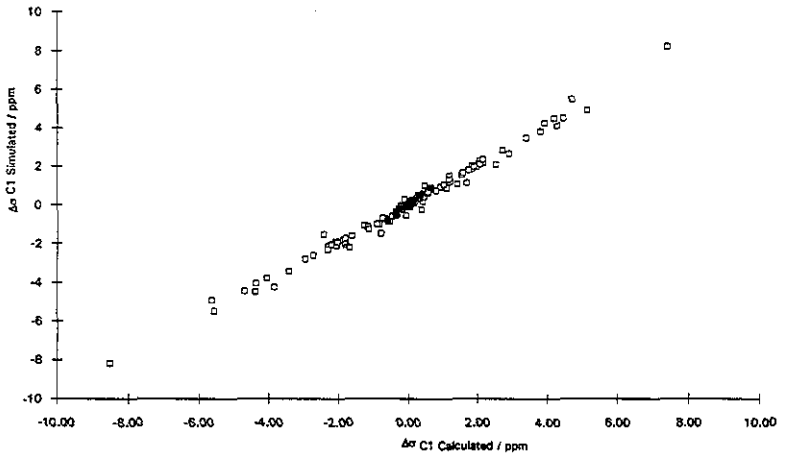

Fig. 4. Ab initio nuclear shieldings versus shieldings calculated from Eq. (1) for ^{13}C carbonyl carbon in ACAM, using geometrical input from both atoms in the bonds. (♦) HF dipolar perturbations.

ab initio work of Augspurger et al. [24,25] a derivative Hartree–Fock approach is used to calculate shielding polarizabilities and hyperpolarizabilities, which are coefficients in an electric field expansion of the shielding [15,16]. As post facto derived quantities according to Eq. (1), our $k_{n,i}$ parameters are akin to, but distinctly different from, the shielding polarizabilities.

The predictions made in this study can be compared to experimental results, although the following points must be taken into account: (i) changes in dielectric constants in solution, (ii) the change in solvation between the charged and the uncharged groups. For proteins changes in local dielectric constants also have to be taken into account; this is not the case for simple amino acids.

C=O titration shifts show that nuclear shielding of the first amide carbonyl carbon of the C-terminus of a peptide or protein is shifted to high field upon deprotonation of the C-terminal carboxylic acid group. This is in good agreement with our theoretical calculations.

For ^{15}N few titration data exist. The glutamine $CONH_2$ nitrogen nuclear shielding shows no effect upon titration of the αCOOH group [8]. The negligible change in shift is in good agreement with an extended side chain, but not with e.g. hydrogen bonding between the acid group and the side-chain amide group as such a closeness would lead to a large shift as judged from the calculations.

^{17}O titration of three dipeptides, Gly–Ala, Gly–Leu and Gly–Glu showed that the $C^{17}ONH$ resonance was shifted 6–12 ppm upfield upon deprotonation of the C-terminal COOH group and 12–16 ppm upfield upon deprotonation of the NH_3^+ group [10] in excellent agreement with the trends of the theoretical results.

We believe that a protocol based on Eq. (1) with the parameters of Table 2 can be of considerable assistance in analyzing changes in ^{13}C, ^{15}N and possibly ^{17}O amide and peptide shieldings caused by charged perturbers. Conversely an approximate location of an atom or group changing charge can be inferred from the chemical shift response of nuclei in its vicinity.

Acknowledgement

The authors wish to thank Director Ib Hendriksens Foundation for support and Associate Professor E. Tüchsen for communicating the results of an analysis of titration data for carbonyl carbon shifts of BPTI prior to publication. The initial calculations were performed by Peter Anker Thorsen. The authors are grateful to Professor C.J. Jameson for a preprint of Ref. [23].

References

[1] M. Christl and J.D. Roberts, J. Am. Chem. Soc. 94 (1972) 4566.

[2] R.E. London, T.E. Walker, V.H. Kollman and N.A. Matwiyoff, J. Am. Chem. Soc. 100 (1978) 3723.
[3] F.R.N. Gurd, P.J. Lawson, D.W. Cohran and E. Wenkert, J. Biol. Chem. 246 (1971) 3725.
[4] Md.A. Khaled, D.W. Urry and R.J. Bradley, J. Chem. Soc. Perkin II (1979) 1693.
[5] A.R. Quirt, J.R. Lyerla Jr., E.R. Peat, J.C. Cohen, W.F. Reynolds and M.H. Freedman, J. Am. Chem. Soc. 96 (1974) 570.
[6] K.L. Marsh, D.G. Maskalich, R.D. England, S. Friend and F.R.N. Gurd, Biochemistry 21 (1982) 5241.
[7] E. Tüchsen and P.E. Hansen, Biochemistry 27 (1988) 8568.
[8] F. Blomberg, W. Maurer and H. Rüterjans, Proc. Natl. Acad. Sci. US 73 (1976) 1409.
[9] J. Glushka, M. Lee, S. Coffin and D. Cowburn, J. Am. Chem. Soc. 111 (1989) 7716.
[10] B. Valentine, A. Steinschneider, D. Dhawan, M.I. Burgar, T.St. Amour and D. Fiat, Intern. J. Peptide Protein Res. 25 (1985) 56.
[11] P.H. Bolton, Progr. NMR Spectry. 22 (1990) 423.
[12] M. Ikura, D. Marion, L.W. Kay, H. Shih, M. Krinks, C.B. Klee and A. Bax, Biochem. Pharm. 40 (1990) 153.
[13] W.J. Horsley and H. Sternlicht, J. Am. Chem. Soc. 90 (1968) 3838;
W.J. Horsley, H. Sternlicht and J.S. Cohen, J. Am. Chem. Soc. 92 (1970) 680.
[14] M.J. Stephen, Mol. Phys. 1 (1958) 223.
[15] A.D. Buckingham, Can. J. Chem. 38 (1960) 300.
[16] J.P. Riley and W.T. Raynes, Mol. Phys. 32 (1976) 569.
[17] J.G. Batchelor, J.H. Prestegaard, R.J. Cushley and S.R. Lipsky, J. Am. Chem. Soc. 95 (1973) 6358.
[18] J.G. Batchelor, J. Am. Chem. Soc. 97 (1975) 3410.
[19] J.G. Batchelor, J. Feeney and G.C.K. Roberts, J. Magn. Reson. 20 (1975) 19.
[20] H.-J. Schneider and W. Freitag, J. Am. Chem. Soc. 99 (1977) 8363.
[21] H.-J. Schneider, W. Freitag, W. Gschwendtner and G. Maldner, J. Magn. Reson. 36 (1979) 273.
[22] J.A. Tossell, ed., Nuclear magnetic shieldings and molecular structure (Kluwer, Dordrecht, 1993).
[23] A.C. de Dios and C.J. Jameson, The NMR Chemical Shfit: Insight into Structure and Environment, in: Ann. Repts. NMR Spectry., ed. G.A. Webb, Vol. 28, to be published.
[24] J.D. Augspurger, C.E. Dykstra and E. Oldfield, J. Am. Chem. Soc. 113 (1991) 2447.
[25] J.D. Augspurger, J.G. Pearson, E. Oldfield, C.E. Dykstra, K.D. Park and D. Schwartz, J. Magn. Reson. 100 (1992) 342.
[26] A.C. de Dios, J.G. Pearson and E. Oldfield, Science 260 (1993) 1491.
[27] Aa.E. Hansen and T.D. Bouman, J. Chem. Phys. 82 (1985) 5035;
T.D. Bouman and Aa.E. Hansen, Intern. J. Quantum Chem. Quantum Chem. Symp. 23 (1989) 381.
[28] Aa.E. Hansen and T.D. Bouman, in: Nuclear magnetic shieldings and molecular structure, ed. J.A. Tossell (Kluwer, Dordrecht, 1993).
[29] K.P. Huber and G. Herzberg, Molecular spectra and molecular structure, Vol. 4. Constants of diatomic molecules (Van Nostrand-Reinhold, New York, 1979).
[30] M.J. Frisch, M. Head-Gordon, G.W. Trucks, J.B. Foresman, H.B. Schlegel, K. Raghavachari, M.A. Robb, J.S. Binkley, C. Gonzalez, D.J. DeFrees, D.J. Fox, R.A. Whiteside, R. Seeger, C.F. Melius, J. Baker, R.L. Martin, L.R. Kahn, J.J.P. Stewart, S. Topiol and J.A. Pople, GAUSSIAN 90 (Gaussian, Pittsburgh, 1990).
[31] T.H. Dunning and P.J. Hay, in: Methods of electronic structure theory, ed. H.F. Schaefer III (Plenum Press, New York, 1977).
[32] T.D. Bouman and Aa.E. Hansen, RPAC Molecular Properties Package, Version 9.0, 1992.
[33] H.O. Kalinowski, S. Berger and S. Braun, ^{13}C-NMR-Spectroskopie (Thieme, Stuttgart, 1984).
[34] S. Berger, S. Braun and H.O. Kalinowski, NMR-Spectroskopie von Nichtmetallen, Vols. 1, 2 (Thieme, Stuttgart, 1992).

Molecular and Vibrational Structure of 1,6,6aλ^4-Trithiapentalene. Infrared Linear Dichroism Spectroscopy and *ab Initio* Normal-Mode Analyses

Kristine B. Andersen, Jens Abildgaard, J. George Radziszewski, and Jens Spanget-Larsen

Department of Life Sciences and Chemistry, Roskilde University, P.O. Box 260, DK-4000 Roskilde, Denmark, and National Renewable Energy Laboratory, 1617 Cole Boulevard, Golden, Colorado 80401

The Journal of Physical Chemistry A®

Reprinted from
Volume 101, Number 24, Pages 4475–4480

J. Phys. Chem. A **1997**, *101*, 4475−4480 **4475**

Molecular and Vibrational Structure of 1,6,6aλ^4-Trithiapentalene. Infrared Linear Dichroism Spectroscopy and *ab Initio* Normal-Mode Analyses†

Kristine B. Andersen,‡ Jens Abildgaard,‡ J. George Radziszewski,*,§ and Jens Spanget-Larsen*,‡

Department of Life Sciences and Chemistry, Roskilde University, P.O. Box 260, DK-4000 Roskilde, Denmark, and National Renewable Energy Laboratory, 1617 Cole Boulevard, Golden, Colorado 80401

Received: March 3, 1997; In Final Form: April 10, 1997®

The vibrational structure of the title compound (TTP) was studied by experimental and theoretical methods. IR absorption spectra were recorded in argon matrix and in stretched polyethylene at 12 K. The linear dichroism (LD) observed in the latter solvent provided experimental symmetry assignments of the observed vibrational states. Molecular geometries and harmonic force fields were calculated *ab initio* with the 6-311G** basis set using three different procedures: restricted Hartree−Fock theory (HF), second-order Møller−Plesset perturbation theory (MP2), and density functional theory (DFT). In the latter, Becke's gradient-corrected exchange functional was combined with Perdew and Wang's correlation functional (BPW91), leading to excellent agreement with observed IR transitions. The combined experimental and theoretical evidence enabled an essentially complete assignment of the fundamental vibrations. Of particular importance is the assignment for the first time of the long-sought "bell-clapper" mode associated with the unique S−S−S structural element of TTP, giving rise to an intense, long-axis polarized transition in the far-IR (153 cm^{-1}).

1. Introduction

The unusual molecular and electronic structure of 1,6,6aλ^4-trithiapentalene (TTP) has been a subject of investigation for

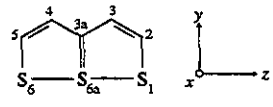

TTP

decades.[1−12] The main question has been whether TTP is adequately described by a rigid C_{2v} symmetrical molecular structure or whether there is rapid equilibration between two equivalent C_s structures, *e.g.*, the valence tautomers I and I′.

I I′

The available evidence indicates that TTP can be considered as a naphthalene-like 10π-electron ring system with C_{2v} symmetrical equilibrium structure, incorporating a unique linear arrangement of three sulfur atoms with weak and unusually long S−S bonds; the bond distance is close to 2.35 Å.[3,4] The central S atom is assumed to be situated in a broad U-shaped potential, giving rise to a low-frequency antisymmetrical S−S stretching vibration, the so-called "bell-clapper" vibration where the central S atom moves in a clapperlike manner toward one or the other of the two neighboring S atoms. The normal coordinate for this vibrational mode would correspond to the reaction coordinate for interconversion of the hypothetical C_s tautomers I and I′.

As emphasized 20 years ago by Gleiter,[5] analysis of the infrared (IR) absorption spectrum of TTP together with a theoretical normal-coordinate analysis would contribute greatly to the understanding of the peculiar properties of TTP. Part of the mid-IR spectrum of 2,5-dimethyl-TTP was published recently,[8] but no experimental investigation of the vibrational structure of the parent compound have been published; in particular, the postulated bell-clapper vibration has never been observed. Theoretical studies of TTP are complicated by the circumstance that *ab initio* Hartree−Fock (HF) calculations fail to reproduce the observed symmetrical structure but predict an equilibrium structure of C_s symmetry.[9,10] Post-HF single-point calculations indicate that inclusion of electron correlation leads to predictions in agreement with the observed symmetrical structure,[9] but complete geometry optimizations and vibrational frequency calculations with correlated wave functions have not been reported.

In this paper we report the results of an extensive experimental and theoretical study of the vibrational transitions of TTP in the mid- and far-IR regions, including linear dichroism (LD) spectroscopy in stretched polyethylene and high-quality *ab initio* calculations of the harmonic vibrational frequencies.

2. Experimental Section

TTP was prepared and purified as previously described.[13] Additional substance was kindly provided by Rolf Gleiter and Carl Th. Pedersen. Ordinary ($-h_4$) and perdeuterated ($-d_4$) stretched polyethylene (PE) samples were prepared using standard procedures.[13,14] The uniaxially stretched samples were pretreated at 60 °C for 28 h to avoid further orientational relaxation. Undesirable fringing effects were minimized by sanding the samples with fine sand paper.

Initial IR absorption spectra were recorded at room temperature on a Perkin Elmer FT-IR SPECTRUM 2000 spectrophotometer. Final spectra were measured at low temperature on Nicolet Magna-550 or evacuated Bomem DA-3 FT spectrophotometers using an APD-Cryogenics 202-E closed-cycle helium cryostat. Mid-IR measurements were carried out with

* Corresponding authors.
† Dedicated to Professor Rolf Gleiter on the occasion of his 60th birthday.
‡ Roskilde University (RUC).
§ National Renewable Energy Laboratory (NREL).
® Abstract published in *Advance ACS Abstracts,* May 15, 1997.

S1089-5639(97)00777-9 CCC: $14.00

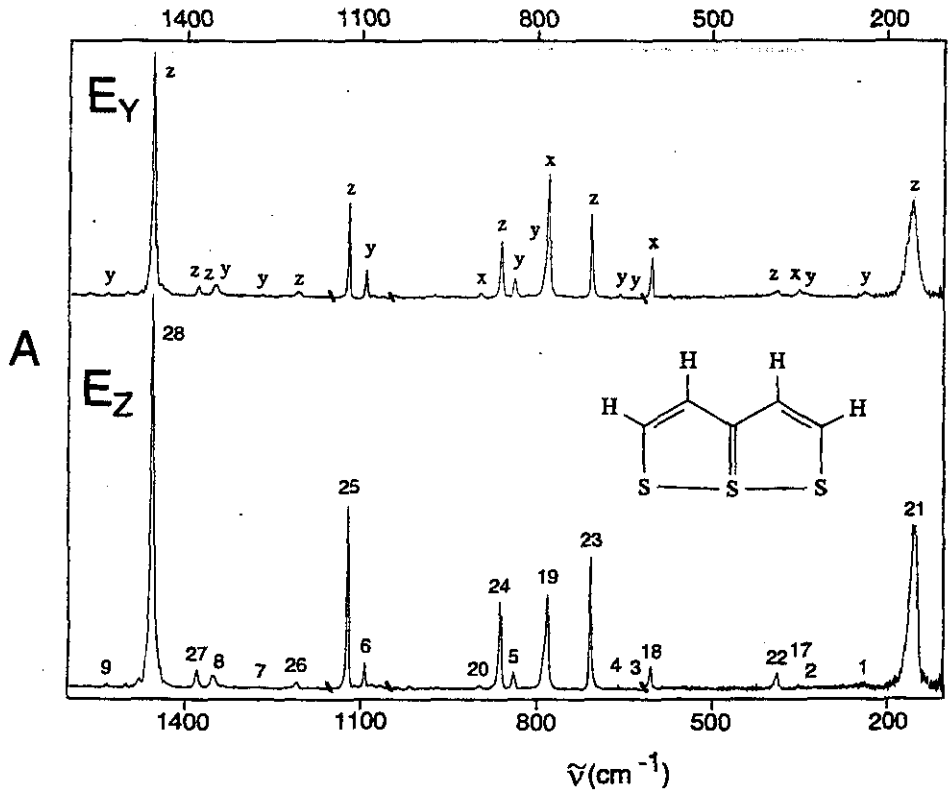

Figure 1. IR linear dichroism spectra of 1,6,6aλ^4-trithiapentalene (TTP) aligned in stretched polyethylene (PE) at 12 K. The figure shows the baseline corrected absorbance curves recorded with the IR electric vector parallel (E_Z, bottom) and perpendicular (E_Y, top) to the stretching direction. The 614−1050 and 1150−1600 cm^{-1} regions were recorded from a perdeuterated PE sample, the remainder from an ordinary PE sample.

a liquid nitrogen cooled MCT-B detector and an IGP-225 polarizer (Cambridge Physical Sciences, Ltd.). In the far-IR region a helium-cooled Si bolometer (Infrared Laboratories), IGP-223 and IGP-224 polarizers, and solid substrate Si beamsplitter were applied. Each spectrum consisted of 1000 scans with a resolution of 0.5 cm^{-1}.

Low-temperature LD spectra were recorded as follows: First, a pure stretched PE sample was mounted in a copper holder, attached to the cold tip of the cryostat, and cooled to 12 K (initially kept under reduced Ar pressure), and two baseline LD spectra were recorded corresponding to $E_Z(\tilde{\nu})$ and $E_Y(\tilde{\nu})$ (see below). The sample was then warmed to room temperature and TTP was introduced from the vapor phase by sublimation in a small evacuated container at 52 °C for 40−60 h. Excess TTP was washed from the surface of the sample with methanol, and after cooling to 12 K two LD absorbance curves were measured: $E_Z(\tilde{\nu})$ with the electric vector of the linearly polarized IR radiation parallel to the stretching direction Z, and $E_Y(\tilde{\nu})$ with the vector perpendicular to it; in both cases the direction of the beam was perpendicular to the surface of the sample sheet.[13,14] The resulting baseline-corrected LD absorbance curves are shown in Figure 1. The 1600−1150 and 1050−614 cm^{-1} regions of the spectra were obtained from a perdeuterated PE sample, the remainder from an ordinary PE sample.

The Ar-matrix sample was prepared on a CsI spectroscopic window attached to the cryostat by subliming TTP at 60 °C into a stream of Ar (0.5 mmol/min for 37 min). The mid-IR absorbance spectrum measured at 12 K is shown in Figure 2. The bands listed in Table 1 were established as belonging to TTP on the basis of identical rate of disappearance during irradiation at 454.5, 514.5 (Ar ion laser), or 248 nm (KrF excimer laser). The photochemistry of TTP in Ar matrix at 12 K is under investigation and the results will be published elsewhere.

Observed wavenumbers $\tilde{\nu}_i$ and relative integrated intensities I_i are given in Table 1. In the stretched PE experiment (Figure 1) I values were determined from the isotropic absorbance curve $E_Z(\tilde{\nu}) + 2E_Y(\tilde{\nu})$[13,14] and normalized relative to the strongest observed transition at 153 cm^{-1}. This transition is not observable in the Ar matrix; the intensities measured in Ar were normalized such that the transition corresponding to the second strongest band in PE (1449 cm^{-1}) appears with equal intensity in both solvents. The wavenumbers observed in Ar and in stretched PE are generally similar, but the relative intensities differ significantly in several instances.

3. Calculations

Molecular geometries and harmonic force fields for TTP were calculated *ab initio* at the restricted Hartree-Fock (HF) level,[15] and by using second-order Møller−Plesset perturbation theory (MP2)[15] and density functional theory (DFT).[15−17] The calculations were performed with GAUSSIAN 94[18] using standard basis set 6-311G**, including 192 basis functions (322 primitive Gaussians). The MP2 expansion considered the complete space of all molecular orbitals (keyword MP2=full).[18] In the DFT calculation Becke's gradient-corrected exchange functional[19] was combined with Perdew and Wang's correlation functional[20] (keyword BPW91).[18]

Within the constraints of C_{2v} symmetry, previous HF calculations on TTP using 4-21G, 3-21G(*), 6-31G(*), and 6-31G* basis sets lead to total energies −1371.413 964,[10] −1377.536 783,[9] −1384.055 281,[12] and −1384.131 800[9] au, respectively, indicating slow basis set convergence. The present HF/6-311G** (C_{2v}) calculation yields −1384.239 116 au; the optimized geometrical parameters are listed in Table 2. However, the C_{2v} structure corresponds to a first-order saddle point on the HF potential energy surface, characterized by one imaginary vibrational

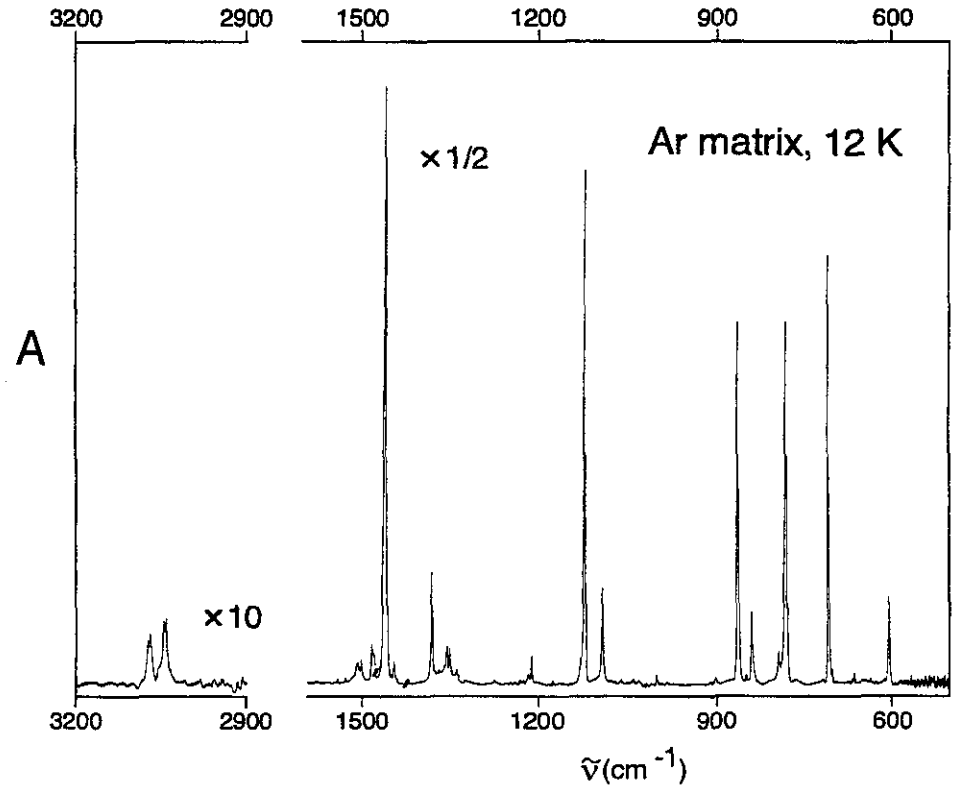

Figure 2. Mid-IR absorption spectrum of 1,6,6aλ^4-trithiapentalene (TTP) isolated in argon matrix at 12 K.

TABLE 1: 1,6,6aλ^4-Trithiapentalene (TTP). Observed Vibrational Absorption Bands and Their Assignment to Calculated Fundamental Transitions[a]

		Ar matrix		stretched PE[c]			BPW91/6-311G**[d]		
	sym[b]	$\tilde{\nu}$	I[e]	$\tilde{\nu}$	I[f]	K[g]	$\tilde{\nu}$	I[h]	approximate description[i]
ν_1	a_1			237	0.1	0.320	220	0.1	$S_{1(6)}-S_{6a}$ st; skel d
ν_2				337	0.02	0.306	320	0.1	$S_1-S_{6a}-S_6$ b; skel d
ν_3		633	0.7	629	0.03	0.303	603	0.1	$C_{3(4)}-C_{3a}$ st + iph $C_{3a}-S_{6a}$ st; skel d
ν_4		661	2.7	654*	1.3	0.310	644	1.0	$C_{3a}-S_{6a}$ st; skel d
ν_5		835	2.9	839	4.9	0.300	825	7.7	$C_{2(5)}-S_{1(6)}$ st + $C_{3(4)}-H$ b; skel d
ν_6		1091	5.1	1090	5.8	0.303	1083	10.4	$C_{2(5)}-H$ b + oph $C_{3(4)}-H$ b
ν_7		1268	0.5	1266	0.3	0.301	1231	0.2	$C_{3(4)}-H$ b
ν_8		1347	0.4	1346	2.23	0.305	1331	6.6	$C_{2(5)}-H$ b + iph $C_{3(4)}-H$ b
ν_9		1534	0.3	1532	0.3	0.31	1507	7.6	$C_{2(5)}-C_{3(4)}$ st + oph $C_{3(4)}-C_{3a}$ st; C−H b
ν_{10}		3044	0.4				3102	0.9	$C_{2(5)}-H$ st
ν_{11}		3073	0.2				3123	8.0	$C_{3(4)}-H$ st
ν_{16}	b_1						127	1.0	S_{6a} op d + iph C_{3a} op d + oph $C_{2(5)}$ op d; op skel d
ν_{17}				347	1.7	0.22	336	1.9	S_{6a} op d + oph C_{3a} op d + iph $C_{2(5)}$ op d; op skel d
ν_{18}		602	6.8	602	11.7	0.240	585	11.5	C_{3a} op d + oph $C_{3(4)}-H$ op b
ν_{19}		781	17.3	778	20.2	0.259	761	55.7	$C_{2(5)}-H$ op b + iph $C_{3(4)}-H$ op b
ν_{20}		904	0.4	896	0.6	0.24	884	0.1	$C_{2(5)}-H$ op b + oph $C_{3(4)}-H$ op b
ν_{21}	b_2			153	100	0.462	228	100	$S_{1(6)}-S_{6a}$ st; skel d (bell-clapper)
ν_{22}				384	3.9	0.520	378	7.4	$S_{1(6)}-S_{6a}$ st + $C_{2(5)}-S_{1(2)}-S_{6a}$ b; skel d
ν_{23}		707	19.3	706*	16.8	0.445	699	17.8	$C_{2(5)}-C_{3(4)}-C_{3a}$ b + $C_{2(5)}-S_{1(2)}-S_{6a}$ b; skel d
ν_{24}		863	23.4	857	14.4	0.457	849	30.3	$S_{1(2)}-C_{2(5)}-C_{3(4)}$ b + C−H b; skel d
ν_{25}		1121	22.4	1121	17.9	0.483	1123	23.3	$C_{2(5)}-H$ b + oph $C_{3(4)}-H$ b
ν_{26}		1207	2.3	1205	2.1	0.435	1207	0.0	$C_{2(5)}-H$ b + iph $C_{3(4)}-H$ b
ν_{27}		1378	5.1	1373	2.8	0.446	1370	4.5	$C_{2(5)}-H$ b + iph $C_{3(4)}-H$ b + $C_{2(5)}-C_{3(4)}-C_{3a}$ b
ν_{28}		1456	75.6	1449*	75.6	0.450	1479	130.2	$C_{2(5)}-C_{3(4)}$ st + oph $C_{3(4)}-C_{3a}$ st + $C_{3(4)}-H$ b
ν_{29}		3040	0.1				3101	0.7	$C_{2(5)}-H$ st
ν_{30}		3068	0.3				3121	1.2	$C_{3(4)}-H$ st

[a] Wavenumbers $\tilde{\nu}$ in cm^{-1}. Additional weak transitions observed, *e.g.*, at 785 (a_1) and 1349 cm^{-1} (b_2) were not assigned as fundamentals, see text. [b] Irreducible representations in the C_{2v} point group. In the designation of symmetry labels, the molecular axes are redefined: z and yz are taken as the C_2 axis and the molecular plane. [c] Stretched polyethylene (12 K); wavenumbers marked with an asterisk (*) indicate transitions observed in perdeuterated polyethylene. [d] Table 3. [e] Integrated intensity relative to $I_{28} \equiv 75.6$. [f] Integrated isotropic intensity $E_z + 2E_y$ relative to $I_{21} \equiv 100$. [g] Orientation factor.[13,14] [h] Theoretical intensities relative to $I_{21} \equiv 100$. [i] st = stretching, b = bending, d = deformation, skel = skeleton, op = out-of-plane, iph = in-phase, oph = out-of-phase.

frequency, ν_{21} (Table 3). This is the transition structure on the reaction coordinate between two equivalent C_s minima on the HF potential energy hypersurface, as mentioned in the Introduction. The HF/6-311G** C_s energy minimum is −1384.255 660 au which is 0.016 544 au (10.38 kcal/mol) lower than the corresponding C_{2v} transition state. But consideration of electron

TABLE 2: 1,6,6aλ⁴-Trithiapentalene (TTP). Calculated C_{2v} Geometries in Comparison with Structural Data from X-ray, Electron Diffraction, and Nematic Phase ^{1}H NMR Investigations

	HF/6-311G**[c]	MP2/6-311G**	BPW91/6-311G**	X-ray[d]	ED[e]	NMR[f]
S1−C2[a]	1.6834	1.6813	1.7019	1.684	1.698	
C2−C3	1.3585	1.3750	1.3774	1.354	1.364	1.387
C3−C3a	1.4110	1.4141	1.4177	1.409	1.422	1.404
C3a−S6a	1.7363	1.7325	1.7633	1.748	1.708	
S1−S6a	2.3797	2.3723	2.4272	2.363	2.328	
C2−H	1.0764	1.0876	1.0920		1.114	1.084
C3−H	1.0736	1.0862	1.0909		1.114	1.109
S1−C2−C3[b]	120.11	119.48	120.41	120.1	118.7	
C2−C3−C3a	119.82	119.97	120.78	120.3	119.4	120.7
C3−C3a−S6a	119.48	119.08	118.70	118.5	119.2	119.0
H−C2−C3	120.69	121.61	121.48			122.3
H−C3−C3a	118.60	118.80	118.48			119.4
C3a−S6a−S1	88.70	89.23	88.99	89.1	90.1	
S6a−S1−C2	91.89	92.24	91.12	92.0	92.6	

[a] Bond lengths in angstrøms. [b] Bond angles in degrees. [c] C_{2v} symmetry imposed. [d] Reference 3. [e] Reference 4. [f] Reference 6.

TABLE 3: 1,6,6aλ⁴-Trithiapentalene (TTP). Comparison of Fundamental Vibrations Calculated at Three Different Levels of Theory (See Text)[a]

		HF/6-311G**[c]				MP2/6-311G**				BPW91/6-311G**			
	sym[b]	$\tilde{\nu}$	I	k	μ	$\tilde{\nu}$	I	k	μ	$\tilde{\nu}$	I	k	μ
ν_1	a_1	260	0.1	0.79	19.7	239	0.1	0.64	19.0	220	0.1	0.55	19.2
ν_2		363	0.1	0.87	11.2	336	0.2	0.75	11.3	320	0.2	0.70	11.7
ν_3		667	0.1	1.66	6.3	626	0.3	1.45	6.3	603	0.2	1.31	6.1
ν_4		703	3.1	2.37	8.1	697	0.5	2.26	7.9	644	1.5	2.10	8.6
ν_5		902	45.1	2.49	5.2	892	10.6	2.27	4.8	825	11.9	2.04	5.1
ν_6		1211	30.2	1.23	1.4	1130	13.5	1.01	1.3	1083	16.0	1.00	1.5
ν_7		1355	0.8	2.43	2.2	1280	0.7	1.88	1.9	1231	0.3	1.69	1.9
ν_8		1510	17.5	2.24	1.7	1383	5.1	2.13	1.9	1331	10.1	1.81	1.7
ν_9		1664	42.3	7.80	4.8	1567	4.1	9.42	6.5	1507	11.7	8.13	6.1
ν_{10}		3329	5.0	7.11	1.1	3201	4.3	6.56	1.1	3102	1.4	6.21	1.1
ν_{11}		3360	9.4	7.29	1.1	3229	7.5	6.73	1.1	3123	12.4	6.29	1.1
ν_{12}	a_2	148	0	0.07	5.3	147	0	0.07	5.4	142	0	0.06	5.4
ν_{13}		468	0	0.44	3.4	425	0	0.43	4.0	436	0	0.39	3.5
ν_{14}		818	0	0.46	1.2	729	0	0.37	1.2	718	0	0.36	1.2
ν_{15}		1054	0	0.86	1.3	879	0	0.56	1.2	875	0	0.58	1.3
ν_{16}	b_1	150	1.5	0.09	6.8	98	1.9	0.03	6.1	127	1.5	0.08	8.0
ν_{17}		353	7.9	0.37	5.0	334	1.5	0.41	6.2	336	2.9	0.35	5.2
ν_{18}		670	11.0	0.81	3.1	561	17.5	0.91	4.9	585	17.7	0.70	3.5
ν_{19}		887	101.1	0.70	1.5	748	91.7	0.44	1.3	761	86.0	0.48	1.4
ν_{20}		1049	1.0	0.89	1.4	877	0.2	0.57	1.3	884	0.1	0.62	1.3
ν_{21}	b_2	392i[d]	342.0	−2.36	26.1	271	159.7	0.86	19.9	228	154.4	0.67	21.8
ν_{22}		416	1.5	1.19	11.7	399	23.1	1.27	13.6	378	11.5	1.08	12.9
ν_{23}		750	233.1	2.94	8.9	730	39.4	2.46	7.9	699	27.6	2.33	8.1
ν_{24}		907	205.7	2.20	4.5	913	77.3	2.07	4.2	849	46.8	1.85	4.4
ν_{25}		1204	407.3	1.27	1.5	1157	54.4	0.85	1.1	1123	36.1	0.83	1.1
ν_{26}		1297	56.8	1.77	1.8	1250	0.5	1.44	1.6	1207	0.0	1.37	1.6
ν_{27}		1469	393.5	3.45	2.7	1428	3.4	4.39	3.7	1370	6.9	4.10	3.7
ν_{28}		1559	175.6	3.47	2.4	1600	288.2	10.34	6.9	1479	201.0	6.84	5.3
ν_{29}		3328	3.2	7.10	1.1	3200	1.3	6.56	1.1	3101	1.1	6.15	1.1
ν_{30}		3353	3.1	7.27	1.1	3226	1.2	6.73	1.1	3121	1.8	6.29	1.1

[a] $\tilde{\nu}$ = wavenumber in cm^{-1} (unscaled), I = IR intensity in km/mol, k = force constant in mdyn/Å, μ = reduced mass in amu. [b] Irreducible representations in the C_{2v} point group. In the designation of symmetry labels, the molecular axes are redefined: z and yz are taken as the C_2 axis and the molecular plane. [c] C_{2v} symmetry imposed. [d] Imaginary wavenumber, see text.

correlation is expected to change the situation in favor of the bridged, symmetrical structure, as indicated by recent single-point MP4/3-21G(*) and MP2/6-31G* results by Cimiraglia and Hofmann.[9] This expectation is confirmed by the present MP2/6-311G** and BPW91/6-311G** calculations with full geometry optimization that predict a stable C_{2v} symmetrical equilibrium structure; no minima coresponding to the valence tautomeric C_s structures I and I′ were found. The calculated total energies are −1385.803 292 6 (MP2) and −1387.600 610 1 (BPW91) au. Calculated bond lengths and angles are in good agreement with experimental data, particularly in the case of MP2. The C−S and S−S bond lengths tend to be slightly overestimated by BPW91; the S−S bond is thus predicted to be 2.43 Å, compared with experimental values in the range 2.33−2.36 (Table 2).

Vibrational transitions computed at the three levels of theory are compared in Table 3, and an approximate description of the IR-active modes is included in Table 1. As anticipated, the ν_{21} mode obtained with MP2 and BPW91 is a low-frequency bell-clapper type vibration (see below).

4. Results and Discussion

The orientational properties that can be determined from the LD curves in Figure 1 are the so-called orientation factors[13,14] for the observed vibrational transitions. The orientation factor K_i for an optical transition i is the average over all solute molecules of cosine square of the angle between the molecular transition moment vector $\mathbf{M}_i$ and the uniaxial stretching direction Z of the sample:[13,14]

$$K_i = \langle \cos^2(M_i,Z) \rangle$$

The K_i value for a nonoverlapped transition i is related to the dichroic ratio $d_i = E_Z(\tilde{\nu}_i)/E_Y(\tilde{\nu}_i)$ through the equation $K_i = d_i/(2 + d_i)$.[13,14] In the present investigation the d values were determined from the ratios of the integrated absorbances and overlapping transitions were analyzed by the TEM method.[14] The resulting K values are given in Table 1.

The observed K_i fall in three distinct groups with values equal to 0.240 ± 0.01, 0.306 ± 0.02, and 0.462 ± 0.02; the three characteristic values add up to unity within experimental error (1.008 ± 0.02). As in the case of 2,5-dimethyl-TTP,[8] this observation is only consistent with the assumption of high molecular symmetry and provides an independent confirmation of the presence of a C_{2v} symmetrical equilibrium molecular geometry on the time scale of IR spectroscopy. Under the assumption that the alignment of TTP in stretched PE reflects its molecular dimensions,[13,14] we assign the three characteristic Ks as $(K_x, K_y, K_z) = (0.240, 0.306, 0.462)$. The labeling of the axes is chosen according to the convention $K_x \leq K_y \leq K_z$. A recently published UV−vis LD investigation of TTP in stretched PE obtained Ks corresponding to $(K_y, K_z) = (0.3, 0.53)$;[12] the larger K_z observed in this experiment can be explained by the circumstance that a freshly stretched (and not annealed) PE sample was applied, resulting in more efficient molecular alignment. The identification of the labels x, y, and z with the individual symmetry axes of the molecule represents an absolute polarization assignment and allows experimental identification of the symmetries of the observed vibrational states. With the present definition of molecular axes, x forms a basis for the b_1, y for the a_1, and z for the b_2 irreducible representation of the C_{2v} point group. The resulting symmetry assignments of the observed transitions are given in Table 1 and indicated graphically in the top panel of Figure 3.

The suggested assignment of observed peaks to fundamental transitions is indicated in Table 1. This assignment is strongly supported by the theoretical results. Calculated wavenumbers and intensities of the 30 fundamental transitions of TTP ($\Gamma = 11a_1 + 4a_2 + 5b_1 + 10b_2$) are listed in Table 3, and illustrated graphically in Figure 3, lower panel. The observed wavenumbers are well reproduced by simple scaling of the theoretical values: $\tilde{\nu}_{obs} = 0.9555\tilde{\nu}_{MP2}$ (SD = 39 cm^{-1}) and $\tilde{\nu}_{obs} = 0.9904\tilde{\nu}_{BPW91}$ (SD = 28 cm^{-1}), indicating an effective scaling factor close to unity in the case of BPW91. The performance of BPW91 is highly satisfactory and slightly superior to that of MP2 (the relative success of BPW91 is remarkable in view of the much shorter computation time). Detailed comparison of observed and calculated IR intensities is complicated by the significant solvent sensitivity of the experimental values, but the observed trends seem well reproduced by the calculations.

One fundamental is apparently not observed, ν_{16}, which is predicted by the theoretical procedures to give rise to a weak transition around 100 cm^{-1}. Experimental features due to this transition are probably obscured by the strong broad band with maximum at 153 cm^{-1} (assigned to ν_{21} as discussed below). A number of additional transitions are observed that are not assigned to fundamentals. Two are indicated in Figure 1, a y-polarized shoulder at 785 cm^{-1} and a z-polarized one at 1349 cm^{-1}; both are observed as distinct peaks in the Ar matrix spectrum (Figure 2). The latter is an alternative candidate for assignment of the ν_{27} fundamental.

Of particular interest is assignment of the first b_2 fundamental (ν_{21}), corresponding to the bell-clapper mode of TTP that has been a topic of discussion for so many years.[1−12] The normal coordinate of this mode calculated with BPW91 is indicated in

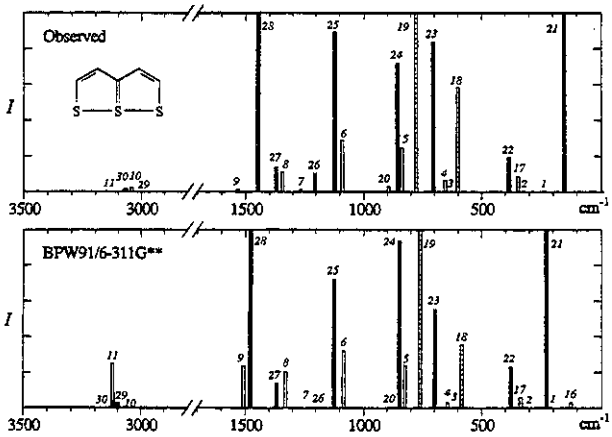

Figure 3. Graphical illustration of observed (top) and calculated (bottom) vibrational transitions for 1,6,6aλ⁴-trithiapentalene (TTP). Solid, white, and hatched bars indicate transitions of b_2, a_1, and b_1 symmetry, respectively. The length of the bars indicates the relative intensity; the transitions labeled 19, 21, and 28 are too intense to be displayed in full on the present scale. The experimental diagram refers to measurements in stretched PE (100−1700 cm^{-1}) and Ar matrix (>1700 cm^{-1}) and indicates the suggested assignment of fundamental transitions. The theoretical diagram shows results obtained with BPW91 density functional theory, see text.

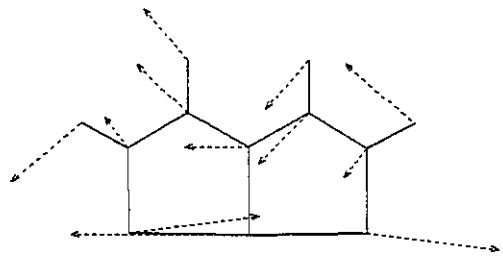

Figure 4. Normal coordinate of the bell-clapper mode ν_{21} for 1,6,6aλ⁴-trithiapentalene (TTP) as predicted with BPW91 density functional theory, see text. The normal coordinate predicted with MP2 theory is very similar.

Figure 4; the molecular vibration can be described as primarily antisymmetric S−S stretching, with admixture of some skeleton deformation. As indicated in Table 3, HF theory yields a negative force constant and an imaginary wavenumber, but MP2 and BPW91 predict this mode to give rise to a strong transition with wavenumber equal to 271 cm^{-1} (MP2) or 228 cm^{-1} (BPW91); the values obtained using the scaling factors defined above are 259 and 226 cm^{-1}. The prominent long-axis polarized absorption band observed in stretched PE with a maximum at 153 cm^{-1} must be assigned to the bell-clapper fundamental. This band is relatively broad and seems to be characteristic for the S−S−S structural element in trithiapentalenes.[21] The theoretical procedures overestimate the wavenumber of the transition; the point for this transition deviates from the regression line by an amount significantly larger than the standard deviation. A preliminary theoretical investigation[22] of the shape of the bell-clapper potential indicates that this can be explained by the expected inadequacy of the harmonic approximation for this vibrational mode, an assumption that is supported by the breadth of the observed band.

5. Concluding Remarks

The experimental and theoretical characterization of the normal vibrational modes of TTP obtained in this study settles a number of questions concerning the unusual molecular structure of this compound that has been investigated for

decades. Most importantly, the so-called bell-clapper mode is observed for the first time in this investigation; it gives rise to a very strong, long-axis polarized, and relatively broad band with maximum at 153 cm^{-1} (stretched polyethylene at 12 K). Harmonic frequencies predicted by *ab initio* MP2 and DFT calculations at the 6-311G** level are in general agreement with the observed data. The DFT procedure, using Becke's gradient-corrected exchange functional and Perdew and Wang's correlation functional, is particularly successful. The results for the bell-clapper mode indicate a possible shortcoming of the harmonic approximation; a detailed theoretical investigation of the anharmonicity of this mode is in progress.

Acknowledgment. The authors are indebted to Professor Rolf Gleiter and Professor Carl Th. Pedersen for kind gifts of compounds and to Professor Barney Ellison for access to the Bomem spectrometer. This project was supported by grants from the Danish National Research Council and Roskilde University. The computational effort was supported by NCSA. J.G.R. thanks Dr. Helena Chum (NREL) for continuing encouragement and support.

References and Notes

(1) Bezzi, S.; Mammi, M.; Carbuglio, C. *Nature* **1958**, *182*, 247. Guillouzo, G. *Bull. Soc. Chim. Fr.* **1958**, 1316. Hertz, H. G.; Traverso, G.; Walter, V. *Justus Liebigs Ann. Chem.* **1959**, *625*, 43.

(2) Lozac'h, N. *Adv. Heterocycl. Chem.* **1971**, *13*, 161.

(3) Hordvik, A.; Saethre, J. *Isr. J. Chem.* **1972**, *10*, 239. Hansen, L. K.; Hordvik, A. *Acta Chem. Scand.* **1973**, *27*, 411.

(4) Shen, Q.; Hedberg, K. *J. Am. Chem. Soc.* **1974**, *96*, 289.

(5) Gleiter, R.; Gygax, R. *Top. Curr. Chem.* **1976**, *63*, 49.

(6) Bjorholm, T.; Jacobsen, J. P.; Pedersen, C. Th. *J. Mol. Struct.* **1981**, *75*, 327.

(7) Pedersen, C. Th. *Sulfur Rep.* **1980**, *1*, 1. Pedersen, C. Th. *Phosphorus, Sulfur Silicon* **1991**, *58*, 17.

(8) Spanget-Larsen, J.; Fink, N. *J. Phys. Chem.* **1990**, *94*, 8423.

(9) Cimaraglia, R.; Hofmann, H.-J. *J. Am. Chem. Soc.* **1991**, *113*, 6449.

(10) Saebø, S.; Boggs, J. E.; Fan, K. *J. Phys. Chem.* **1992**, *96*, 9268.

(11) Duus, F. In *Methoden der organischen Chemie (Houben-Weyl), Vol. E8a*; Schaumann, E., Ed.; Georg Thieme Verlag: Stuttgart, 1993; pp 553–583.

(12) Spanget-Larsen, J.; Chen, E.; Shim, I. *J. Am. Chem. Soc.* **1994**, *116*, 11433.

(13) Radziszewski, J. G.; Michl, J. *J. Am. Chem. Soc.* **1986**, *108*, 3289.

(14) Michl, J.; Thulstrup, E. W. *Spectroscopy with Polarized Light. Solute Alignment by Photoselection, in Liquid Crystals, Polymers and Membranes*; VCH Publishers: New York, 1986, 1995. Thulstrup, E. W.; Michl, J. *Elementary Polarization Spectroscopy*; VCH Publishers: New York, 1989.

(15) Head-Gordon, M. *J. Phys. Chem.* **1996**, *100*, 13213. Foresman, J. B.; Frisch, Æ. *Exploring Chemistry with Electronic Structure Methods*; Gaussian, Inc.: Pittsburgh, PA, 1996.

(16) Parr, R. G.; Yang, W. *Ann. Rev. Phys. Chem.* **1995**, *46*, 701. Kohn, W.; Becke, A. D.; Parr, R. G. *J. Phys. Chem.* **1996**, *100*, 12974.

(17) Stephens, P. J.; Devlin, F. J.; Chabalowski, C. F.; Frisch, M. J. *J. Phys. Chem.* **1994**, *98*, 11623. Wong, M. W. *Chem. Phys. Lett.* **1996**, *256*, 391.

(18) Frisch, M. J.; Trucks, G. W.; Schlegel, H. B.; Gill, P. M. W.; Johnson, B. G.; Robb, M. A.; Cheeseman, J. R.; Keith, T.; Petersson, G. A.; Montgomery, J. A.; Raghavachari, K.; Al-Laham, M. A.; Zakrzewski, V. G.; Ortiz, J. V.; Foresman, J. B.; Peng, C. Y.; Ayala, P. Y.; Chen, W.; Wong, M. W.; Andres, J. L.; Replogle, E. S.; Gomperts, R.; Martin, R. L.; Fox, D. J.; Binkley, J. S.; Defrees, D. J.; Baker, J.; Stewart, J. P.; Head-Gordon, M.; Gonzalez, C.; Pople, J. A. *Gaussian 94, Revisions B.3 and C.3*; Gaussian, Inc.: Pittsburgh, PA, 1995.

(19) Becke, A. D. *Phys. Rev. A* **1988**, *38*, 3098.

(20) Perdew, J. P.; Wang, Y. *Phys. Rev. B* **1992**, *45*, 13244.

(21) A similar intense, broad band with maximum at 185 cm^{-1} is observed in the far-IR spectrum of 2,5-dimethyl-TTP (PE tablet, room temp.); Andersen, K. B., unpublished result.

(22) Abildgaard, J., Spanget-Larsen, J., unpublished results.

Reprinted from *Spectrochimica Acta Part A*, **The Vibrational Spectrum of Acenaphthylene: Linear Dichroism and ab initio Model Calculations**, volume **53**, Juliusz G. Radziszewski, Jens Abildgaard, Erik W. Thulstrup, pages 2095 - 2107,

Reprinted from

SPECTROCHIMICA ACTA

PART A:

Spectrochimica Acta Part A 53 (1997) 2095–2107

The vibrational spectrum of acenaphthylene: linear dichroism and ab initio model calculations

Juliusz G. Radziszewski [a], Jens Abildgaard [b], Erik W. Thulstrup [b,*]

[a] *Department of Life Sciences and Chemistry, Roskilde University, P.O. Box 260, DK-4000 Roskilde, Denmark*
[b] *The National Renewable Energy Laboratory, Golden, CO 80309, USA*

ELSEVIER

ELSEVIER

Spectrochimica Acta Part A 53 (1997) 2095–2107

SPECTROCHIMICA ACTA PART A

The vibrational spectrum of acenaphthylene: linear dichroism and ab initio model calculations

Juliusz G. Radziszewski [a], Jens Abildgaard [b], Erik W. Thulstrup [b,*]

[a] *Department of Life Sciences and Chemistry, Roskilde University, P.O. Box 260, DK-4000 Roskilde, Denmark*
[b] *The National Renewable Energy Laboratory, Golden, CO 80309, USA*

Received 3 March 1997; accepted 6 May 1997

Abstract

Complete infrared linear dichroism spectra were recorded between 50 and 3200 cm^{-1} of acenaphthylene aligned in stretched polyethylene and polyethylene-d_4 as well as Raman solution spectra. The information obtained from the infrared spectra made it possible to separate the electric dipole allowed transitions into three groups, corresponding to three different excited state symmetries. The separation is possible for the C_{2v} symmetric molecule, since the three groups of transitions correspond to three mutually perpendicular transition moment directions, which in the stretched polymer obtain different average alignments. This information makes a safe assignment of all allowed fundamental vibrational transitions, belonging to three of the four C_{2v} symmetry classes, possible. Similarly, the Raman spectra permitted an assignment of vibrations belonging to the fourth symmetry class. The assignments were supported by ab initio quantum mechanical modelling calculations at various levels. A comparison of the present assignments with those from recent linear dichroism studies of acenaphthylene aligned in a nematic liquid crystal matrix confirmed most assignments, but also led to new assignments and reassignment of several transitions. This was possible because of the additional information that becomes available in the stretched polyethylene method, which provide an excellent separation of the excited state symmetries corresponding to the two in-plane transition moment directions. © 1997 Elsevier Science B.V.

Keywords: Acenaphthylene; Linear dichroism; Vibrational spectrum

1. Introduction

Infrared linear dichroism studies of large polycyclic aromatic compounds (PACs) are today relatively simple to perform using stretched polymers or nematic liquid crystals as anisotropic solvents for the PACs. These studies often allow complete assignments of vibrational spectra; such assignments are likely to become useful in future studies of the occurance of the environmentally important PACs, both in nature and the workplace. One example is the complex, carcinogenic PAC content of soot which in recent years has increasingly attracted interest among environmental researchers.

* Corresponding author. Tel.: +45 46742709; fax: +45 46743000; e-mail: ewt@ruc.dk

PII S1386-1425(97)00130-3

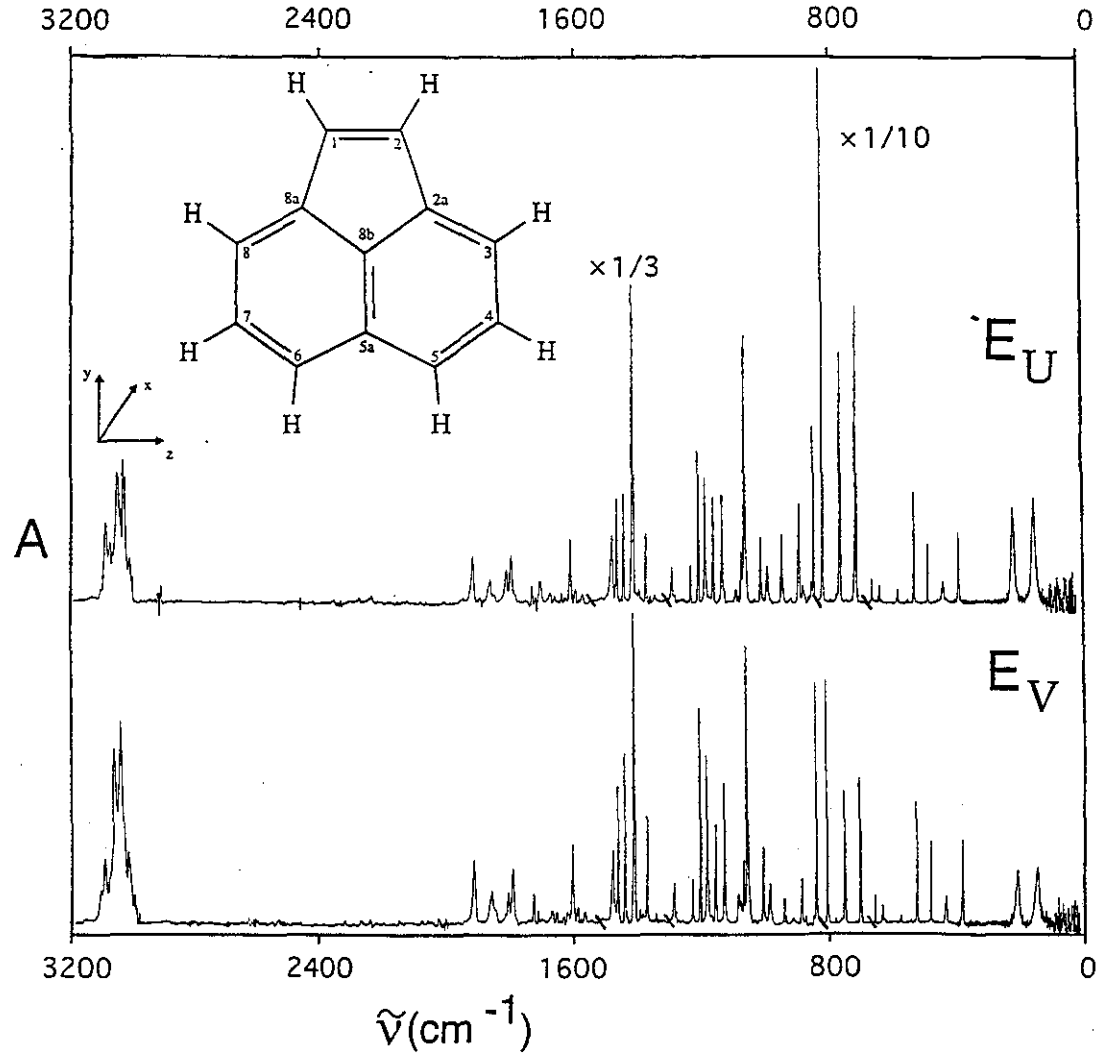

Fig. 1. The baseline corrected IR absorption spectrum of acenaphthylene in stretched polyethylene sheets, recorded at 12 K, as described in the next. Top: the spectrum recorded with the electric vector along the stretching direction. Bottom: the spectrum recorded with the electric vector perpendicular to the stretching direction.

In the following we shall present a complete assignment of the vibrations of acenaphtylene as an example of an almost disk-shaped small PAC, which nevertheless may be aligned sufficiently in stretched polyethylene sheets to achieve a complete resolution of the three IR active transition moment directions. This study follows a recent investigation of the vibrations of acenaphthylene molecules aligned in nematic liquid crystals [1] and a more than 20 year old similar study of the electronic transitions in acenaphthylene aligned in stretched polyethylene [2].

The recent study of the vibrational spectrum of acenaphthylene is described in a paper by Baranovic, Jordanov, and Schrader [1] who used linear dichroism spectroscopy on a sample of acenaphthylene aligned in a ZLI-1695 nematic liquid crystal (Merck). The liquid crystal served as a

uniaxial, anisotropic solvent and produced an effective alignment of the dissolved acenaphthylene molecules. However, it was a major problem in these studies that the average alignments of the in-plane molecular axes were the same. This prevented a separation of the two possible in-plane transition moment directions observed in the planar C_{2v} symmetric molecule; the directions correspond to excited vibrational states of a_1 and b_2 symmetry. Although these two directions could be distinguished from the third, out-of-plane transition moment direction corresponding to vibrations of b_1 symmetry, the study did not allow a safe assignment of all fundamentals. The spectra presented in the present paper, based on alignment in stretched polyethylene sheets, allow a clear separation of all three transition moment directions which, as we shall see, turned out to be essential for the assignment process.

The ability of stretched polyethylene to produce a difference in the average alignment of different molecular directions has been shown to be sufficient for a separation of transitions along three perpendicular molecular axes in numerous molecules of C_{2v} or D_{2h} symmetry. Many examples are found in the literature [3,4], demonstrating the impressive degree of alignment that may be produced, even of quite small molecules, such as ethylene or phthalic anhydride [5,6]. In addition to the use of stretched polyethylene, solid argon matrices were also used as solvents for the latter molecules and the alignment of guest molecules was produced by photoorientation [3,4].

The 20-year-old linear dichroism spectroscopic investigation of the electronic transitions of acenaphthylene aligned in stretched polyethylene [2] had demonstrated a considerable difference between the average alignment of the two in-plane, symmetry-determined axes, corresponding to A_1 and B_2 electronic transitions; see also [3] in which a more general discussion of this spectrum may be found. This difference in average alignment was so large in this-almost perfectly disk shaped-molecule that a resolution of a long A_1 symmetry vibronic band series underneath a stronger B_2 symmetry band was possible.

The investigation of the electronic spectrum of acenaphthylene [2,3] showed that the molecule is aligned in stretched polyethylene in such a way that the in-plane axis z, perpendicular to the symmetry axis y, becomes the 'long axis' (the axis which on the average is best aligned, see later, it is usually labelled z). However, it is interesting to note that an 1,2-Br disubstitution could be shown to change the alignment so much that the symmetry axis y became the molecular 'long' axis [2,3].

The distinction between the two in-plane transition moment directions and between these and the out-of-plane transtition moment direction, which is possible when the molecular sample is aligned in stretched polyethylene, is crucial in the present investigation. In particular, it allows a clarification of several assignments which could not be safely made in the recent liquid crystal study [1]. The resulting assignments are further confirmed by comparison with ab initio quantum mechanical modelling calculations.

2. Experimental

A sample of pure acenaphthylene was provided by Niels Jørgen Hansen of Aarhus University. Polyethylene sheets of linear, low-density polyethylene (du Pont) or of high-density perdeuterated polyethylene (Merck), in both cases about 0.4 mm thick, were stretched 400% and baselines corresponding to two different polarizer positions (U and V, see later) were recorded. Then the sheets were either soaked for 40 h in saturated chloroform solutions of acenaphthylene or they were left for a week in a small, evacuated and sealed vial, containing some crystals of acenaphthylene. Although it is more time consuming, introduction of acenaphthylene from the vapour phase is preferable; it eliminates problems with removal of the chloroform or compensation for peaks due to solvent remaining in the sheet. In the present case, it also made it possible to obtain a higher concentration in the sheet and thus higher absorbance, which is important in these and most other infrared absorption spectra of large molecules in a stretched polyethylene matrix. Alternatively, remaining chloroform might have

Table 1
Acenaphthylene experimental and calculated vibrational spectral data

	Symmetry	Experimental				AM1		PM3		RHF/6-311G**			BPW91/6-311G**		Assignment
		υ	I^{b}	I^{Rc}	K	υ	I^{d}	υ	I^{d}	υ	I^{d}	I^{Re}	υ	I^{d}	
1	a_1	415	2.1	7.5	0.369	460	0.4	440	0.3	449	1.9	2.1	412	1.9	$C_5-C_{5a}-C_6b$
2		551	2.2	15.4	0.358	591	1.3	560	1.1	599	3.3	14.2	545	3.0	$C_{2a}-C_{8b}-C_{8a}b$
3		659	0.5	31.1	0.379	803	0.2	760	0.2	703	0.5	31.1	657	0.2	Skeletal breathing
4		804	0.5	8.9	0.352	906	1.2	868	1.3	868	2.1	4.1	796	0.2	$C_{4(7)}-C_{3(8)}-C_{2a(8a)}$ b + $C_{8b}-C_{2a(8a)}-C_{3(8)}b$
5		1010	2.1	7.4	0.363	1108	0.4	1070	0.5	1090	1.9	6.7	1005	0.7	$C_{2a(8a)}-C_{2(1)}$st + $C_{2(1)}-H_{2(1)}b$
6		1031	2.2	19.5	0.369	1158	2.4	1088	2.8	1115	3.7	14.9	1035	2.1	$C_{3(8)}-C_{4(7)}$st + $C_{3,5(8,6)}-H_{3,5(8,6)}b$
7		1080	11.1	17.2	0.363	1167	3.9	1111	2.5	1191	7.0	45.0	1072	13.6	$C_{2(1)}-H_{2(1)}b$
8		1176	2.8	1.6	0.342	1248	4.9	1171	2.0	1285	2.1	6.0	1174	3.6	$C_{4(7)}-C_{4(7)}b$ oph$C_{5(6)}-C_{5(6)}b$
9		1248	0.9	4.2	0.369	1336	16.2	1265	15.4	1363	1.1	19.2	1241	1.1	Five-member ring st + $C_{3(8)}-H_{3(8)}b$
10		1356	1.1	27.3	0.371	1467	0.1	1441	2.1	1484	6.1	73.3	1351	0.5	$C_{5a}-C_{8b}$st + $C_{3(8)}-H_{3(8)}b$
11		1406	0.7	0.5	0.381	1512	5.9	1481	3.0	1537	33.3	131.4	1405	2.0	Five-member ring breathing
12		1425	33.0	73.3	0.345	1633	49.3	1612	52.5	1562	3.1	21.7	1436	34.6	$C_{3(8)}-C_{4(7)}$st + $C_{4,7,5,6}-H_{4,7,5,6}b$
13		1491	9.9	39.2	0.358	1693	0.2	1715	0.5	1701	13.8	123.7	1490	11.6	$C_2=C_1$st + $C_{2(1)}-H_{2(1)}b$
14		1584	0.5	1.1	0.340	1818	0.2	1839	3.2	1795	0.0	105.8	1588	0.0	'Kekule' mode + C–Hb
15		1605	0.6	2.3	0.364	1852	11.7	1841	7.5	1809	0.1	104.1	1608	0.6	$C_{5a}-C_{8b}$st iph$C_{3(8)}-C_{4(7)}$st
16		3062	9.4	—	0.379	3176	0.0	3050	0.1	3317	1.6	48.6	3098	1.1	$C_{3,5(8,6)}-H_{3,5(8,6)}$st oph$C_{4(7)}-H_{4(7)}$st
17		3076	0.2	—	0.343	3191	80.4	3066	47.3	3331	33.8	124.9	3108	25.1	$C_{3(8)}-H_{3(8)}$st oph$C_{5(6)}-H_{5(6)}$ st
18		3086	0.4	–	0.366	3198	2.8	3077	0.0	3345	16.3	482.8	3122	14.4	$C_{3,4,5(8,7,6)}-H_{3,4,5(8,7,6)}$ st
19		3100	3.2	—	0.354	3264	48.5	3148	31.1	3379	21.5	211.8	3163	17.3	$C_{2(1)}-H_{2(1)}$st
20	a_2	209	0.0	0.2	—	198	0.0	191	0.0	232	0.0	0.6	203	0.0	
21		371	0.0	2.1	—	342	0.0	330	0.0	407	0.0	0.5	361	0.0	
22		571	0.0	1.4	—	513	0.0	506	0.0	629	0.0	3.5	564	0.0	
23		642	0.0	1.7	—	644	0.0	626	0.0	729	0.0	6.6	653	0.0	
24		742	0.0	0.2	—	815	0.0	781	0.0	850	0.0	0.1	739	0.0	
25		897	0.0	0.8	—	937	0.0	918	0.0	1027	0.0	0.9	882	0.0	
26		918	0.0	1.1	—	959	0.0	969	0.0	1064	0.0	7.0	894	0.0	
27		—	—	—	—	994	0.0	998	0.0	1094	0.0	0.3	939	0.0	
28	b_1	168	12.3	0.2	0.210	163	5.8	156	4.9	175	7.3	0.0	156	6.9	'Flapping' mode (skeletal bend)
29		236	7.6	0.5	0.225	229	9.0	223	7.0	252	7.2	0.6	220	4.8	Skeletal torsion
30		450	0.2	0.7	0.193	435	1.0	423	0.8	501	0.0	0.2	442	0.0	Skeletal bend
31		601	0.4	0.3	0.201	594	0.3	573	0.1	663	0.3	0.8	597	0.2	Skeletal bend
32		726	45.8	0.9	0.203	768	52.4	753	64.8	820	57.2	0.1	714	45.1	$C_{2(1)}-H_{2(1)}b+C_{5(6)}-H_{5(6)}b$
33		775	43.5	0.8	0.210	839	32.4	797	16.0	870	30.8	0.9	760	42.6	C–Hb
34		831	48.1	0.3	0.200	895	80.2	872	46.1	930	72.0	1.1	814	48.1	C–Hb
35		911	3.3	1.7	0.201	961	1.1	944	2.3	1038	4.7	2.7	895	1.9	$C_{5(6)}-H_{5(6)}b+C_{3(8)}-H_{3(8)}b$
36		967	2.1	0.6	0.193	1000	3.2	1008	3.4	1103	1.0	2.6	948	0.8	$C_{5(6)}-H_{5(6)}b+C_{4(7)}-H_{4(7)}b$
37	b_2	462	1.1	0.0	0.410	515	0.3	496	0.1	499	1.3	0.1	460	1.4	$C_{3(8)}-C_{2a(8a)}-C_{2(1)}b$
38		510	1.3	17.9	0.422	550	0.3	521	0.4	553	1.4	10.9	503	1.5	'Napthalene' skewing mode
39		682	0.5	1.1	0.397	758	0.0	719	0.0	735	0.2	0.6	676	0.0	As st of "napthalene" rings
40		864	4.0	1.6	0.417	914	3.0	870	2.0	936	4.3	1.7	854	3.8	$C_{2a(8a)}-C_{2(1)}$st

Table 1 (continued)

Symmetry	Experimental				AM1		PM3		RHF/6-311G**			BPW91/6-311G**		Assignment
	υ	I^b	I^{Rc}	K	υ	I^d	υ	I^d	υ	I^d	I^{Rc}	υ	I^d	
41	1005	0.2	0.5	0.397	1156	0.1	1084	0.2	1056	2.5	1.4	1017	0.8	$C_{3(8)}-C_{4(7)}$st
42	1091	0.9	12.7	0.420	1180	0.1	1122	1.4	1186	2.5	0.3	1085	2.1	$C_{2a(6a)}-C_{2(1)}$st+C–Hb
43	1149	4.6	3.2	0.412	1212	1.0	1153	0.0	1224	13.9	15.3	1152	2.7	$C_{8(7)}-C_{8(7)}$b
44	1202	5.1	10.2	0.421	1257	2.1	1163	0.5	1303	4.1	6.8	1193	1.4	$C_{5a(8b)}-C_{5(2a)}$st+$C_{3,4}-H_{3,4}$b ophi$C_{5a(8b)}$–$C_{6(8a)}$st+
45	1223	4.6	3.7	0.415	1320	32.3	1250	32.4	1328	0.6				$C_{8,7}-H_{8,7}$b
46	1304	1.4	0.2	0.403	1356	0.1	1325	0.0	1421	0.0	3.5	1219	5.8	$C_{5a}-C_{5}$st ophi$C_{5a}-C_{6}$st+C–Hb
47	1386	5.4	27.7	0.429	1500	1.8	1472	0.1	1514	2.4	3.2	1302	1.3	$C_{2a(4)}-C_{3(5)}$st ophi$C_{8a(7)}-C_{8(6)}$st+$C_{2(1)}-H_{2(1)}$b
48	1451	15.4	11.1	0.440	1625	16.4	1622	6.1	1613	8.4	43.1	1393	2.8	$C_{3}-C_{2a}-C_{2}$st ophi$C_{8}-C_{8a}-C_{3}$st+$C_{2(1)}-H_{2(1)}$b
49	1476	13.7	6.9	0.417	1665	3.9	1655	11.2	1637	28.0	18.3	1453	16.9	$C_{8b}-C_{2b,8a}$st ophi$C_{5a}-C_{5,6}$st+C–Hb
50	1622	2.8	34.4	0.400	1826	10.3	1841	13.2	1821	1.2	27.0	1476	12.0	$C_{3,4,5}-H_{3,4,5}$st ophi$C_{8,7,6}-H_{8,7,6}$st
51	3012	0.2	—	0.430	3176	30.2	3050	15.0	3316	1.2	56.3	3098	0.0	$C_{2a,5a,8b,7}-C_{3,5,8a,6}$st ophi$C_{8b,4,8a,5a}-C_{2a,5,8,6}$st
52	3022	0.4	—	0.420	3191	0.6	3067	0.1	3330	5.2	103.7	3108	8.1	$C_{3,7,5}-H_{3,7,5}$ st ophi $C_{8,4,6}-H_{8,4,6}$ st
53	3041	9.9	—	0.425	3197	117.0	3077	62.6	3344	60.8	21.7	3121	46.7	$C_{3(6)}-H_{3(6)}$st ophi$C_{8(9)}-H_{8(9)}$ts st
54	3114	0.2	—	0.437	3254	50.2	3132	23.0	3356	2.0	80.9	3143	2.3	$C_{3,4,5}-H_{3,4,5}$ st oph $C_{8,7,6}-H_{8,7,6}$st
														$C_{2(1)}-H_{2(1)}$ts st

[a] RHF calculated (RHF/6-311G**) values.
[b] DFT calculated (BPW91/6-311G**) values.
[c] *Integrated relative infrared absorbtion intensity* (E_0+2E_v).
[d] Calculated infrared absorbtion intensity.

been completely removed by placing the soaked sample in a vacuum line, but this would have been counterproductive, since it would have removed part of the acenaphthylene molecules as well.

The infrared absorption spectra were obtained on a Nicolet Magna 550 FTIR equipped with KRS-5 or polyethylene based polarizers (IGP-225 or IGP-228, Cambridge Physical Sciences). They were corrected for the wavelength-dependent polarizer efficiency [8]. All FTIR spectra were recorded with a 0.5 cm^{-1} resolution, using a liquid nitrogen cooled MCT detector (mid-IR) or a liquid helium cooled Si bolometer (FIR). These spectra were obtained at a temperature near 12 K, in a closed-cycle helium refrigerator (Displex 202-E, Air Products). In this setup the sample was placed in a massive copper holder, well shielded from external radiation; the temperature was recorded by a thermocouple at the holder. Experiments performed with two thermocouples, one placed on a 1.5 mm thich polyethylene sample, the other on the copper holder, showed a difference in temperature of only 1.5 K between the holder and the sample after equilibrium had been reached.

The solution Raman spectra were recorded at room temperature with a 2.5 cm^{-1} resolution using a Spex Ramalog instrument and an Ar-ion laser (514.5 nm, 350 mW) as the excitation source. The infrared linear dichroism spectra of acenaphthylene aligned in stretched polyethylene and (when polyethylene baseline absorption made it necessary) stretched perdeuterated polyethylene are shown in Fig. 1 and listed in Table 1, which also contains the results of the Raman spectroscopic studies.

3. Computational details

Acenaphtylene was geometry optimized with the Gaussian 94 programs [9] at the AM1, PM3, RHF/6-311G**, BPW91/6-311G**, and MP2 = FULL/6-311G** levels within C_{2v} constraints, in agreement with the experimental structure [10,11]. The calculated results were compared with experimental structures determined by neutron diffraction [11] and the lowest average distance between the positions of corresponding atoms in the calculated and experimental structures was found by rotating and translating the theoretical structure relative to the experimental one. The bond lengths and angles obtained are shown in Table 2.

Recent reviews have suggested that several combinations of exchange and correlation terms in density functional theory (DFT) outperforms MP2 type calculations with respect to the prediction of vibrational frequencies [12,13]. This is in agreement with the findings for trithiapentalene [14] using the Becke's exchange [15] and a Perdew–Wang (1991) correlation term [16] (BPW91). Another reason for choosing the DFT method over MP2 was the expected amount of computational time needed for the latter which, due to lack of a direct MP2 frequency method in the Gaussian 94 program [9], would also require in excess of 24 Gb of scratch-diskspace.

The frequency calculations unequivocally establish the AM1, the PM3, the RHF, and the BPW91 geometries to be minima on the respective potential energy surfaces, and due to the agreement between the BPW91 and MP2 geometries we expect the MP2 structure to be a minimum as well.

Bond orders were calculated with the NBO 4.0 program [17] linked to Gaussian 94. The natural resonance theory (NRT) option in this program makes it possible to fit the electron density matrix as a sum of one electron densities associated with each significant resonance structure. The natural bond orders (based on the weight of the individual resonance structures times the bond order) and the covalent-ionic ratios obtained were compared with Wiberg bond orders in a natural orbital basis.

4. Results and discussion

The alignment of organic molecules in stretched polyethylene is usually assumed to be uniaxial around the stretching direction *U*. In other words,

all directions perpendicular to U are equivalent. This is also assumed to be the case in a thin polymer sheet; a verification of this assumption has been demonstrated in a recent study [7]. It is important to realize that absorption spectroscopy performed on an aligned sample with unknown molecular orientation can usually not produce a complete distribution function. The only orientational quantities which may be determined in an absorption experiment performed with linearly polarized light on a uniaxially aligned sample are average values of squares of directional cosines, for example [3,4]:

$$K_i = \langle \cos^2(U, i) \rangle$$

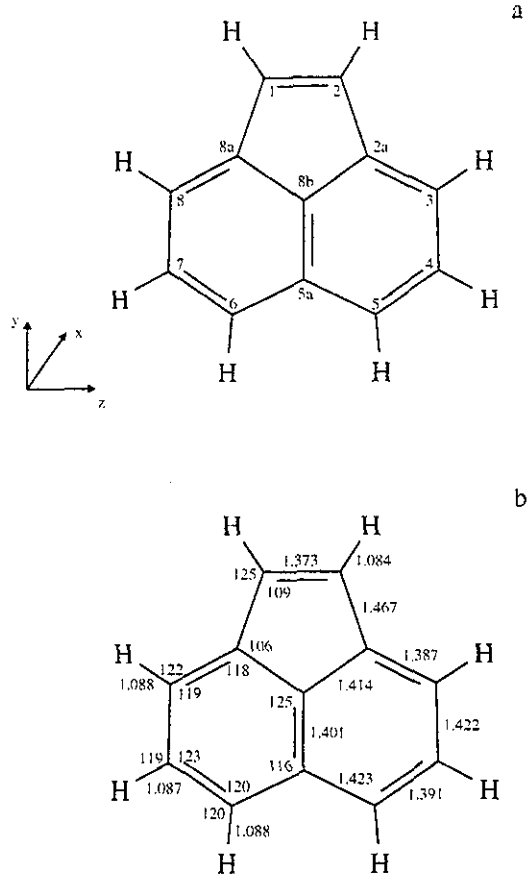

Fig. 2. MP2 = FULL/6-311G** calculated geometry, (a) axes and atomic numbering. (b) Bond lengths and bond angles (in Å and degrees).

where $i = x, y, z$ represents the molecule-fixed axes system, here determined by the molecular symmetry (due to the molecular shape, we have chosen y as the symmetry axis), U is the (macroscopic) unique sample axis (the stretching direction), (U, i) is the angle between directions U and i, and the brackets ($\langle\ \rangle$) indicate an averaging over all molecules in the sample, since the alignment of individual guest molecules in stretched polyethylene varies. The set of three K_is contains the only information on the molecular alignment available from an absorption experiment; they are called orientation factors. Since the three K_is are linearly dependent (by definition their sum is equal to one [3,4]) the orientational information is overdetermined and thus may provide a test of the interpretation and quality of the spectra.

Use of the orientation factors makes it is possible to write the result of absorption experiments on aligned samples performed with linearly polarized light in a very simple, but still exact form. The observed absorbance, when the electric vector of the light is parallel to the unique sample axis U, may be written:

$$E_U(\nu) = \Sigma K_i A_i(\nu)$$

where the sum goes over the three molecular axes x, y, and z, and $A_i(\nu)$ is three times the combined absorbance of all i-polarized transitions in an otherwise similar, isotropic sample (in such a sample all orientation factors are identical and equal to 1/3). If the polarizer is rotated so that the electric vector is along V, perpendicular to U (the laboratory axes are chosen so that U and V defines the plane of the polyethylene sheet), we obtain:

$$E_V(\nu) = \tfrac{1}{2}\Sigma(1 - K_i)A_i(\nu)$$

K_i values may be directly determined for all non-overlapping peaks; from the above expressions for $E_U(\nu)$ and $E_V(\nu)$, applied to a peak at ν_i corresponding to polarization I, we obtain:

$$K_i = E_U(\nu_i)/[E_U(\nu_i) + 2E_V(\nu_i)]$$

Even if transitions overlap it is possible to determine K_i. This may be done by means of a trial and error technique, the TEM method [3,4]

Table 2
Experimental and calculated geometries

	Neutron [11]	AM1	PM3	RHF	BPW91	MP2
Bond lengths (Å)						
C_1–C_2	1.395	1.371	1.362	1.340	1.372	1.373
C_1–H_1	1.052	1.089	1.088	1.073	1.088	1.084
C_{2a}–C_3	1.381	1.370	1.367	1.359	1.388	1.387
C_{2a}–C_{8b}	1.441	1.438	1.428	1.409	1.420	1.414
C_2–C_{2a}	1.466	1.475	1.473	1.480	1.472	1.467
C_3–C_4	1.424	1.426	1.424	1.427	1.427	1.422
C_3–H_3	1.090	1.099	1.094	1.076	1.092	1.088
C_4–C_5	1.382	1.379	1.424	1.365	1.391	1.391
C_4–H_4	1.094	1.101	1.096	1.076	1.092	1.087
C_{5a}–C_{8b}	1.386	1.391	1.386	1.377	1.402	1.401
C_5–C_{5a}	1.433	1.425	1.424	1.424	1.429	1.423
C_5–H_5	1.077	1.100	1.095	1.076	1.092	1.088
Bond angles (°)						
C_1–C_2–C_{2a}	108.8	109.6	109.4	109.2	108.9	108.8
C_{2a}–C_2–H_2	126.0	123.1	123.3	124.9	125.2	125.4
C_{2a}–C_3–C_4	118.7	118.5	118.2	118.4	118.8	118.6
C_{2a}–C_3–H_3	119.5	122.2	122.0	122.2	121.8	121.8
C_2–C_{2a}–C_{8b}	106.9	105.3	105.5	105.7	106.0	106.2
C_3–C_{2a}–C_{8b}	116.6	117.7	118.1	118.3	117.8	117.9
C_3–C_4–C_5	123.9	123.1	123.1	122.5	122.6	122.7
C_3–C_4–H_4	117.2	117.5	117.7	118.3	118.5	118.5
C_4–C_5–C_{5a}	118.9	120.1	120.0	119.9	119.9	119.8
C_{5a}–C_5–H_5	120.3	119.1	119.1	120.1	120.1	120.2
C_{5a}–C_{8b}–C_{2a}	125.7	124.9	124.9	124.9	125.0	125.0
C_5–C_{5a}–C_{8b}	116.1	115.7	115.7	115.9	115.9	116.0

in which linear combinations of the observed spectra are formed:

$$(1-K)E_U(\nu) - 2KE_V(\nu)$$

and applied to a specific peak or other spectral feature i at $\nu = \nu_i$. K is then varied until the peak or feature disappears. This will happen only when $K = K_i$ and often produces a very accurate determination of K_i.

The infrared linear dichroism absorption spectra obtained (see Fig. 1) allow the determination of numerous K_i values. As expected these are grouped around three distinctly different K-values: $K_x = 0.204$, $K_y = 0.369$, and $K_z = 0.407$, which correspond to the three 'allowed' symmetry classes as discussed below. Assuming a perfect C_{2v} symmetry, the sum of these three values (each averaged within the respective symmetry class) should be equal to unity; thus they provide a check of the accuracy. We find that the sum of the three orientation factors is 0.982 which, within the experimental error, is equal to the theoretical value of one. These K-values are almost identical to those determined in the ultraviolet spectroscopic studies of acenaphthylene in stretched polyethylene [2] although these studies were performed on samples in much thinner polethylene sheets. The UV studies produced the following K-values: $K_x = 0.20$ (this value was determined indirectly from $K_x = 1 - K_y - K_z$, since no x-polarized intensity is observed in the spectral region studied), $K_y = 0.38$, and $K_z = 0.42$. Since no value for K_x is experimentally determined, the sum rule does not provide a check for the electronic spectra as it does for the vibrational.

The observed infrared wavenumbers, intensities (both infrared and relative Raman scattering intensities), and K_i values (which in this C_{2v} molecule provide information about the symmetry of excited state i), as well as theoretical results for

these key properties, determined by the best computational method (see below), are listed in Table 1 together with proposed vibrational assignments. As we shall see later, the stretched polyethylene sheet and Raman results make it possible to account for all significant bands and to propose reliable assignments corresponding to all infrared active fundamentals.

The calculated normal modes of acenaphthylene were animated using the VISVIB program [18] and dominant atomic motions for each mode were recorded visually and are listed in Table 1. The convention we have used to describe a mode in a condensed form may be best illustrated by its application to a concrete example. Consider, for example, n_{44} which we have listed as

$$C_{5a(8b)} - C_{5(2a)}st + C_{3,4} - H_{3,4}b\ ophC_{5a(8b)} - C_{6(8a)}st + C_{8,7} - H_{8,7}b$$

This should be interpreted in the following way: The C_{5a}–C_5 bond stretching is proceeding in-phase with the C_{8b}–C_{2a} bond stretching and the C_3–H_3 and C_4–H_4 bendings. The amplitude of all these motions is positive. At the same time these displacements are synchronous with bond stretches of C_{5a}–C_6 and C_{8b}–C_{8a} and bendings of C_8–H_8 and C_7–H_7. The latter motions proceed with the opposite amplitude of those mentioned before-they may be said to be 'out-of-phase' ('oph') although we realize that, strictly speaking, motions of all atoms within any particular normal mode are perfectly in-phase with respect to each other, regardless of the sign of their relative amplitudes. In the case of simple stretching vibrations 'oph' might be replaced by a minus sign. Other notations used are: as, asymmetric; iph, in-phase; b, bending; s, symmetric; st, stretch.

The distribution among the irreducible representations of the 54 normal modes in acenaphthylene is:

$$\Gamma = 19_{a1} + 8_{a2} + 9_{b1} + 18_{b2}$$

Among these, we do not expect to observe the $8a_2$ vibrations in infrared absorption spectra. In the linear dichroism absorption spectra, which are shown in Fig. 1, 19 candidates for a_1 symmetry fundamentals are present. They have an average orientation factor $K_y = 0.369 \pm 0.01$; the earlier IR study [1] determined the average K value for these transitions to 0.44. Our results show that the transitions are polarized along the short, in-plane (symmetry) axis, which we have labelled y in order to reserve the label z for the molecular long axis, which turns out to be the in-plane direction perpendicular to y. In the earlier study [1], based on alignement in nematic liquid crystals, 7 out of the 19 allowed a_1 fundamental vibrations were assigned. Three of these, previously reported at 510, 1154 and 1226 cm^{-1} and now recorded at 510, 1149 and 1223 cm^{-1} can be reassigned to b_2 symmetry vibrations, since their orientation factors are 0.422, 0.412, and 0.415, respectively.

The 18 peaks (including the three discussed above) with the highest K values in the present study have been assigned to 18 b_2 symmetry fundamentals (transitions along the long in-plane axis). The average orientation factor for these peaks was found to be $K_z = 0.407$, compared with 0.44 in the earlier liquid crystal based study [1] the latter value is identical to that obtained for y-polarized transitions in the liquid crystal. Out of the six vibrations in the b_2 symmetry class, which previously were assigned [1], we believe that the one at 416 cm^{-1} was incorrectly assigned. We find the band observed at 415 cm^{-1} to be polarized along the C_2 axis (y). It has the orientation factor $K_y = 0.369 \pm 0.01$.

Very strong candidates for all nine fundamentals belonging to the b_1 symmetry class are present in the spectra shown in Fig. 1. In the previous LD study on acenaphthylene aligned in nematic liquid crystals [1] only three b_1 vibrations were assigned. Not surprisingly for out-of-plane polarized transitions, the nine fundamentals produce the lowest observed orientation factor among all, both in our study and in [1], namely $K_x = 0.204 \pm 0.01$ in our work and 0.13 in the nematic liquid crystal study [1].

For all observed infrared and Raman transitions (the latter are only shown in Table 1) we have determined relative intensities. Infrared isotropic integrated intensities are normalized

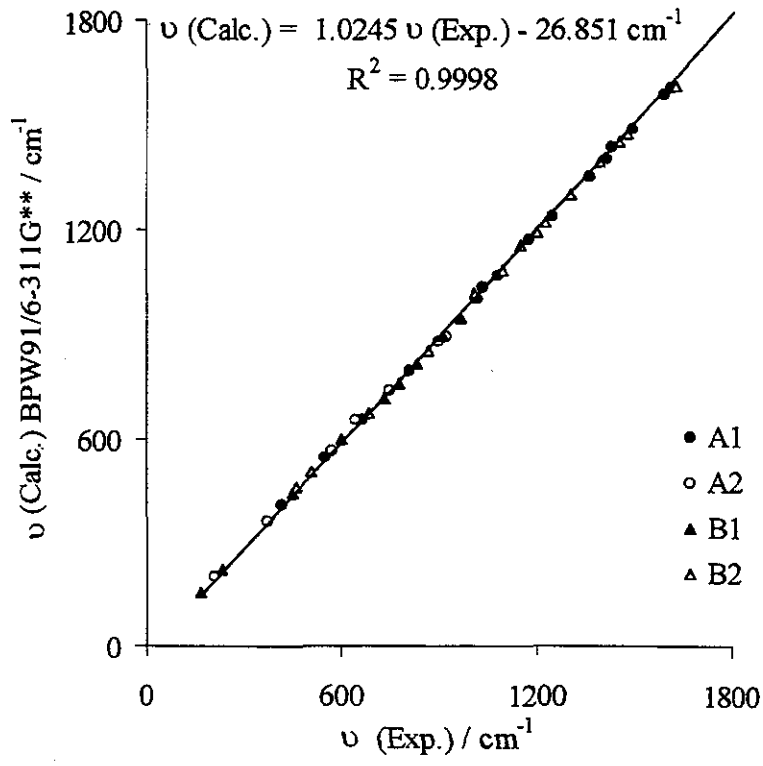

Fig. 3. Comparison of BPW91/6-311G** calculated and experimental wavenumbers.

using the strong out-of-plane polarized transition ν_{34}, calculated at to be at 814 cm^{-1} with an intensity of 48.1 km mol^{-1}. The Raman scattering relative intensities are normalized using the non-overlapping ν_3 vibration, rather than the strongest band, which would be the normal choice, since this most likely is not properly placed by the lower level RHF/6-3116** calculations. We have not calculated Raman scattering intensities at the DFT level.

A comparison of the calculated structures with the experimental one, determined by neutron diffraction [11], shows that the sum of the bond length differences between calculated and experimental results falls through the series: RHF > PM3 > MP2 ~ BPW91 ~ AM1 (Table 2).

The results obtained in the bond length calculations confirm the systematic errors which are expected in RHF theory: the calculated bonds are too short.

The bond angle differences between calculated and experimental angles decrease systematically through the series: AM1 > PM3 > RHF > BPW91 > MP2. For both BPW91 and MP2, the calculated bond angles are in excellent agreement with the experimental geometry. The MP2 calculated bond lengths and angles are shown in Fig. 2.

The lowest average distance between the positions of corresponding atoms in the calculated and experimental structures were 0.0181, 0.0167, 0.0242, 0.0155, and 0.0141 Å, respectively, for the structures determined in the AM1, PM3, RHF, BPW91, and MP2 models.

The calculated vibrational frequencies all agree well with experiment using scaling factors for AM1:PM3:RHF:BPW91 of, respectively, 1.065:1.030:1.096:1.010. Standard errors were 57.1:74.2:27.7:20.4 cm^{-1}, respectively. A comparison of experimentally determined frequencies and intensities for each symmetry group with the re-

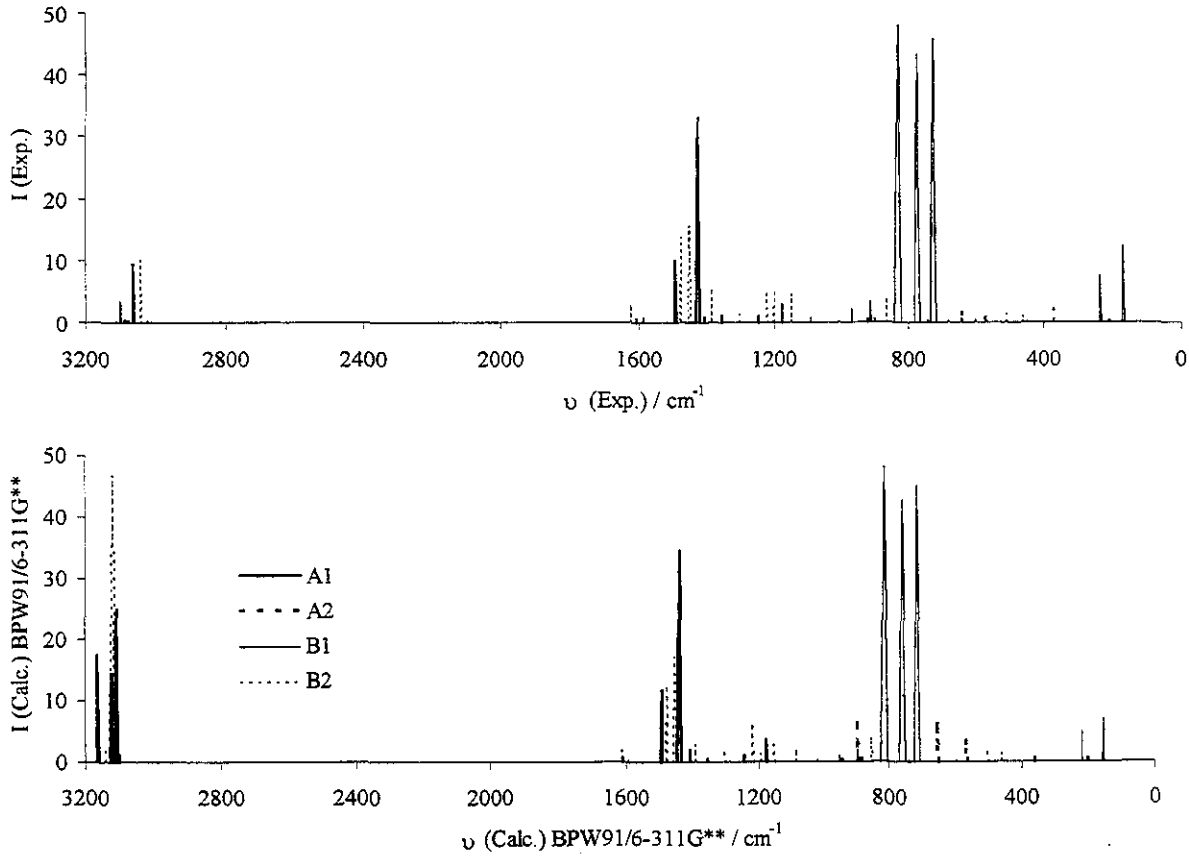

Fig. 4. Top: Experimental, and bottom: Calculated transition energies and intensities.

sults obtained by the four theoretical methods is given in Table 1. See also Figs. 3 and 4.

The agreement with experiment is considerably better for the BPW91 calculation than for the other three calculations; this is the reason that BPW91 results were chosen for comparison with experiment in Table 1. Fig. 3 shows the BPW91 calculated frequencies versus the experimental frequencies; the results demonstrate an almost perfect linear relation. Fig. 4(a) and (b), respectively, show the synthetic experimental and BPW91 calculated spectra; not surprisingly, the two pictures are very similar.

The NBO 4.0 calculated bond orders are presented in Fig. 5; the values obtained for bond lengths and bond orders show that the ethylene part of acenapthylene (C_1 and C_2) has a very localized double bond and does not 'resonate' with the highly aromatic napthalene part of the molecule. The natural resonance theory bond orders and the covalent ionic ratios agree well with the Wiberg bond orders in a natural orbital basis. The two predominant, non-symmetry related Kekulé resonance structures account for most electron density, and none of the bonds in the molecule show any significant ionic character.

We have demonstrated the efficiency of the linear dichroism method applied to samples aligned in stretched polyethylene sheets. Especially when these experimental results are combined with theoretical calculations of a good quality, a complete determination of vibrational assignments in infrared spectra of aromatic compounds often becomes possible. The experimen-

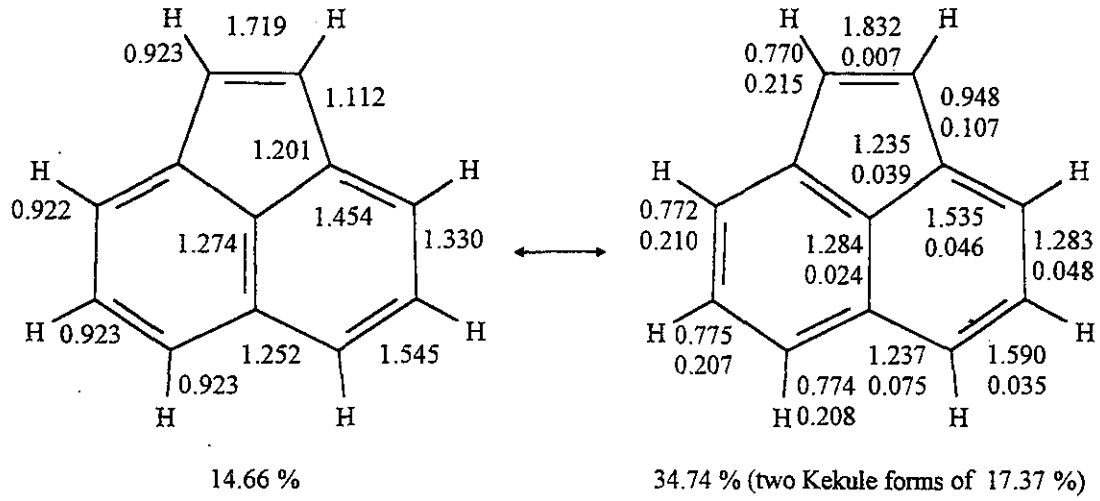

Fig. 5. The BPW91/6-311G** electronic structure. Top, left: Wiberg bond orders in NBO basis. Top, right: Natural Resonance Structures average covalent (upper) and ionic (lower) bond orders. Bottom: Natural Resonance Structure weights in %. If only the two reference structures shown are included, the individual constributions become 36.62% and 63.38% (two Kekule forms of 31.69%), respectively.

tally simple linear dichroism method, based on stretched polymer sheets, is in most cases superior to traditional polarization studies of vibrational and electronic spectra based on oriented single or mixed crystals. It is similar to linear dichroism investigations of molecules aligned in nematic liquid crystals [1,3,4] but will often provide information with a slightly different content, which sometimes, like in the present case, has additional detail, crucial for a safe assignment.

Acknowledgements

The project was supported by the Danish Natural Science Research Council; in addition, the computational efforts were supported by the National Center for Supercomputing Applications. Niels Jørgen Hansen of Aarhus University is gratefully acknowledged for a gift of pure acenaphthylene.

References

[1] G. Baranovic, B. Jordanov, B. Schrader, J. Mol. Struct. 323 (1994) 103.
[2] E.W. Thulstrup, J. Michl, J. Am. Chem. Soc. 98 (1976) 4533.
[3] J. Michl, E.W. Thulstrup, Spectroscopy with polarized light. Solute alignment by photoselection, in Liquid Crystals, Polymers and Membranes, Paperback Edition, VCH, New York, 1995
[4] E.W. Thulstrup, J. Michl, Elementary Polarization Spectroscopy, VCH, New York, 1989.
[5] J.G. Radziszewski, V. Balaji, P. Carsky, Erik W. Thulstrup, J. Phys. Chem. 95 (1991) 5064.
[6] P.R. Biernacki, P. Kaszynski, B.A. Hess, E.W. Thulstrup, J.G. Radziszewski, J. Phys. Chem. 99 (1995) 6309.
[7] F.R. Steenstrup, K. Christensen, C. Svane, E.W. Thulstrup, J. Mol. Struct. (1997) in press.
[8] J.G. Radziszewski, C.A. Arrington, J.W. Downing, V. Balaji, G.S. Murthy, J. Michl, J. Mol. Struct. (Theochem) 163 (1988) 191.
[9] M.J. Frisch, G.W. Trucks, H.B. Schlegel, P.M.W. Gill, B.G. Johnson, M.A. Robb, J.R. Cheeseman, T.A. Keith, G.A. Petersson, J.A. Montgomery, K. Raghavachari, M.A. Al-Laham, V.G. Zakrzewski, J.V. Ortiz, J.B. Foresman, C.Y. Peng, P.Y. Ayala, M.W. Wong, J.L. Andres, E.S. Replogle, R. Gomperts, R.L. Martin, D.J. Fox, J.S. Binkley, D.J. Defrees, J. Baker, J.P. Stewart, M. Head-Gordon, C. Gonzalez, J.A. Pople. Gaussian, 94 (Revision), Gaussian, Pittsburgh, 1995.
[10] T.R. Welberry, Proc. R. Soc. Lond. Ser. A 334 (1973) 19.
[11] R.A. Wood, T.R. Welberry, A.D. Rae, J. Chem. Soc. Perkin Trans. 2 (1985) 451.
[12] P. Scott, L. Radom, J. Phys. Chem 100 (1996) 16502.
[13] W. Wong, Chem. Phys. Lett. 256 (1996) 391.

[14] K. Birklund Andersen, J. Abildgaard, J.G. Radziswski, J. Spanget-Larsen, J. Phys. Chem. 101 (1997) 4475.
[15] D. Becke, Phys. Rev. A 38 (1988) 3098.
[16] P. Perdew, Y. Wang, Phys. Rev. B 45 (1992) 13244.
[17] NBO 4.0-E.D. Glendening, J.K. Badenhoop, A.E. Reed, J.E. Carpenter, F.A. Weinhold, Theoretical Chemistry Institute, University of Wisconsin, Madison, WI, 1996.
[18] T. Preiss VISVIB—this graphical program for generation, display and animation of normal modes was kindly provided by Professor Maier from the University of Giessen, Germany.

Cumulative alphabetic list of references

Abildgaard, J.; Bolvig, S.; Hansen, P. E. *J. Am. Chem. Soc.* **120** (35), 9063 (1998)

Abildgaard, J.; Duus, F.; Hansen, P.E. *J. Am. Chem. Soc.* (In preparation)

Abildgaard, J.; Hansen, P. E., *Wiadomosci Chemiczne* (Chemical News), Polish Chemical Society, (1998) (in press)

Abildgaard, J.; Hansen, P. E.; Hansen, Aa. E. Poster at "Frontiers of NMR in Molecular Biology IV", Keystone, Colorado, USA 3-9.4.1995. Abstract In *J. Cell. Biochem.* **Supplement 21B**, 68 (1995)

Abildgaard, J.; Hansen, P. E.; Hansen, Aa. E.; Wang, A.; Bax, A. *J. Am. Chem. Soc.* (In preparation)

Abildgaard, J.; Hansen, P. E.; Josephsen, J.; Lycka, A. *Inorg. Chem.* **33**, 5271 (1994)

Abildgaard, J.; Josephsen, J.; Hansen, P. E.; Larsen, S. *Inorg. Chem.* (In preparation)

Abildgaard, J.; Wang, A.; Bax, A.; Hansen, P. E.; In preparation.

Altman, L. J.; Laungani, D. L.; Gunnarson, G.; Wennerstöm, H.; Forsén, S. *J. Am. Chem. Soc.* **100**, 8264 (1978)

Andersen, K. B.; Abildgaard, J.; Radziszewski, J. G.; Spanget-Larsen, J. *J. Phys. Chem.* **101**, 4475 (1997)

Augspurger, J. D.; de Dios, A. C.; Oldfield, E.; Dykstra, C. E.; *Chem. Phys. Lett.* **213**, 211 (1993)

Augspurger, J. D.; Dykstra, C. E.; *J. Am. Chem. Soc.* **115**, 12016 (1993)

Augspurger, J. D.; Dykstra, C. E.; Oldfield, E. *J. Am. Chem. Soc.* **113**, 2447 (1991)

Augspurger, J. D.; Pearson, J. G.; Oldfield, E.; Dykstra, C. E.; Park K. D.; Schwartz, D. *J. Mag. Res.* **100**, 342 (1992)

Augspurger, J. D.; Pearson, J. G.; Oldfield, E.; Dykstra, C. E.; Park K. D.; Schwartz, D. *J. Mag. Res.* **100**, 342 (1992)

Baranovic, G.; Jordanov, B.; Schrader, B. *J. Mol Struct*, **323**, 103 (1994)

Barfield, M.; Fagerness, P. *J. Am. Chem. Soc.* **119**, 8699 (1997)

Bartlett; R. J. Purvis, G. D. *Int. J. Quant. Chem.* **14**, 516 (1978)

Batchelor, J. G. Feeney, J.; Roberts, G. C. K. *J. Mag. Res.* **20**, 19 (1975)

Batchelor, J. G. *J. Am. Chem. Soc.* **97**, 3410 (1975)

Batchelor, J. G.; Prestegaard, J. H.; Cushley R. J.; and Lipsky, S. R. *J. Am. Chem. Soc.* **95**, 6358 (1973)

Bax, A.; Freeman, R. *J. Am. Chem. Soc.* **104**, 1099 (1982)

Becke, A. D. *J. Chem. Phys.* **98**, 5648 (1993)

Becke, A. D. *Phys. Rev. A*, **38**, 3098 (1988)

Berger, S.; Braun, S.; Kalinowski, H. O. NMR-Spectroskopie von Nichtmetallen, Volumes 1 and 2, Georg Thieme,

Stuttgart (1992)

Bernardi, F.; Bottini, A.; McDougall, J. J. W.; Robb M. A.; Schlegel, H. B. *Far. Symp. Chem. Soc.* **19**, 137 (1984)

Bezzi, S.; Mammi, M.; Carbuglio, C. *Nature* **182**, 247 (1958)

Biernacki, P. R.; Kaszynski, P. Hess, B. A.; Thulstrup, E. W.; Radziszewski, J. G. *J. Phys. Chem.* **99**, 6309 (1995)

Bingham, R. C.; Dewar, M. J. S.; Lo?, *J. Am. Chem. Soc.* **97**, 1285,1294,1302,1307 (1975)

Bjorholm, T.; Jacobsen, J. P.; Pedersen, C. Th. *J. Mol. Struct.* **75**, 327 (1981)

Blomberg, F.; Maurer, W.; Rüterjans, H. *Proc. Natl. Acad. Sci. USA*, **73**, 1409 (1976)

Bolton, P. H. *Prog. NMR Spectrosc.* **22**, 423 (1990)

Bolvig, S.; Hansen, P. E.; *Mag. Res. Chem.* **34**, 467 (1996)

Bordner, J.; Hammen, P. D.; Whipple, E. B. *J. Am. Chem. Soc.* **11**, 6572 (1989)

Borisenko, K. B.; Bock, C. W.; Hargittai, I. *J. Phys. Chem.* **100**, 7426 (1996)

Borisov, E. V.; Zhang, W.; Bolvig, S.; Hansen, P. E. *Mag. Res. Chem.* In press.

Bouman, T. D.; Hansen, Aa. E.RPAC Molecular Properties Package, Version 9. 0, (1992)

Bouman; T. D.; Hansen, Aa. E. *Intern. J. Quantum Chem. : Quantum Chem. Symp.* **23**, 381 (1989)

Brünger, A. T.; Clore, G. M.; Gronenborn A. M.; Karplus, M.*Proc. Natl. Acad. Sci. (USA)*, **83**, 3801 (1986)

Buckingham, A. D. *Can. J. Chem.* **38**, 300 (1960)

Burant, J. C.; Strain, M. C.; Scuseria, G. E.; Frisch, M. J. *Chem. Phys. Lett.* **248**, 43 (1996)

Burant, J. C.; Strain, M. C.; Scuseria, G.; Frisch, M. J. *Chem. Phys. Lett.*, **258**, 45 (1996)

Challacombe, M.; Schwegler E.; Almlof, J. in Computational Chemistry: Review of Current Trends, Ed. J. Leczsynski *World Scientific* (1996)

Challacombe, M.; Schwegler, E. *J. Chem. Phys.* **105**, 4685 (1996)

Cheeseman, J. R.; Trucks, G. W.; Keith, T. A.; Frisch, M. J. *J. Chem. Phys.* **104** (14), 5497 (1996)

Chesnut, D. B.; Foley, C. K.; *J. Chem. Phys.* **84**, 852 (1986)

Christl, M.; Roberts, J. D. *J. Am. Chem. Soc.* **94**, 4566 (1972)

Cimaraglia, R.; Hofmann, H.-J. *J. Am. Chem. Soc.* **113**, 6449 (1991)

Cizek, J. Adv. *Chem. Phys.* **14**, 35 (1969)

Dahl, J. P.; Springborg, M. *J. Chem. Phys.* **88**, 4335 (1988)

Davis, L. P. et. al.? *J. Comp. Chem.* **2**, 433 (1981)

de Dios, A. C. *J. Prog. NMR*, **29**, 229 (1996)

de Dios, A. C.; Jameson, C. J. : "The NMR Chemical Shift: Insight into Structure and Environment", to appear in *Ann. Repts. NMR Spectroscopy* (ed. G. A. Webb) vol. **29**, 1 (1994)

de Dios, A. C.; Laws, D. D.; Oldfield, E. *J. Am. Chem. Soc.* **116**, 7784 (1994)

de Dios, A. C.; Oldfield, E. *Chem. Phys. Lett.* **205**, 108 (1993)

de Dios, A. C.; Oldfield, E. *J. Am. Chem. Soc.* **116**, 11485 (1994)

de Dios, A. C.; Oldfield, E. *J. Am. Chem. Soc.* **116**, 5307 (1994)

de Dios, A. C.; Oldfield, E. *J. Am. Chem. Soc.* **116**, 7453 (1994)

de Dios, A. C.; Oldfield, E. *Solid state NMR* **6**, 101 (1996)

de Dios, A. C.; Pearson J. G.; Oldfield, E. *Science*, **260**, 1491 (1993)

de Dios, A. C.; Pearson, J. G.; Oldfield, E. *J. Am. Chem. Soc.* **115**, 9768 (1993)

de Dios, A. C.; Pearson, J. G.; Oldfield, E. *Science.* **260**, 1491 (1993)

Desai, R. D.; Ekhlas, M. *Proc. Ind. Acad. Sci.* **8**, 194 (1938)

Dewar, A. M.; Thiel, W. *J. Am. Chem. Soc.* **99**, 4499 (1977)

Dewar, M. J. S. et. al.? *Organometallics* **4**, 1964 (1985)

Dewar, M. J. S.; Grady, G. L.; Stewart, J. J. P *J. Am. Chem. Soc.* **106**, 6771 (1984)

Dewar, M. J. S.; McKee, M. L. *J. Comp. Chem.* **4**, 84 (1983)

Dewar, M. J. S.; McKee, M. L.; Rzepa, H. S. *J. Am. Chem. Soc.* **100**, 3607 (1978)

Dewar, M. J. S.; Rzepa, H. S. *J. Am. Chem. Soc.* **100**, 777 (1978)

Dewar; M. J. S.; Healy, E. F. *J. Comp. Chem.* **4**, 542 (1983)

Dewar; M. J. S.; Reynolds, C. H. *J. Comp. Chem.* **2**, 140 (1986)

Dewar; M. J. S.; Thiel, W. *J. Am. Chem. Soc.* **99**, 4899 (1977)

Dewar; M. J. S.; Zoebisch, E. G.; Healy, E. F. *J. Am. Chem. Soc.* **107**, 3902 (1985)

Ditchfield, R. *Mol. Phys.* **27**, 789 (1974)

Ditchfield, R.; Hehre W. J.; Pople, J. A. *J. Chem. Phys.* **54**, 724 (1971)

Dodds, J. L.; McWeeny R.; Sadlej, A. J. *Mol. Phys.* **41**, 1419 (1980)

Dunning, T. H.; Hay, P. J. in Methods of Electronic Structure Theory, H. F. Schaefer III, ed. Plenum, New York (1977)

Duus, F. In Methoden der organischen Chemie (Houben-Weyl), Vol. E8a; Schaumann, E., Ed.; Georg Thieme Verlag: Stuttgart, pp 553 (1993)

Dziembowska, T.; Rozwadowski, Z.; Hansen, P. E. *J. Mol. Struct.* **436-437**, 189 (1997)

Eade R. H. E.; Robb, M. A. *Chem. Phys. Lett.* **83**, 362 (1981)

Facelli, J. C.; Grant, D. M.; Bouman, T.

D.; Hansen, Aa. E. *J. Compt. Chem.* **11**, 32 (1990)

Feeney, J.; McCormick, J. E.; Bauer, C. J.; Birdsall, B.; Moody, C. M.; Starkmann, B. A.; Young, D. W.; Francis, P.; Havlin, R. H.; Arnold, W. D.; Oldfield, E. *J. Am. Chem. Soc.* **118**, 8700 (1996)

Foresman, J. B.; Frisch, Æ. Exploring Chemistry with Electronic Structure Methods; Gaussian, Inc.: Pittsburgh, PA (1996)

Foresman, J. B.; Head-Gordon, M.; Pople J. A.; Frisch, M. J. *J. Phys. Chem.* **96**, 135 (1992)

Forsyth, D.; Sebag, A. B. *J. Am. Chem. Soc.* **119**, 9483 (1997)

Frisch, M. J. Head-Gordon, M.; Pople, J. A. *Chem. Phys. Lett.* **166**, 275 (1990)

Frisch, M. J.; Head-Gordon, M.; Trucks, G. W.; Foresman, J. B.; Schlegel, H. B.; Raghavachari, K.; Robb, M. A.; Binkley, J. S.; Gonzalez, C.; Defrees, D. J.; Fox, D. J.; Whiteside, R. A.; Seeger, R.; Melius, C. F.; Baker, J.; Martin, R. L.; Kahn, L. R.; Stewart, J. J. P.; Topiol, S.; Pople, J. A.; Gaussian90, Gaussian Inc, Pittsburgh, PA (1990)

Frisch, M. J.; Ragazos, I. N.; Robb M. A.; Schlegel, H. B. *Chem. Phys. Lett.* **189**, 524 (1992)

Frisch, M. J.; Trucks, G. W.; Schlegel, H. B.; Gill, P. M. W.; Johnson, B. G.; Robb, M. A.; Cheeseman, J. R.; Keith, T.; Petersson, G. A.; Montgomery, J. A.; Raghavachari, K.; Al-Laham, M. A.; Zakrzewski, V. G.; Ortiz, J. V.; Foresman, J. B.; Peng, C. Y.; Ayala, P. Y.; Chen, W.; Wong, M. W.; Andres, J. L.; Replogle, E. S.; Gomperts, R.; Martin, R. L.; Fox, D. J.; Binkley, J. S.; Defrees, D. J.; Baker, J.; Stewart, J. P.; Head-Gordon, M.; Gonzalez, C.; Pople, J. A. Gaussian 94, Revisions B.3, C.3, and E1 Gaussian, Inc.: Pittsburgh, PA (1995)

Gauss J.; Cremer, C. *Chem. Phys. Lett.* **150**, 280 (1988)

Gilli, G.; Bertolasi, V. in *The Chemistry of Enols*. Eds. Z. Rappoport; S. Patai, Wiley, Chichester (1990)

Gilli, G.; Bertulucci, F.; Ferretti, V.; Bertolasi, V. *J. Am. Chem. Soc.* **111**, 1023 (1989)

Gilli, P.; Ferretti, V.; Bertolasi, V.; Gilli, G. *Adv. Mol. Struc. Res.* **2**, 67 (1996)

Gleiter, R.; Gygax, R. Top. *Curr. Chem.* **63**, 49 (1976)

Glushka, J.; Lee, M.; Coffin, S.; Cowburn, D. *J. Am. Chem. Soc.* **111**, 7716 (1989)

Gordon, M. S. *Chem. Phys. Lett.* **76**, 163 (1980)

Grech, E.; Kliemkiewicz, J.; Nowicka-Scheibe, J.; Pietrzak, M.; Stefaniak, L.; Bolvig, S.; Abildgaard J.; Hansen, P. E. *J. Am. Chem. Soc.* (In preparation)

Greengard, L. MIT Press: Cambridge, MA, (1988)

Greengard, L.; Rokhlin, V. *J. Comput. Phys.* **73**, 325 (1987)

Greengard, *Science,* **265**, 909 (1994)

Guillouzo, G. *Bull. Soc. Chim. Fr.* 1316 (1958)

Gurd, F. R. N.; Lawson, P. J.; Cohran, D. W.; Wenkert, E. *J. Biol. Chem.* **246**, 3725 (1971)

Göschke, A.; Tambor, J. *Ber.* **45**, 1237 (1912)

Hansen, L. K.; Hordvik, A. *Acta Chem. Scand.* **27**, 411 (1973)

Hansen, P. E. in *The Chemistry of Double Bonded Functional Groups*, ed. S. Patai, Wiley, New York, p. 83. (1989)

Hansen, P. E. *J. Mol. Struct.* **321**, 79 (1994)

Hansen, P. E. *Mag. Res. Chem.* **31**, 23 (1993)

Hansen, P. E. *Org. Mag. Res.* **24**, 903. (1986)

Hansen, P. E. *Prog. NMR Spectrosc.* **20**, 207 (1988)

Hansen, P. E.; Abildgaard, J.; Hansen, Aa. E. *Chem. Phys. Lett.* **224**, 275 (1994)

Hansen, P. E.; Abildgaard, J.; Hansen, Aa. E. Poster at "Frontiers of NMR in Molecular Biology III", Taos, New Mexico, USA 8-14.3.1993. Abstract In *J. Cell. Biochem.* **Supplement 17C,** 306 (1993)

Hansen, P. E.; Bolvig, S.; Duus, F.; Petrova, M. V.; Kawecki, R.; Krajewski, P.; Kozerski, L. *Mag. Res. Chem.* **33**, 621 (1995)

Hansen, P. E.; Bolvig, S.; *Mag. Res. Chem.* **35**, 520 (1997)

Hansen, P. E.; Christoffersen, M.; Bolvig, S. *Mag. Res. Chem.* **31**, 893 (1993)

Hansen, P. E.; Duus, F.; Bolvig, S.; Jagodzinski, T. S.; *J. Mol. Struct.* **378**, 45 (1996)

Hansen, P. E.; Ibsen, S. N.; Kristensen, T.; Bolvig, S. *Mag. Res. Chem.* **32**, 399 (1994)

Hansen, P. E.; Kawecki, R.; Krowczynski, A.; Kozerski, L. *Acta Chem. Scand.* **44**, 826 (1990)

Hansen, P. E.; Langgård, M.; Bolvig, S. *Polish J. Chem.* **72**, 269 (1998)

Hansen, Aa. E.; Bouman, T. D. in *Nuclear Magnetic Shieldings and Molecular Structure*, ed. J. A. Tossell, Kluwer Academic Publishing Dordrecht, (1993)

Hansen, Aa. E.; Bouman, T. D. *J. Chem. Phys.* **82**, 5035 (1985)

Hansen, Aa. E.; Bouman, T. D. J. *Chem. Phys.* **82**, 5035 (1985)

Hariharan P. C.; Pople, J. A. *Mol. Phys.* **27**, 209 (1974)

Hariharan P. C.; Pople, J. A. *Theo. Chim. Acta.* **28**, 213 (1973)

Havlin; R. H.; Le; H.; Laws; D. D.; deDios; A. C.; Oldfield; E.; *J. Am. Chem. Soc.* **119**, 11951 (1997)

Head-Gordon, M. *J. Phys. Chem.* **100**, 13213 (1996)

Head-Gordon, M.; Head-Gordon, T. *Chem. Phys. Lett.* **220**, 122 (1994)

Head-Gordon, M.; Pople, J. A.; Frisch, M. J. *Chem. Phys. Lett.* **153**, 503 (1988)

Hegarty D.; Robb, M. A. *Mol. Phys.* **38**, 1795 (1979)

Hehre, W. J.; Ditchfield R.; Pople, J. A. *J. Chem. Phys.* **56**, 2257 (1972)

Heller; J.; Laws; D. D.; Tomaselli; M.; King; D. S.; Wemmer; D. E.; Pines; A.; Havlin; R. H.; Oldfield; E. *J. Am. Chem. Soc.* **119**, 7827 (1997)

Hertz, H. G.; Traverso, G.; Walter, V. *Justus Liebigs Ann. Chem.* **625**, 43 (1959)

Hofacker, G. L.; Marchal, Y.; Ratner, M. A.; in *The Hydrogen Bond*, p. 1. P. Schuster, G. Zundel and C. Sandody, eds. North-Holland, Amsterdam (1976)

Hohenberg, P.; Kohn, W. *Physical Review* **136**, B864 (1964)

Hordvik, A.; Saethre, J. *Isr. J. Chem.* **10**, 239 (1972)

Horsley, W. J.; Sternlicht, H. *J. Am. Chem. Soc.* **90**, 3838 (1968)

Horsley, W. J.; Sternlicht, H.; Cohen, J. S. *J. Am. Chem. Soc.* **92**, 680 (1970)

Huber, K. P.; Herzberg, G. *Molecular Spectra and Molecular structure*, **IV**. Constants of Diatomic Molecules, Van Nostrand-Reinhold New York (1979)

Humbel, S.; Sieber, S.; Morokuma, K. *J. Chem. Phys.* **105**, 1959 (1996).

Ichikawa, M. *Acta Cryst.* **B34**, 2074 (1978)

Ikura, M.; Marion, D.; Kay, L. E.; Shih, H.; Krinks, M.; Klee, C. B.; Bax, A. *Biochem. Pharm.* **40**, 153 (1990)

Jameson, C. J. in *Encyclopedia of NMR*, **vol. 6.** , John Wiley, New York, (1995)

Jameson, C. J. in *Isotopes in the Physical and Biomedical Sciences, Isotopic Applications in NMR Studies*, edited by E. Buncel; J. R. Jones, p. 1. Elsevier, Amsterdam (1991)

Kalinowski, H. O. Berger, S.; Braun, S.^{13}C-NMR-Spectroskopie, Georg Thieme, Stuttgart (1984)

Kessler, H.; Griesinger, C.; Zarbock, J.; Loosli, H. R.; *J. Mag. Res.* **57**, 331 (1984)

Khaled, Md. A.; Urry, D. W.; Bradley, R. J. *J. C. S. Perkin II*, 1693 (1979)

Khatipov, S. A.; Shapet'ko, N. N.; Bogavev, Yu. S.; Andreichikov, Yu. S.*Russ. J. Phys. Chem.* **59**, 2097 (1985)

Kohn, W.; Becke, A. D.; Parr, R. G. *J. Phys. Chem.* **100**, 12974 (1996)

Kohn, W.; Sham, L. J.*Physical Review* **140**, A1133 (1965)

Kokoila, M. K.; Nirmala, K. A.; Puttaraja, Shamala, N.; *Acta. Cryst.* **C48**, 1133. (1992)

Krishnan, R.; Schlegel H. B.; Pople, J. A. *J. Chem. Phys.* **72**, 4654 (1980)

Kutteh, R.; Apra E.; Nichols, J. *Chem. Phys. Lett.* **238**, 173 (1995)

Kutzelnigg, W. *Isr. J. Chem.* **19**, 193 (1979)

Kutzelnigg, W. *Isr. J. Chem.* **19**, 193 (1980)

Kutzelnigg, W. *J. Mol. Struct. (Theochem)*, **202**, 11 (1989)

Lampert, H.; Mikenda, W.; Karpfen, A. *J. Phys. Chem.* **101**, 2254 (1997)

Lampert, H.; Mikenda, W.; Karpfen, A.; *J. Phys. Chem.* **100**, 7418 (1996)

Laws, D. D.; de Dios, A. C.; Oldfield, E. *J. Biomol. NMR.* **3**, 607 (1993)

Laws, D. D.; Le, H.; de Dios, A. C.; Havlin, R. H.; Oldfield, E. *J. Am. Chem. Soc.* **117**, 9542 (1995)

Le, H.; Oldfield, E. *J. Biomol. NMR*, **4**, 341 (1994)

Le, H.; Oldfield, E. *J. Phys. Chem.* **100**, 16423 (1996)

Le, H.; Pearson, J. G.; de Dios, A. C.; Oldfield, E. *J. Am. Chem. Soc.* **117**, 3800 (1995)

Lee, T.-S.; York, D. M.; Yang, W. *American Institute of Physics* **105**, 2744 (1996)

Liepins, E.; Petrova, M. V.; Gudriniece, E.; Paulins, J.; Kuznetsov, S. L. *Mag. Res. Chem.* **27**, 907 (1989)

London, F. *J. Phys. Radium, Paris* **8**, 397 (1937)

London, R. E.; Walker, T. E.; Kollman, V. H.; Matwiyoff, N. A. *J. Am. Chem. Soc.* **100**, 3723 (1978)

Lozac'h, N. Adv. *Heterocycl. Chem.* **13**, 161 (1971)

Marsh, K. L.; Maskalich, D. G.; England, R. D.; Friend, S.; Gurd, F. R. N. *Biochemistry* **21**, 5241 (1982)

Martin, J. M. L.; El-Yazal J.; Francois, J.-P. *J. Phys. Chem.* **100**, 15358 (1996)

Maseras, F; Morokuma, K. *J. Comp. Chem.* **16**, 1170 (1995)

McMahon, M. T.; deDios, A. C.; Godbout, N.; Salzmann, R.; Laws, D. D.; Le, H.; Havlin, R. H.; Oldfield, E. *J. Am. Chem. Soc.* **120**, 4784 (1998)

McWeeny, R. *Phys. Rev.* **126**, 1028 (1962)

McWeeny, R.; Dierksen, G. *J. Chem. Phys.* **49**, 4852 (1968)

Michl, J.; Thulstrup, E. W. Spectroscopy with Polarized Light. Solute Alignment by Photoselection, in Liquid Crystals, Polymers and Membranes; VCH Publishers: New York, (1986, 1995)

Munch, M.; Hansen, P. E.; Hansen, Aa. E.; Bouman, T. D. *Acta Chem. Scand.* **46**, 1065 (1992)

Ng, S.; Lee, H. -H.; Bennett, G. J. *Mag. Res. Chem.* **28**, 337 (1990)

Nieto, M.; Simmons, L. M. Jr.; *Phys. Rev. A*, **19**, 438 (1979)

O'Brien, D. H.; Stipanovich, R. D. *J. Org. Chem.* **43**, 1105 (1978)

Oldfield, E. *Abs. Papers. Am. Chem. Soc.* **208**, 146 (1994)

Oldfield, E. *J. Biomol. NMR*, **5**, 217 (1995)

Oldfield, E.; de Dios, A. C.; Pearson, J. G. *Abs. Papers. Am. Chem. Soc.* **205**, 36 (1993)

Oldfield, E.; de Dios, A. C.; Pearson, J. G. *Abs. Papers. Am. Chem. Soc.* **206**, 256 (1993)

Pardi, G.; Wagner; K. Wüthrich, *Eur. J. Biochem.* **137**, 445 (1983)

Parr, R. G.; Yang, W. *Ann. Rev. Phys. Chem.* **46**, 701 (1995)

Pearson, J. G.; Le, H.; Sanders, L. K.; Godbout, N.; Havlin, R. H.; Oldfield, E. *J. Am. Chem. Soc.* **119**, 11941 (1997)

Pearson, J. G.; Montez, B.; Le, H.; Oldfield, E.; Chien, E. Y. T.; Sligar, S. G.; *Biochem.* **36**, 3590 (1997)

Pearson, J. G.; Oldfield, E.; Lee, F. S..; Warshel, A. *J. Am. Chem. Soc.* **115**, 6851 (1992)

Pearson, J. G.; Wang, J.-F.; Markley, J. L.; Le, H.; Oldfield, E. *J. Am. Chem. Soc.* **117**, 8823 (1995)

Pearson; J. G.; Le; H.; Sanders; L. K.; Godbout; N.; Havlin; R. H.; Oldfield; E. *J. Am. Chem. Soc.* **119**, 11941 (1997)

Pedersen, C. Th. *Phosphorus, Sulfur Silicon* **58**, 17 (1991)

Pedersen, C. Th. *Sulfur Rep.* **1**, 1 (1980)

Perdew J. P.; Wang, Y. *Phys. Rev. B*, **45**, 13244 (1992)

Perdew, J. P.; Zunger, A. *Phys. Rev. B*, **23**, 5048 (1981)

Perez-Jorda, J. M.; Yang, W. Chem. Phys. Lett. 247, 484 (1995).

Perez-Jorda, J. M.; Yang, W. *J. Chem. Phys.* **104**, 8003 (1996)

Petersen, H. G.; Soelvason, D.; Perram, J. W. *J. Chem. Phys.* **101**, 8870 (1994)

Pople, J. A.; Beveridge D.; Dobosh, P. *J. Chem. Phys.* **47**, 2026 (1967)

Pople, J. A.; Head-Gordon M.; Raghavachari, K. *J. Chem. Phys.* **87**, 5968 (1987)

Pople, J. A.; Krishnan, R.; Schlegel H. B.; Binkley, J. S. *Int. J. Quant. Chem.* **XIV**, 545 (1978)

Pople, J. A.; Nesbet, R. K. *J. Chem. Phys.* **22,** 571 (1959)

Pople, J. A.; Seeger R.; Krishnan, R. *Int. J. Quant. Chem. Symp.* **11**, 149 (1977)

Purvis G. D.; Bartlett, R. J. *J. Chem. Phys.* **76**, 1910 (1982)

Quirt, A. R.; Lyerla Jr. , J. R.; Peat, E. R.; Cohen, J. C.; Reynolds, W. F.; Freedman, M. H. *J. Am. Chem. Soc.* **96**, 570 (1974)

Radhi, M. M.; El-Bermani, M. F.*Spectrochim. Acta,* **46A**, 33 (1990)

Radziszewski, J. G.; Abildgaard, J.; Thulstrup, E. W. *Spectrochimica Acta Part A*, **53**, 2095 (1997)

Radziszewski, J. G.; Arrington, C. A.; Downing, J. W.; Balaji, V.; Murthy, G. S. Michl, J. *J Mol. Struct. (Theochem)***163**, 191, (1997)

Radziszewski, J. G.; Balaji, V.; Carsky, P.; Thulstrup, E. W. *J. Phys. Chem.* **98**, 5064 (1991)

Radziszewski, J. G.; Kaszynski, P.; Friderichsen, A.; Abildgaard, J. *Coll. Czech. Chem. Comm.* **63**, 1094 (1998)

Radziszewski, J. G.; Michl, J. *J. Am. Chem. Soc.* **108**, 3289 (1986)

Raghavachari K.; Pople, J. A. *Int. J.*

Quant. Chem. **20**, 167 (1981)

Reuben, J. *J. Am. Chem. Soc.* **108**, 1735. (1986)

Reuben, J. *J. Am. Chem. Soc.* **109**, 316 (1987)

Riley, J. P.; Raynes, W. T *Mol. Phys.* **32**, 569 (1976)

Roothan, C. C. J. *Rev. Mod. Phys.* **23**, 69 (1951)

Saeb, S.; Boggs, J. E.; Fan, K. *J. Phys. Chem.* **96**, 9268 (1992)

Saebo, S.; Almlof, J. *Chem. Phys. Lett.* **154**, 83 (1989)

Salter, E. A.; Trucks G. W.; Bartlett, R. J. *J. Chem. Phys.* **90**, 1752 (1989)

Schindler M.; Kutzelnigg, W. *J. Am. Chem. Soc.* **105**, 1360 (1983)

Schindler M.; Kutzelnigg, W. *J. Chem. Phys.* **76**, 1919 (1982)

Schindler M.; Kutzelnigg, W. *Mol. Phys.* **48**, 781 (1983)

Schlegel H. B.; Robb, M. A.*Chem. Phys. Lett.* **93**, 43 (1982)

Schneider, H.-J.; Freitag, W. *J. Am. Chem. Soc.* **99**, 8363 (1977)

Schneider, H.-J.; Freitag, W.; Gschwendtner, W.; Maldner, G.; *J. Mag. Res.* **36**, 273 (1979)

Scott, A. P.; Radom, L. *J. Phys. Chem.* **100**, 16502 (1996)

Scuseria G. E. ; Schaefer, III, H. F. *J. Chem. Phys.* **90**, 3700 (1989)

Scuseria, G. E.; Janssen C. L.; Schaefer, III, H. F. *J. Chem. Phys.* **89**, 7382 (1988)

Segal, G.; Pople, J. A. *J. Chem. Phys.* 3289 (1966)

Shapet'ko, N. N.; Bogachev, Yu. S.; Radushnova, L. V.; Shigorin, D. N. *Dokl. Akad. Nauk, SSSR* **231**, 409 (1976)

Shen, Q.; Hedberg, K. *J. Am. Chem. Soc.* **96**, 289 (1974)

Singh, O. N.; Srivastava, M. P.; Singh, I. S. *Curr. Sci.* **23**, 630 (1967)

Slater, J. C. *Quantum Theory of Molecular and Solids*. Vol. 4: *The Self-Consistent Field for Molecular and Solids,* McGraw-Hill: New York, 1974.

Smirnov, S. N.; Golubev, N. S.; Denisov, G. S.; Benedict, H.; Schah-Mohameddi, P.; Limbach, H.-H. *J. Am. Chem. Soc.* **118**, 4094 (1996)

Spanget-Larsen, J.; Chen, E.; Shim, I. *J. Am. Chem. Soc.* **116**, 11433 (1994)

Spanget-Larsen, J.; Fink, N. *J. Phys. Chem.* **94**, 8423 (1990)

Steenstrup, F. R.; Chrstensen, K.; Svane, C.; Thulstrup, E. W. *J Mol. Struct.* **408/409,** 139 (1997)

Steiner, Th.; Saenger, W.; *Acta Cryst.* **B50**, 348 (1994)

Stephen, M. J. *Mol. Phys.* **1**, 223 (1958)

Stephens, P. J.; Devlin, F. J.; Chabalowski, C. F.; Frisch, M. J. *J. Phys. Chem.* **98**, 11623 (1994)

Stewart, J. J. P. *J. Comp. Chem.* **10**, 209

(1989)

Strain, M. C.; Scuseria G. E.; Frisch, M. J. *Science,* **271**, 51 (1996)

Svensson, M.; Humbel, S.; Froese, R. D. J.; Matsubara, T.; Sieber S.; Morokuma, K. *J. Phys. Chem.* **100**, 19357 (1996)

Thulstrup, E. W.; Michl, J. Elementary Polarization Spectroscopy; VCH Publishers: New York, (1989)

Thulstrup, E. W.; Michl, J. *J. Am. Chem. Soc.* **98**, 4533 (1976)

Tossell, J. A. ed. *Nuclear Magnetic Shieldings and Molecular Structure*, Kluwer academic Publishing, Dordrecht (1993)

Tozer, D. J. *J. Chem. Phys.* **104**, 4166 (1996)

Trucks, G. W.; Frisch, M. J.; Andres J. L.; Schlegel, H. B. *J. Chem. Phys.* submitted? (1995?)

Tüchsen, E.; Hansen, P. E. *Biochemistry*, **27**, 8568 (1988)

Valentine, B.; Steinschneider, A.; Dhawan, D.; Burgar, M. I.; Amour, T. St.; Fiat, D. *Int. J. Peptide Protein Res.* **25**, 56 (1985)

Vosko, S. H. Wilk L.; Nusair, M. *Canadian J. Phys.* **58**, 1200 (1980)

Wajsman, E.; Grabowski, M. J.; Stepien, A.; Cygler, M. *Chryst. Struct. Comm.* **7**, 233 (1978)

Welberry, T. R. *Proc. R. Soc. London.Ser. A,* **334**, 19 (1973)

White C. A.; Head-Gordon, M. *American Institute of Physics,* **105**, 5061 (1996)

White, C. A.; Head-Gordon, M. *J. Chem. Phys.* **104**, 2620 (1996)

Wilkens; S. J.; Xia; B.; Volkman; B. F.; Weinhold; F.; Markley; J. L.; Westler; W. M. *J. Phys. Chem. B,* **102**, 8300 (1998)

Wolinski, K.; Hilton J. F.; Pulay, P. *J. Am. Chem. Soc.* **112**, 8251 (1990)

Wong, M. W. *Chem. Phys. Lett.* **256**, 391 (1996)

Wood, R. A.; Welberry, T. R.; Rae, D. *J. Chem. Soc. Perkin Trans. 2*, 451 (1985)

Xia; B.; Wilkens; S. J.; Westler; W. M.; Markley; J. L. *J. Am. Chem. Soc.* **120**, 4893 (1998)

Yamamoto, N; Vreven, T; Robb, M. A.; Frisch, M. J.; Schlegel, J. B. *Chem. Phys. Lett.* **250**, 373 (1996)

Zheglova, D.; Genov, D. G.; Bolvig, S.; Hansen, P. E.; *Acta Chem. Scand.* **51**, 1016 (1997)